

ACTA

*Visa Isteri*

ALTERNATIVE YE'ELIMITE  
(CSA) CEMENT CLINKERS  
FROM INDUSTRIAL  
BYPRODUCTS

UNIVERSITY OF OULU GRADUATE SCHOOL;  
UNIVERSITY OF OULU,  
FACULTY OF TECHNOLOGY





ACTA UNIVERSITATIS OULUENSIS  
C Technica 880

*VISA ISTERI*

**ALTERNATIVE YE'ELIMITE (CSA)  
CEMENT CLINKERS FROM  
INDUSTRIAL BYPRODUCTS**

Academic dissertation to be presented with the assent of  
the Doctoral Programme Committee of Technology and  
Natural Sciences of the University of Oulu for public  
defence in the Arina auditorium (TA105), Linnanmaa, on  
19 May 2023, at 12 noon

UNIVERSITY OF OULU, OULU 2023

Copyright © 2023  
Acta Univ. Oul. C 880, 2023

Supervised by  
Professor Timo Fabritius  
Professor Mirja Illikainen  
Docent Katja Ohenoja

Reviewed by  
Doctor Frank Winnefeld  
Doctor Mohsen Ben Haha

Opponent  
Doctor Alexander Pisch

ISBN 978-952-62-3663-6 (Paperback)  
ISBN 978-952-62-3664-3 (PDF)

ISSN 0355-3213 (Printed)  
ISSN 1796-2226 (Online)

Cover Design  
Raimo Ahonen

PUNAMUSTA  
TAMPERE 2023

## **Isteri, Visa, Alternative ye'elimate (CSA) cement clinkers from industrial byproducts.**

University of Oulu Graduate School; University of Oulu, Faculty of Technology

*Acta Univ. Oul. C 880, 2023*

University of Oulu, P.O. Box 8000, FI-90014 University of Oulu, Finland

### ***Abstract***

The production of ordinary Portland cement (OPC) is responsible for ~8% of global anthropogenic CO<sub>2</sub>. Two thirds of the emissions arise from the calcination of limestone (CaCO<sub>3</sub> -> CaO + CO<sub>2</sub>). Meanwhile, huge volumes of inorganic industrial sidestreams with necessary ingredients for cement production (Al<sub>2</sub>O<sub>3</sub>, CaO, SiO<sub>2</sub>, and Fe<sub>2</sub>O<sub>3</sub>) are landfilled across the globe. Locally these raw materials can be used to replace virgin raw materials of cement manufacture and provide a source of already decarbonized CaO that can reduce the carbon footprint of cement manufacture while promoting the circular economy. The driving factors for industry to utilize their industrial sidestreams are to find a way to enhance waste valorization, to cover the rising expenses of landfilling due to taxation and regulations, and to tackle resource scarcity.

The aim of this thesis is to utilize Finnish metallurgical slags (argon oxygen decarburization (AOD) slag, ladle slag (LS), fayalitic slag (FS), burned jarosite slag (Fe slag)), and phosphogypsum (PG) which is a byproduct of fertilizer production as a raw material source for the production of two alternative ye'elimate (CSA) cement clinkers; CSAB (calcium sulfoaluminate belite), and AYF (alite-ye'elimate-ferrite). The chemical composition of ye'elimate clinkers requires less calcium than conventional OPC and allows the use of sulfur- and aluminum-containing raw materials. To allow the use of iron-containing slags, the produced clinkers had a high ferrite phase content. The main concern to use industrial sidestreams as raw materials are the impurities that may affect the clinkering parameters and mineralogy. Detailed microstructural analyses were performed on the clinker to reveal the clinker composition, as well as the partition of the minor elements. The usability of the raw materials for cement manufacture was first tested in laboratory-scale experiments and was then translated to a pilot demonstration in a 7-meter semi-industrial kiln.

It was found through mineralogical analysis that impurities from raw materials affected the produced clinker phases in both clinker types when compared to natural raw materials. CSAB clinker was found to be successful in a pilot demonstration. The raw meal of pilot CSAB was composed of 85% industrial residues, and the CO<sub>2</sub> emissions caused by chemical reactions were 90% lower than that of PC cement made with virgin raw materials. CSAB clinker from pilot demonstration was mixed with anhydrite, sand, and water to make concrete mortars that led to 28-day performance equaling reference PC cement (CEM II/B-M (S-LL) 42,5 N). AYF clinker was successfully produced in laboratory conditions, but the use of fluorine-containing AOD slag was found challenging in a pilot-scale demonstration and requires further experiments.

*Keywords:* clinkering, CSA cement, low-carbon, waste valorization, ye'elimate



## **Isteri, Visa, Teollisuuden sivuvirtoihin perustuvien kalsiumsulfoaluminaattisementtien (CSA) valmistus.**

Oulun yliopiston tutkijakoulu; Oulun yliopisto, Teknillinen tiedekunta

*Acta Univ. Oul. C 880, 2023*

Oulun yliopisto, PL 8000, 90014 Oulun yliopisto

### ***Tiivistelmä***

Sementtiteollisuus aiheuttaa 8 % kaikista ihmisen aiheuttamista CO<sub>2</sub> päästöistä, joista kaksi kolmasosaa (2/3) syntyy kalkkikiven kalsinoinnista (CaCO<sub>3</sub> -> CaO + CO<sub>2</sub>). Samanaikaisesti teollisuus tuottaa maailmanlaajuisesti suuret määrät läjitettäviä epäorgaanisia jättemateriaaleja, joiden sisältämät alkuaineet (Al<sub>2</sub>O<sub>3</sub>, CaO, SiO<sub>2</sub> ja Fe<sub>2</sub>O<sub>3</sub>) sopivat sementin raaka-aineeksi. Paikallisesti näitä materiaaleja voitaisiin hyödyntää sementin valmistuksessa, ne tarjoavat lähteen CO<sub>2</sub> vapaalle kalkille (CaO), joka voisi alentaa sementin valmistuksen CO<sub>2</sub> päästöjä samalla edistää kiertotaloutta. Tiukentuva lainsäädäntö ja verotus läjitettävälle jätteelle on ajava voima yrityksille löytää keinoja hyödyntää ja tuotteistaa jättemateriaaleja.

Väitöskirjatutkimuksessani tutkin ye'elimiitti (kalsiumsulfoaluminaatti eli CSA) pitoisten sementtien valmistusta hyödyntäen metallurgisen teollisuuden kuonia (AOD-kuona, senkkakuona, fayaliittikuona ja pyrometallurgisesti käsitelty jarosiittikuona), sekä fosforilannoitteen valmistuksessa syntyvää fosforikipsiä. Vaihtoehtoiset sementit nimetään yleisesti niissä ilmenevien päämineraalien mukaan. Tässä työssä valmistetut vaihtoehtoiset sementtiklinkkerit ovat CSAB (ye'elimiitti-beliitti) ja AYF (aliitti-ye'elimiitti-ferriitti). Tutkimuksessa kehitettyjen CSA-sementtien perusidea on korvata perinteisen sementin päämineraaleja alhaisemman kalkkipitoisuuden omaavilla mineraaleilla, joka mahdollistaa sulfaatti-, rauta- ja alumiinioksidipitoisten jättemateriaalien monipuolisen käyttämisen raaka-aineena. Työssä valmistetut sementit sisälsivät tavanomaista sementtiä korkeamman pitoisuuden rautapitoista brownmilleriitti (ferriitti) mineraalia, joka mahdollisti rautapitoisten kuonien käytön. Jättemateriaalien sisältämien epäpuhtauksien vaikutusta sementtiklinkkerin mikrorakenteeseen ja muodostuviin mineraaleihin tutkittiin monipuolisesti. Jättemateriaalien käyttöä sementin raaka-aineina tutkittiin aluksi laboratoriomit-takaavassa, jonka jälkeen valmistusta kokeiltiin 7-metrisessä pilottimittakaavan jatkuvatoimisessa sementtiuunissa. Mineralogisissa analyyseissä huomattiin, että jättemateriaalien epäpuhtaudet johtivat muutoksiin valmistettujen sementtiklinkkerien mineralogiassa ja mineraaleissa verratta-essa puhtaista raaka-aineista valmistettuihin verrokkeihin.

CSAB-klinkkerin valmistus onnistui laboratorioissa ja pilottimittakaavassa. Valmistetussa sementtiklinkkerissä parhaimmillaan 85 % raaka-aineista oli korvattu teollisuuden jättemateriaaleilla ja raaka-aineista peräisin olevat CO<sub>2</sub>-päästöt alenivat 90 % verrattuna kalkkikivestä valmistettuun OPC-sementtiklinkkeriin. CSAB-sementtiklinkkeristä, anhydriitistä (CaSO<sub>4</sub>), vedestä ja hiekasta valmistettujen betonikappaleiden 28 päivän lujuusominaisuudet vastasivat kaupallisen OPC-sementin (CEM II/B-M (S-LL) 42,5 N) lujuutta. AYF-sementtiklinkkereitä pystyttiin valmistamaan laboratorio-olosuhteissa, mutta pilottimittakaavassa fluoria sisältävän AOD-kuonan käyttö osoittautui vaikeaksi ja vaatisi lisätutkimusta.

*Asiasanat:* CSA sementti, jätteen hyötykäyttö, klinkkerin valmistus, vähähiilisyys, ye'elimiitti





*The world is a dangerous place to live; not because of the people who are evil, but because of the people who don't do anything about it. Albert Einstein*



## Acknowledgments

This study was carried out in the Process Metallurgy and Fiber and Particle Engineering Research Units at the University of Oulu between 2017 and 2022. The study was funded by the Business Finland CECIRE (1415/31/2015) project, with the following companies: Boliden Harjavalta; Boliden Kokkola; Yara Suomi; Fortum Waste Solutions; and Outokumpu Stainless. The authors appreciate the companies' support with materials and their financial support for the pilot demonstration. In addition, we thank Simo Isokääntä from SSAB Europe Oy for providing ladle slag for the pilot demonstration, and Dr. Martin Radke from IBUtec for setting up the pilot configuration and for technical support during the pilot study.

I would like to thank my principal supervisor, Professor Timo Fabritius, for his valuable guidance and suggestions during my PhD studies. My sincere gratitude goes to my secondary supervisors, Associate Professor Katja Ohenoja and Professor Mirja Illikainen for their immense mentoring, encouragement, and inspiring talks throughout the journey. I especially thank Pekka Tanskanen MSc, who provided me with the subject for the thesis. During my thesis work, it was a pleasure to make a research visit to Sheffield. I would like to thank my supervisors Dr. Theodore Hanein and Dr. Hajime Kinoshita for their wise and beneficial guidance during my stay at the Department of Materials Science and Engineering at the University of Sheffield for the pilot demonstration and their reviewing of the publications. I cannot exaggerate how beneficial the research visit was for my thesis work after I met Theodore, who guided and gave me the most valuable comments for my research and publications and helped me conduct the pilot demonstration.

It is my great pleasure that Dr. Frank Winnefeld and Dr. Mohsen Ben Haha are reviewing my thesis. It is my great honor to have Dr. Alexander Pisch as my opponent. I would like to express my sincere gratitude to my follow-up group members, Associate Professor Eetu-Pekka Heikkinen and Assistant Professor Priyadharshini Perumal, for their valuable suggestions. I am also grateful for the support of Dr. Tuomas Stoor and Riku Mattila MSc in my business and office-related issues.

I would like to acknowledge my co-authors for their assistance with my research and publications during my PhD: Dr. Theodore Hanein, Dr. Hajime Kinoshita, Dr. Holger Kletti, Dr. Christiane Rößler, and Pekka Tanskanen MSc. I would also like to thank the lab technicians from the process metallurgy unit, Mr. Tommi Kokkonen and Mr. Riku Mattila, and from the fiber and particle engineering unit: Mrs. Elisa Wirkkala, Mr. Jarno Karvonen, and Mr. Jani Österlund, for helping

me with lab work. I thank Tun Tun Nyo, Marcin Selent, Markus Riihimäki, Pasi Juntunen, Holger Kletti, and Christiane Rößler for their help with materials characterization. I also wish to thank all the research trainees and students who lent helping hands to my research.

Special thanks go to all my co-workers and colleagues for creating a warm, supportive, and cheerful working environment. It has been a great honor to be a part of both research groups of bright and talented people. My deepest gratitude goes to my friends who helped me through the darkest hours of my PhD by providing company for lunch breaks, travel, games, and free time. I would like to express my loving gratitude to my family, who have always given me the opportunity to chase my dreams.

November 22, Oulu

Visa Isteri

## Abbreviations

AOD	argon oxygen decarburization
AOD_C	CSAB clinker produced from RGC and AOD slag
ABY	alite-belite-ye'elinite
AFm	monosulfate
AFt	ettringite
AYF	alite-ye'elinite-ferrite
CO <sub>2e</sub>	equivalent CO <sub>2</sub> emissions
CSA	calcium sulfoaluminate
BAY	belite-alite-ye'elinite
BOF	basic oxygen furnace
BSE	back-scattered electron detector
CSA	calcium sulfoaluminate/ye'elinite
CSAB	calcium sulfoaluminate-belite
CSABF	calcium sulfoaluminate-belite-ferrite
Fay_C	CSAB clinker produced from RGC and fayalitic slag
Fe_C	CSAB clinker produced from RGC and Fe slag/BJA
EAF	electric arc furnace
EDX	energy-dispersive X-ray spectroscopy
ICDD	the International Centre for Diffraction Data
ICP-OES	inductively coupled plasma atomic emission spectroscopy
FESEM	field emission scanning electron microscope/microscopy
OPC	Ordinary Portland cement
PC	Portland cement
PDF	powder diffraction file
PG	phosphogypsum
PSD	particle size distribution
R <sub>wp</sub>	weighted profile R-factor
LOI	loss on ignition
LS	ladle slag
RGC	reagent grade chemicals
RC_C	CSAB clinker produced from reagent grade chemicals
SCM's	supplementary cementitious materials
TGA	thermal gravimetric analysis
WPPF	Whole powder pattern fit
XRD	X-ray diffraction

XRF	X-ray fluorescence
	Greek symbols
$\beta$ -C <sub>2</sub> S	larnite
$\gamma$ -C <sub>2</sub> S	calcio-olivine

Standard cement chemistry notations were used; hence, C denotes CaO, A is Al<sub>2</sub>O<sub>3</sub>, S is SiO<sub>2</sub>, F is Fe<sub>2</sub>O<sub>3</sub>, \$ is SO<sub>4</sub>, M is MgO, and H is H<sub>2</sub>O.

## Original publications

This thesis is based on the following publications, which are referred to throughout the text by their Roman numerals:

- I Isteri, V., Ohenoja, K., Hanein, T., Kinoshita, H., Tanskanen, P., Illikainen, M., Fabritius, T. (2020). Production and properties of ferrite-rich CSAB cement from metallurgical industry residues, *Science of the Total Environment*, 712, 136208. <https://doi.org/10.1016/j.scitotenv.2019.136208>.
- II Isteri, V., Ohenoja, K., Hanein, T., Kinoshita, H., Tanskanen, P., Illikainen, M., Fabritius, T. (2021). The Effect of Fluoride and Iron Content on the Clinkering of Alite-Ye'elimite-Ferrite (AYF) Cement Systems, *Frontiers in Built Environment*, 7, 89. <https://doi.org/10.3389/fbuil.2021.698830>.
- III Isteri, V., Ohenoja, K., Hanein, T., Kinoshita, H., Kletti, H., Rößler, C., Tanskanen, P., Illikainen, M., Fabritius, T. (2022). Ferritic calcium sulfoaluminate belite cement from metallurgical industry residues and phosphogypsum: Clinker production, scale-up, and microstructural characterization. *Cement and Concrete Research*, 154, 106715. <https://doi.org/10.1016/j.cemconres.2022.106715>.
- IV Isteri, V., Ohenoja, K., Hanein, T., Kinoshita, H., Kletti, H., Rößler, C., Tanskanen, P., Illikainen, M., Fabritius, T. (manuscript). The effect of slag variability and the fate of minor elements in the attempted manufacture of AYF (alite-ye'elimite-ferrite) cement clinker at both laboratory and pilot scale.

The author of this thesis was the first author of the above publications. The author was mainly responsible for designing and conducting the experiments, analyzing and reporting the data with the guidance of the supervisors (Katja Ohenoja, Theodore Hanein, and Pekka Tanskanen). The co-authors (Hajime Kinoshita, Katja Ohenoja, Theodore Hanein, Pekka Tanskanen, Mirja Illikainen, and Timo Fabritius) provided valuable help with editing and proofreading the manuscripts, comments, and corrections.

Holger Kletti and Cristiane Rößler provided part of the mineralogical characterization experiments (XRF, XRD and EDX) for Papers III & IV. The author was responsible for the design and reporting of these experiments.





# Contents

<b>Abstract</b>	
<b>Tiivistelmä</b>	
<b>Acknowledgments</b>	<b>9</b>
<b>Abbreviations</b>	<b>11</b>
<b>Original publications</b>	<b>13</b>
<b>Contents</b>	<b>15</b>
<b>1 Introduction</b>	<b>17</b>
1.1 Background .....	17
1.2 Approach and aims of the thesis .....	18
1.3 Outline of the thesis .....	20
<b>2 Literature review</b>	<b>21</b>
2.1 Portland cement (PC), calcium sulfoaluminate cement (CSA) and alite-ye'elinite-ferrite cement (AYF) .....	21
2.1.1 Portland cement (PC) .....	22
2.1.2 Calcium sulfoaluminate cement (CSA) .....	23
2.1.3 Alite-ye'elinite-ferrite cement (AYF) .....	25
2.2 Mineralogy of clinkers .....	25
2.3 Production of CSA & AYF .....	28
2.3.1 Calcium sulfoaluminate cement (CSA) .....	28
2.3.2 Alite-ye'elinite-ferrite cement (AYF) .....	29
2.4 Hydration of CSA and AYF .....	29
2.5 Sidestream materials: Metallurgical slags and phosphogypsum .....	30
2.5.1 AOD slag .....	31
2.5.2 Ladle slag (LS) .....	32
2.5.3 Burned jarosite slag (BJA) – Fe slag .....	32
2.5.4 Fayalitic slag .....	33
2.5.5 Phosphogypsum (PG) .....	33
2.6 Utilization of metallurgical slags as raw materials for CSA-based cements and other applications .....	33
2.7 Applications of CSA-based concretes .....	35
<b>3 Materials and Methods</b>	<b>37</b>
3.1 Materials .....	37
3.1.1 Reagent-grade chemicals (RGC) .....	37
3.1.2 Industrial sidestreams .....	38
3.1.3 Aggregates and cements .....	40

3.2	Methods.....	41
3.2.1	Pretreatment and characterization of materials.....	41
3.2.2	Design of the clinker recipes .....	46
3.2.3	Production of clinkers in laboratory .....	47
3.2.4	Production of clinkers in pilot kiln .....	51
3.2.5	Preparation of samples for hydration studies: Workability, setting time and compressive strength.....	54
<b>4</b>	<b>Results and discussion</b>	<b>57</b>
4.1	Laboratory-scale CSAB clinker production .....	57
4.1.1	Mineralogy .....	58
4.1.2	Chemical composition .....	60
4.1.3	Effect of impurities .....	61
4.2	CSAB(F) clinker production in pilot demonstration.....	62
4.2.1	Granules.....	62
4.2.2	Ground and mixed clinker .....	65
4.2.3	Chemical composition of clinker.....	65
4.2.4	Mineralogy of clinker .....	66
4.2.5	Effect of minor elements on phases.....	70
4.3	AYF clinker production in laboratory scale .....	72
4.3.1	Effect of industrial byproducts .....	75
4.4	AYF clinker production in pilot demonstration.....	77
4.4.1	Chemical composition of granules and clinker.....	79
4.4.2	Ground and mixed clinker .....	82
4.4.3	Mineralogy .....	82
4.5	Hydration of cement pastes and mortars .....	88
4.5.1	CSAB.....	88
4.5.2	CSAB(F).....	90
4.5.3	AYF .....	91
4.6	Brief sustainability assessment.....	92
<b>5</b>	<b>Summary and concluding remarks</b>	<b>95</b>
	<b>References</b>	<b>99</b>
	<b>Appendices</b>	<b>119</b>
	<b>Original publications</b>	<b>133</b>

# 1 Introduction

## 1.1 Background

Concrete is the fundamental building material that consists of three basic components: binder (cement clinker and gypsum), aggregate (e.g., sand), and reactant (e.g., water). The manufacture of Portland cement (PC) is responsible for 6–9% of global man-made CO<sub>2</sub> [1], [2]. Over half of emissions are associated with the burning of natural limestone (CaCO<sub>3</sub>), where almost half of the mass of limestone is released as CO<sub>2</sub> [2], [3]. Meanwhile, huge volumes of industrial sidestream materials suitable for raw materials cement manufacture are landfilled. The world is seeking a solution to reduce CO<sub>2</sub> emissions from anthropogenic activities, but the demand of concrete is continuing to increase, especially in the developing world. This compels the cement industry to find new methods to reduce the CO<sub>2</sub> burden of manufacturing. The most relevant mitigation strategies to cut CO<sub>2</sub> emissions of cement manufacture are the use of supplementary cementitious materials (SCMs), the efficient use of PC, and the development of alternative cements [2]. A recently widely studied alternative cement type is calcium sulfoaluminate cements (CSA). CSA cements have been commercially used in China and the USA for decades with the names “third cement series” [4] and BCSA [5]. In Europe, the use of CSA has developed slowly because of a lack of standardization, but some manufacturers today have received technical approval for CSA applications [6]. The common applications for CSA cements have been pre-cast concrete (e.g., slabs, pipes, and beams), cold concreting, roads, bridges, airports, and fast repairs [4], [5]. The PC-CSA-calcium sulfate ternary systems has been commonly used in fast setting dry-mix mortars such as tile adhesives, self-levelling floors [3].

CSA can be produced at a ~200 °C lower production temperature and with less calcium than conventional PC. This means the net CO<sub>2</sub> emissions of CSA cement manufacture are around 25–35% lower than of PC [7]. The lower calcium content than with PC can be achieved by replacing most calcium-bearing phase alite (C<sub>3</sub>S) with less calcium-containing cementitious phases such as ye’elimite (C<sub>4</sub>A<sub>3</sub>S), belite (C<sub>2</sub>S), and ferrite (C<sub>2</sub>(A,F)). The main hydration product of CSA clinker mixed with gypsum/anhydrite is ettringite (AFt), which produces rapid strength gain, high durability, and sulfate resistance superior to PC [8], [9]. Ettringite can be beneficial

when industrial raw materials are used because it has high potential for capsule and stabilizes hazardous elements, promoting environmental safety [10], [11].

PC cement is superior because of the availability of the globally cheap raw materials limestone and clays. To make alternative cements more affordable locally, it is investigated if industrial sidestream materials can be used as raw materials. In this thesis, limestone and other virgin raw materials are replaced by metallurgical slags and phosphogypsum to produce CSA (calcium sulfoaluminate) and AYW (alite-ye'elinite-ferrite) clinkers. To increase the yield of iron-rich slags, the produced cement clinkers had higher ferrite phase content than typical cements. The Finnish industrial sidestreams used were: argon oxygen decarburization (AOD) slag resulting from the steel refining process at Outokumpu Stainless Oy (Tornio), ladle slag originating in the secondary metallurgical ladle treatment process of SSAB (Raahe, Finland), fayalitic slag from the nickel flash furnace process at Boliden Harjavalta, Fe slag from the pyrometallurgically treated jarosite at Kokkola Boliden, and phosphogypsum from phosphoric acid production at Yara (Siilinjärvi, Finland).

## **1.2 Approach and aims of the thesis**

This thesis focused on finding a way to utilize Finnish metallurgical slags and phosphogypsum as raw materials to introduce two types of alternative cement clinkers, CSAB and AYW, which could further be utilized as low-CO<sub>2</sub> cement binders as alternatives to conventional PC. The overview of the thesis and the journal papers included in the study are presented in Fig. 1. The aims of each journal paper are also listed below.

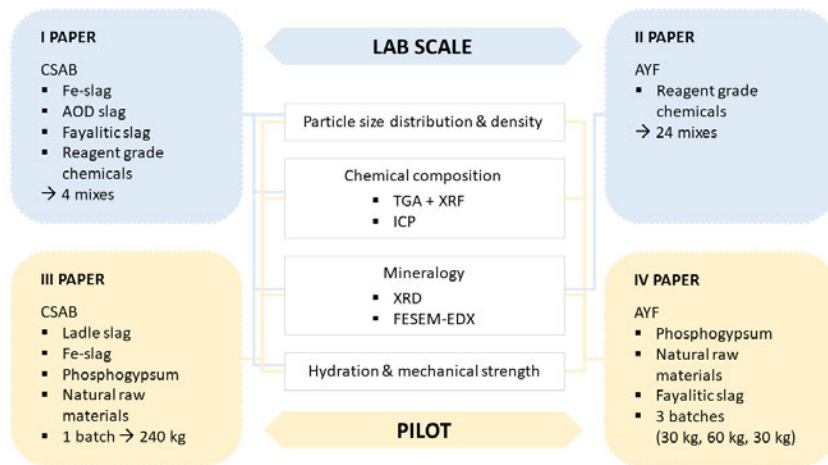


**Fig. 1. Overview of the thesis.**

1. The aim of Paper I was to utilize as much of each raw material, which were Finnish metallurgical slags: AOD (argon oxygen decarburization) slag from stainless-steel production, Fe slag from zinc production, and fayalitic slag from nickel production. The production of CSAB clinker was investigated at a laboratory scale, and the aim was to find if the impurities from industrial sidestreams affected the final chemical and phase composition.
2. The aim Paper II was to find the optimal fluoride content and raw mix for alite-ye'elinite-ferrite (AYF) clinkers. A total of 24 raw mixes was produced at a laboratory scale, and the goal was to find the effect of iron, sulfur, and fluoride on mineralogy by changing the target phase compositions.
3. The aim of Paper III was to translate production of CSAB with high ferrite content from a lab-scale to a pilot demonstration in a 7-meter kiln. The aim was to produce clinker in which limestone was replaced with carbon-free calcium originating in industrial sidestream materials (ladle slag, Fe slag, and phosphogypsum). The goal of the microstructural analyses was to reveal the clinker composition and the partition of the minor elements originating in the industrial sidestreams.
4. The aim of Paper IV was to produce AYF (alite-ye'elinite-ferrite) clinker by using fluorine-bearing AOD slag as a fluorine source to work as a mineralizer to produce alite instead of  $\text{CaF}_2$ , which was previously successfully used in

Paper II. The aim of the study was first to produce AYF clinker in laboratory conditions using industrial sidestream materials (AOD slag, ladle slag, fayalitic slag, and phosphogypsum) and then to scale to a pilot demonstration in a 7-meter kiln. In a pilot demonstration, three clinkers with different amounts of AOD slag were produced (Paper IV). *(Manuscript was submitted to Cement and Concrete Research and is under review)*

### **1.3 Outline of the thesis**

This thesis is divided into five chapters. Chapter 1 serves as an introduction to the topic. Chapter 2 provides an overview of raw materials used in this study and the state-of-the-art of CSA type cements. The materials and methods used in this study are presented in Chapter 3, while Chapter 4 contains the key results and a discussion. Conclusions regarding the main findings of the thesis are drawn in Chapter 5.

## 2 Literature review

### 2.1 Portland cement (PC), calcium sulfoaluminate cement (CSA) and alite-ye'elimite-ferrite cement (AYF)

In this study, the focus was on CSA (Papers I & III) and AYF (Papers II & IV) cements. The different cement types consist of different chemical compositions, listed in Table 1, and the cement types are described in more detail in this chapter's subsections. CSA and AYF clinkers differ from PC, with higher  $\text{Al}_2\text{O}_3$  and  $\text{SO}_3$  content, because of the existence of the ye'elimite phase. BYF (belite-ye'elimite-ferrite) belongs to a subgroup of the CSA cement type. BYF is commercially produced belitic clinker, in which belite ( $\text{C}_2\text{S}$ ) content is dominant over ye'elimite ( $\text{C}_4\text{A}_3\text{S}$ ) [12].

**Table 1. Typical compositional ranges of PC, CSA, and AYF clinkers. Values for PC and CSA adapted from [12], and for AYF types from [13]–[17].**

Oxide	PC (%)	CSA types (%)	AYF types (%)
CaO	55–75	35–45	50–60
SiO <sub>2</sub>	15–25	5–10	10–25
Al <sub>2</sub> O <sub>3</sub>	2–6	25–35	10–25
Fe <sub>2</sub> O <sub>3</sub>	0–6	0–9	2–12
SO <sub>3</sub>	0.3–1.5	6–30	2–7

The composition ranges of mineralogical phase assemblages are presented in Table 2. PC and CSA are commercially produced, but AYF is a novel cement type that has recently been studied, and its potential is still under research. The variations of CSA cements can be classified according to the main crystalline phases of the clinkers of which they consist [18]. The BYF type covers CSAB and CSABF produced in this thesis study. Alite is the dominant phase of PC and AYF types. Belite is dominant in BYF along with ye'elimite. In CSA, the ye'elimite type of clinker content is highest of those listed and is alternated according to impurities from raw materials and the designed application. Free lime is only added to CSA cements as additive to improve expansion if it is required by the application [19].

**Table 2. Comparison of typical compositional ranges of the mineralogical phase assemblages of PC, CSA, and AYF clinkers. Values for PC and CSA adapted from [12]. AYF types adapted from [13]–[17].**

Phase	PC (%)	CSA (%)	AYF (%)
Clinker phases			
C <sub>3</sub> S (alite)	55–75	0–5	30–50
C <sub>2</sub> S (Belite)	10–20	0–55	0–30
C <sub>3</sub> A, CA, C <sub>12</sub> A <sub>7</sub> , CA <sub>2</sub> (aluminates)	5–10	0–20	0–7
C <sub>4</sub> AF (ferrites)	5–10	0–30	5–45
C <sub>4</sub> A <sub>3</sub> \$ (ye'elimite)		45–75	7–45
The additives to produce cement			
C\$ · xH (calcium sulfates)	3–6	0–30	0–30
C\$ & CH (free lime & portlandite)	0–2	0–25	0–2

### 2.1.1 Portland cement (PC)

Concrete produced from conventional cement—ordinary Portland cement OPC—is the most produced and versatile construction material. Modern PC was developed in the 18<sup>th</sup> century and has undergone only minor modifications for the past two centuries [3]. PC is produced from abundant raw materials like limestone, clays, and shale, which are cheaply and widely available throughout the world.

PC is produced in a continuous rotary kiln, where an intermediately ground raw mix of limestone and clay is calcined (heat-treated) at around 1450 °C. The product of heat treatment is called clinker. It is ground to a fine powder and mixed with 3–5 wt.% gypsum [2] to form PC cement. More than half of CO<sub>2</sub> emissions are from the breaking of CaCO<sub>3</sub> (56% CaO and 44% CO<sub>2</sub>), and the rest are from the combustion of fossil fuels to heat the kiln. The total CO<sub>2</sub> emissions per tonne of clinker are around 840 kg CO<sub>2</sub> [2]. With the total annual production of 4 Gt cement, the total emissions of cement manufacture are 3 Gt of CO<sub>2</sub>, which is around 8% of global human-made CO<sub>2</sub> emissions [2], [20].

The proportion of the main mineral of PC alite (C<sub>3</sub>S) is determined with the lime saturation factor ( $LSF = 100 \cdot CaO / (2.8 \cdot SiO_2 + 1.18 \cdot Al_2O_3 + 0.65 \cdot Fe_2O_3)$ ). LSF 100% indicates the maximum alite content in the clinker. The typical LSF values are between 94 and 98%. The major phases of PC in the order of appearance are tricalcium silicate (alite; Ca<sub>3</sub>SiO<sub>5</sub>; C<sub>3</sub>S), dicalcium silicate (belite; Ca<sub>2</sub>SiO<sub>4</sub>; C<sub>2</sub>S), tricalcium aluminate (Ca<sub>3</sub>Al<sub>2</sub>O<sub>6</sub>; C<sub>3</sub>A), calcium aluminoferrite (Ca<sub>4</sub>Al<sub>2</sub>Fe<sub>2</sub>O<sub>10</sub>; C<sub>4</sub>AF), and gypsum (CaSO<sub>4</sub>·2H<sub>2</sub>O; CSH<sub>2</sub>) [3]. When PC cement is mixed with water and possible additives to improve the properties, the main hydration product



of  $C_3S$  and  $C_2S$  is calcium silicate hydrate C-S-H, which is responsible for the mechanical strength of the PC concrete. The hydration speed of  $C_2S$  is slower than  $C_3S$ , and it is therefore usually referred to as increasing the long-term strength of concrete. Alumina and iron-containing phases  $C_3A$  and  $C_4AF$  react with gypsum and hydrate to ettringite ( $Ca_6Al_2(SO_4)_3(OH)_{12} \cdot 26H_2O$ ;  $C_6AS_3H_{32}$ ). The hydration speed of  $C_3A$  is faster than  $C_4AF$  [21].

### **2.1.2 Calcium sulfoaluminate cement (CSA)**

Calcium sulfoaluminate cements and clinkers (CSA) were discovered by Alexander Klein in the late 1950s [22]. CSA cement was used to compensate for shrinkage in PC concrete [22]. CSA cement was patented in the USA as ASTM K cement, which is specified as ASTM C845-04 [23]. In China, CSA-based concrete was used under the name third cement series for cold concreting pre-cast concrete for structural and non-structural applications [4]. Sulfoaluminate (SAC) and ferroaluminate cements (FAC) are standardized in China in the Chinese GB 20472-2006 [24] cement standard. In the USA, BCSA (Belite- Calcium sulfoaluminate) has been successfully used in high volumes for 30 years for applications which need a rapid setting time, such as the restoration of a highway or an airfield pavement [5]. The fast reaction kinetics and high early-stage heat of hydration of CSA cements benefits in cold weather applications [25], [26]. In Europe, the use of CSA-based concrete has thus far been limited because of the lack of standardization. There have been some positive developments recently: In 2020, CSA cements obtained technical approval in Germany [27]. In Europe, a few industrial-scale producers of CSA cements exist.

The typical cement phases of CSA are ye'elimite ( $C_4A_3S$ ), belite ( $C_2S$ ), brownmillerite/ferrite  $C_4AF$ , and anhydrite (CS). There are numerous variations of CSA cements, and they are usually named after the quantity of each phase existing in the clinker i.e., high-belite-containing CSA is BCSA, and one with ye'elimite as the dominant phase with belite and a notable amount of ferrite phase can be called CSABF. CSA is typically used as a blend with PC, where it offers a control for setting time, high early-strength, and compensates for shrinkage [4], [9]. CSA concrete has good sulfate [9], [28], sodium chloride, seawater [9], [28], and carbonation resistance [9], [28]. The workability of CSA is comparable to PC, and the setting time can be controlled using retarders [4]. The high early heat of hydration of CSA cements allows its use in cold weather applications [29]–[31]. The superior properties of CSA cement compared to PC cement are achieved due to the main hydration

product ettringite ( $\text{Ca}_6\text{Al}_2(\text{SO}_4)_3(\text{OH})_{12}\cdot 26\text{H}_2\text{O}$ ) [4], [9]. The formation of ettringite (AFt) from ye'elimitite requires the addition of calcium sulfate and water according to the equation  $\text{C}_4\text{A}_3\text{S} + 2\text{C}_2\text{S} + 34\text{H} \rightarrow \text{C}_3\text{A} \cdot 3\text{C}_2\text{S} \cdot 32\text{H} + 2\text{AH}_3$ . Monosulfate (AFm) forms together with AFt especially in the early stages of hydration. The content and ratio of AFt and AFm are dependent of calcium sulfate available [32]. With an insufficient amount of calcium sulfate, the hydration product of ye'elimitite is AFm besides with  $\text{AH}_3$  [33], [34]. In addition, intermediate microcrystalline phases ( $\text{CaH}_{10}$  etc.) may precipitate from C-A-H gel [3], [6].

In CSA cements, the  $\text{CO}_2$  emissions are reduced by modifying the phase composition of PC towards minerals that require less limestone and can be produced with reduced energy. Table 3 shows  $\text{CO}_2$  emissions associated with each cement phase. Alite ( $\text{C}_3\text{S}$ ) is the most lime-dominant phase, requiring a production temperature of 1450 °C, around 200 °C higher than the production temperature for CSA cement phases (belite, ye'elimitite, and ferrite) [35]. When alite (and  $\text{C}_3\text{A}$ ) is substituted with ye'elimitite ( $\text{C}_4\text{A}_3\text{S}$ ) and belite ( $\text{C}_2\text{S}$ ), the  $\text{CO}_2$  emissions associated with the calcination of limestone can be drastically reduced. It is estimated that the production of CSA can reduce overall net emissions by 25–35% compared to PC [7]. Emissions can be further reduced by replacing limestone with calcium-bearing byproducts that have been decarbonized in the original process.

**Table 3.  $\text{CO}_2$  emissions of cement phases per tonne when produced from  $\text{CaCO}_3$  [18].**

Phase	CaO	$\text{CaCO}_3$	t $\text{CO}_2$ /t of phase
$\text{C}_3\text{S}$	73.7	131.5	0.58
$\text{C}_2\text{S}$	65.1	116.2	0.51
$\text{C}_3\text{A}$	62.2	111.0	0.49
$\text{C}_4\text{AF}$	46.2	82.5	0.36
$\text{C}_4\text{A}_3\text{S}^1$	36.7	49.1	0.22

<sup>1</sup> Ye'elimitite  $3\text{CaCO}_3 + 3\text{Al}_2\text{O}_3 + \text{CaSO}_4 \rightarrow \text{Ca}_4\text{Al}_6\text{O}_{12}\text{SO}_4 + 3\text{CO}_2$

Natural raw materials for cement production, namely limestone, clays and silicon oxides, are cheaply available throughout the world. The disadvantage of CSA cements is the required alumina, which comes with a much higher price and is scarce. The cost of CSA cement limits the use of CSA cements to special applications in which rapid setting, cold concreting properties, or shrinkage control are needed. The access to alumina can be locally overcome by using aluminum containing waste materials, which also leads to increasing industrial sustainability through the circularity of resources.

### 2.1.3 Alite-ye'elimate-ferrite cement (AYF)

The second alternative cement clinker studied in this study (Papers II & IV) is a novel yet to be commercially produced Alite-ye'elimate-ferrite cement (AYF), in which alite is produced at 1250 °C instead of the typical 1450 °C [3]. AYF cement is designed to be an alternative/modified PC that combines the favorable properties of PC and CSA cements. In AYF, all the tricalcium aluminate ( $C_3A$ ) is replaced with ye'elimate ( $C_4A_3S$ ), and the ferrite ( $C_4AF$ ) content is increased; thus, as shown in Table 1 the CaO content of raw meal decreases and less  $CO_2$ -bearing limestone is required for production. The production of AYF requires the use of mineralizers, i.e., fluoride, which decreases the formation temperature of the alite phase. AYF is therefore an interesting option for opening new ways to use fluoride-containing industrial waste materials such as argon oxygen decarburization (AOD) slags for cement production. The production of AYF clinker requires precise adjustments to chemical composition and dopants [13], [14]. There are several studies on AYF clinker production from industrial byproducts. Bauxite residue was successfully used to produce AYF clinkers at 1250–1275 °C, with a ferrite ( $C_4AF$ ) phase content between 5 and 45% [13]. The production of the alite-ye'elimate type of clinker has also been studied, using different raw materials and target phase compositions. The produced clinkers were successfully synthesized and are listed with references according to the type of clinker: AYF (alite-ye'elimate-ferrite) [16]; ABY (alite-belite-ye'elimate)[14]; and BAY (belite-alite-ye'elimate) [17].

## 2.2 Mineralogy of clinkers

### *Alite $Ca_3SiO_5$*

Alite ( $C_3S$ ) is an impure form of tricalcium silicate ( $C_3S$ ). Alite is the most abundant phase of PC clinker. Alite is already thermodynamically stable above 1200–1250 °C [3], [36] but in the PC system, the production temperature in the cement kiln needs to be above 1350 °C to prevent free lime and assure constant cement quality [37]. The production temperature of alite in a pure system without impurities needs to be much higher because of the absence of the melt formers iron and alumina.

Alite has a total of seven polymorphs with very similar structures: R (rhombohedral) >1100 °C; Monoclinic 1060 °C  $M_{III}$ ; 1050 °C  $M_{II}$ ; 990 °C  $M_I$  and triclinic 980 °C  $T_{III}$ ; 920 °C  $T_{II}$ ; 600 °C  $T_I$ . The most common polymorphs of alite

found in industrially produced PC are  $M_I - M_{III}$  due to the quenching and stabilizing effect of impurities such as Mg, Al, Fe, S, P, and Mn [3], [36], [38]. A low Mg content is reported to stabilize  $T_{III}$  type, but higher Mg content favors  $M_{III}$  [38].

Fluorine (F) has a strong mineralizing effect on alite that is beneficial for reducing the production temperature of alite-based cement clinkers, which reduces energy consumption. In a pure CaO – SiO<sub>2</sub> 3:1 solid solution with the addition of Al and F, the thermodynamical stability of high temperature form (rhombohedral) of alite (Ca<sub>3</sub>Si<sub>1-x</sub>Al<sub>x</sub>O<sub>5-x</sub>F<sub>x</sub>) can be decreased from 1250°C (X = 0) to 1050°C (X = 0.15) [39]. The mineralization effect in the solid state in the presence of F and Al is based on a coupled substitution of F<sup>-</sup> for O<sup>2-</sup> and Al<sup>3+</sup> for Si<sup>4+</sup> [39], [40]. Melt formation makes fluorine addition inefficient because fluorine is portioned to melt and solid phases but prefers melt [39]. Other suggested dopants that can be used as a mineralizer/fluxing agent to decrease the formation temperature (lower free energy) of alite are B, Na, Zn, Mg, and Cu [14], [41]–[44].

### *Belite Ca<sub>2</sub>SiO<sub>4</sub>*

Dicalcium silicate (C<sub>2</sub>S) is referred to in cements as belite. Belite also exists in slags and refractories. C<sub>2</sub>S has various polymorphs,  $\alpha$ ,  $\alpha'$ ,  $\alpha'_H$ ,  $\alpha'_L$ ,  $\beta$ , and  $\gamma$ , which depend on the formation temperature and substituting elements [3], [18]. When cooled from elevated temperatures,  $\alpha$  polymorph passes through  $\alpha'$ ,  $\alpha'_H$ ,  $\alpha'_L$ , and  $\beta$ -form is stable from 630 °C [3], with insufficient quenching and a lack of stabilizing elements of almost non-hydraulic  $\gamma$ -C<sub>2</sub>S. The formation of  $\gamma$ -C<sub>2</sub>S causes volume expansion, which leads to dusting [45]. In cements, C<sub>2</sub>S exists most of the time as  $\beta$ -C<sub>2</sub>S, which has weaker hydration properties than C<sub>3</sub>S but is still very important for late strength formation.

Many studies address the chemical stabilization of  $\beta$ -C<sub>2</sub>S by foreign ions such as S [46]–[48], P [46], [48], [49], B [48]–[50], Cr [46], [48], [49], K [51], Na [52], and Mn [48]. The most common method to stabilize  $\beta$ -C<sub>2</sub>S that is adapted to an industrial scale is to use borax Na<sub>2</sub>[B<sub>4</sub>O<sub>5</sub>(OH)<sub>4</sub>]·8H<sub>2</sub>O [53], [54]. In CSA cement systems, the addition of borax allows the stabilization of high temperature polymorphs ( $\alpha'$ ) at the lower synthesis temperatures. The method has been patented [55]. The motivation to stabilize high temperature forms of belite ( $\alpha$ ,  $\alpha'$ ,  $\alpha'_H$ ,  $\alpha'_L$ ) is the better hydration activity compared to  $\beta$ -form [18].

### *Ye'elimite $\text{Ca}_4\text{Al}_6\text{O}_{12}\text{SO}_4$*

Calcium sulfoaluminate – ye'elimite belongs to the sodalite family, in which sodium is substituted with calcium. Stoichiometric ye'elimite has an orthorhombic structure at room temperature, but foreign ions can stabilize the cubic/pseudo-cubic polymorph [56]–[58]. In a pure system, the cubic/pseudo-cubic form is stable above 800 °C [59]. The structure of ye'elimite is  $\text{M}_4[\text{T}_6\text{O}_{12}]\text{X}$ , where M presents low-charge cations (e.g.,  $\text{Na}^+$ ,  $\text{Ca}^{2+}$ , or  $\text{Sr}_2^+$ ), X is an anion ( $\text{Cl}^-$ ,  $\text{SO}_4^{2-}$ ,  $\text{WO}_4^{2-}$  and  $\text{CrO}_4^{2-}$ ), and T represents  $\text{Si}^{4+}$  or  $\text{Al}^{3+}$ , which occupy tetrahedral sites [58], [60]. It is reported that iron ( $\text{Fe}^{3+}$ ) can substitute alumina in the ye'elimite structure (T), which leads to the stabilization of pseudo-cubic ye'elimite [57].

There is still some controversy in the literature if the hydration of ye'elimite is enhanced or reduced by the iron substitution or is the major cause the polymorphism of ye'elimite or the presence of minor phases such as mayenite. The iron doped cubic polymorph of ye'elimite is considered to have faster hydration kinetics but the other factors such as presence of minor phases may affect the results [12], [57]. The production temperature of the ye'elimite type of cements is restricted to around 1300 °C, at which ye'elimite decomposes in normal processing conditions [61].

### *Ferrite/brownmillerite ( $\text{C}_4\text{AF}$ )*

Iron is needed in cement manufacture to enhance burnability [62]–[64]. Iron can originate in raw materials or can be added if necessary [20]. According to Bogue equations, each gram of iron produces three grams of stoichiometric  $\text{C}_4\text{AF}$  [65]. Bogue calculation is a method for approximating proportions of four major phases of OPC cement through chemical compositions. Ferrite (calcium aluminoferrite) can be present in cement clinker as multiple solid solutions from the series ( $\text{C}_2\text{F} - \text{C}_6\text{A}_2\text{F}$ ). The most common mineral end-members existing in cement clinkers are brownmillerite ( $\text{C}_4\text{AF}$ ) and srebrodolskite ( $\text{C}_2\text{F}$ ) [66].

The continuous solid solution of ferrite series ( $\text{C}_2\text{F} - \text{C}_6\text{A}_2\text{F}$ ) can be defined by the value of x in the formula  $\text{Ca}_2(\text{Fe}_{1-x}\text{Al}_x)_2\text{O}_5$ , where  $0.0 < x < 0.7$  [66]. Fe can be substituted for Ti to a certain limit before the ferrite starts to transform towards a perovskite structure [67], [68]. Zn, Si, Mg, Mn, Na, and S are also known to incorporate into the ferrite phase [69]–[73]. In CSA mixes, some of the iron can also be substituted for ye'elimite, which decreases the available iron to form ferrite [57], [74].

## *Most notable minor phases in PC, CSA, and AYW clinkers*

Periclase (MgO) crystallizes from the liquid during the firing process if the excess MgO cannot be incorporated into the clinker phases of alite, belite intermediate phases, and glass/amorphous and ferrite phases [70], [75]. The formation of excess periclase should be avoided due to the hydration of periclase to brucite  $\text{Mg}(\text{OH})_2$ , which causes expansion in the cement matrix and is harmful for cement properties [3], [76]. Standards limit the allowed amount of MgO in PC cement to a maximum of 3–6% [3], [42], [77].

Mayenite ( $\text{C}_{12}\text{A}_7$ ) is a common minor phase in CSA cements. The common formula of mayenite is  $\text{Ca}_{12}\text{Al}_{14}\text{O}_{32-x}(\text{OH})_{3x}[\text{W}_{6-3x}]$ , where  $X = 0-2$ , W can be occupied with anions  $\text{OH}^-$ ,  $\text{F}^-$ , and  $\text{Cl}^-$  and  $\text{Al}^{3+}$  can be replaced with  $\text{Fe}^{3+}$  and  $\text{Si}^{4+}$  [78], [79]. Without retarders such as citric acid [80]–[83], the presence of mayenite leads to the flash setting of the cement [3], [84]. Depending on the grade of the calcium sulfate addition, the hydration product of mayenite is ettringite or monosulfate [82]. Other common calcium aluminates in PC and CSA cements are tricalcium aluminate ( $\text{C}_3\text{A}$ ), krotite (CA), and grossite ( $\text{CA}_2$ ). The hydration reactivity of these phases can be present in the order  $\text{C}_3\text{A} < \text{C}_{12}\text{A}_7 < \text{CA} < \text{CA}_2$  [12].

Fluorellestadite ( $3\text{C}_2\text{S} \cdot 3\text{CS} \cdot \text{CaF}_2$  or  $\text{Ca}_{10}(\text{SiO}_4)_3(\text{SO}_4)_3\text{F}_2$ ), with an apatite structure, may form in clinkers when fluorine is present with sulfur [44]. During the clinkering of PC and CSA, fluorellestadite decomposes above 1250 °C to  $\text{C}_2\text{S}$  (s),  $\text{SO}_2$  (g),  $\text{O}_2$  (g), and the liquid phase and can thereby be avoided by controlling the temperature and cooling [16], [85]–[87]. Fluorellestadite has poor hydraulic properties and should be avoided in clinker [3], [6].

Gehlenite ( $\text{C}_2\text{AS}$ ) is the alumina-rich end-member in melilite solid solution series, in which the other end-member is åkermanite ( $\text{C}_2\text{MS}$ ). Gehlenite is undesired because of the poor/non-hydraulic phase [6]. The formation of gehlenite can be prevented by adjusting the lime content of the raw mix (ternary system  $\text{CaO}-\text{Al}_2\text{O}_3-\text{SiO}_2$ ) [3]. Part of Paper III studied whether gehlenite formation could be prevented in CSA cements by controlling the lime content in the raw mix.

## **2.3 Production of CSA & AYW**

### **2.3.1 Calcium sulfoaluminate cement (CSA)**

The major benefits of CSA compared to conventional PC are a 200 °C lower production temperature and lower  $\text{CO}_2$  emissions due to less limestone ( $\text{CaCO}_3$ ) in

the raw mix. CSA clinker can be produced from natural raw materials such as limestone, bauxite/clay, and gypsum in a conventional rotary cement kiln without major modifications to the configuration. However, because of the narrow production temperature of ye'elimite between 1200 and 1300 °C [61], [88]–[90], the kiln facilities should have good control of the process temperature, atmospheric conditions (oxidizing), residence time, and quality control of the clinker phases [6].

The production temperature of CSA clinker is highly dependent on the chemical composition of the clinker and impurities from the raw materials. One way to further decrease CO<sub>2</sub> emissions is to use alternative fuels for kiln burners. Elemental sulfur can be successfully used as both a fuel and source of SO<sub>3</sub> for CSA cement production to replace natural gas [91].

### **2.3.2 Alite–ye'elimite–ferrite cement (AYF)**

The production procedure and raw materials of alite-ye'elimite clinkers is very similar to those for CSA clinkers. Novel AYF and BAY clinkers can be produced at a temperature range between 1250 and 1300 °C [14]–[16]. The coexistence of ye'elimite and alite is challenging because of their different thermal stability ranges. The upper limit is the decomposition temperature of ye'elimite (~1300 °C) [90], [92]. The lower limit is the temperature required for alite formation in the presence of dopants [14], [15]. In the alite-ye'elimite system, sulfur tends to stabilize belite over alite because of the presence of the S<sup>6+</sup> ion, which can replace Si<sup>4+</sup> in belite, which prevents the formation of alite. To overcome the stabilization effect and ensure the formation of alite, a mineralizer needs to be used [40], [42]. The use of F as a mineralizer has been adapted to the production of novel BAY and AYF clinkers [13], [14], [16], [17], [86], [93], [94]. The use of mineralizers has been discussed in more detail in Paper II. It is also stated that fluoride and sulfates in the raw mix leads to liquid formation, which improves ion mobility. This is called the fluxing effect [85], [87]. Because of the addition of fluorine, a non-hydraulic fluorellestadite phase can form as a minor phase [44]. To prevent fluorellestadite formation, the production temperature should be above the decomposition temperature of fluorellestadite, which is 1250 °C [85]–[87].

## **2.4 Hydration of CSA and AYF**

The early strength of CSA concrete is achieved with the hydration of ye'elimite. The hydration of ye'elimite consists of the dissolution of ye'elimite and the

formation of monosulfate (AFm) or ettringite (Aft) along with nanocrystalline  $\text{Al}(\text{OH})_3$ , depending on the amount of available Ca-sulfate [8], [34]. If there is an insufficient amount of calcium sulfate in the system, the hydration product is monosulfate (AFm) [34]. Gypsum and anhydrite can both be used as a calcium sulfate source, from which gypsum accelerates ye'elimite hydration more efficiently than anhydrite [95]. Anhydrite is used for a practical reason to increase the shelf-life of the cement. The water solubility of different polymorphs of anhydrite (I,II and III) varies, that has an effect on the hydration kinetics of anhydrite [12], [96], [97]. The late strength properties develop with the hydration of  $\text{C}_2\text{S}$  and  $\text{C}_4\text{AF}$ .  $\text{C}_2\text{S}$  hydrates to C-S-H in high belite systems [6] and if  $\text{AH}_3$  is present,  $\text{C}_2\text{S}$  can hydrate to stätlingite [98].  $\text{C}_4\text{AF}$  can hydrate with  $\text{C}_2\text{S}$  to form hydrogarnet [99], [100].

The hydration of AYF cement can be considered similar to the hydration of blended PC/CSA. Alite ( $\text{C}_3\text{S}$ ) hydrates to portlandite (CH) and calcium-silicate-hydrates (C-S-H) nanocrystalline gel [101]. As with CSA cement, ye'elimite reacts with the water and sulfate source to produce ettringite [98].

## **2.5 Sidestream materials: Metallurgical slags and phosphogypsum**

This chapter presents the Finnish industrial sidestreams used in this study: Argon Oxygen Decarburisation (AOD) slag resulting from the stainless-steel refining process at Outokumpu Stainless (Tornio); fayalitic slag from the nickel flash furnace process at Boliden (Harjavalta); Fe slag from the pyrometallurgically treated jarosite at Boliden (Kokkola); ladle slag from steel production at SSAB Europe (Raahe); and phosphogypsum from fertilizer production at Yara Suomi (Siilinjärvi). The chemical composition of the raw materials obtained through XRF (X-ray fluorescence) is presented in Table 4. The estimates of the annual production of the slags and phosphogypsum in Finland are presented in Table 5.



**Table 4. Chemical composition based on XRF analysis of industrial sidestreams used in this study as raw materials for alternative cements (adapted under CC BY 4.0 license from Paper I © 2020 and Paper III © 2022 Authors).**

Raw material	AOD slag	Ladle slag	Phospho gypsum	Burned Jarosite Fe slag	Fayalitic slag
Oxide	wt. %	wt. %	wt. %	wt. %	wt. %
CaO	55.6	37.6	29.1	12.2	2.1
SiO <sub>2</sub>	29.7	8.5	0.3	20.6	34.4
Al <sub>2</sub> O <sub>3</sub>	1.7	22.9	0.1	6.8	2.9
Fe <sub>2</sub> O <sub>3</sub>	0.8	1.6	0.1	49.3	51.3
SO <sub>3</sub>	0.5	0.5	39.8	0.7	0.5
MgO	8.9	6.1	0.1	1.5	6.9
SUM Major oxides	97.2	77.2	69.5	91.1	98.1
LOI (1000 °C, 1h)	-0.41 <sup>1</sup>	19.17	29.31	-4.9 <sup>1</sup>	-4.45 <sup>1</sup>
Minor elements	Mn, Ti, Cr, F	Mn, Ti, V, Cr	P, Sr, F	Na, K, Cr, Ba, Mn, P, Sr, Ti	Na, K, Cr, Ni, Ti, Cu
SUM minor elements	2.5	2	1.6	8.9	2.8

<sup>1</sup>negative LOI is due to the oxidization of iron

**Table 5. Estimated annual production of raw materials in Finland used in this study. Slag/PG produced for each tonne of product, amount of product (metal or fertilizer) produced annually, and the estimate of annual slag/PG production in Finland (adapted under CC BY 4.0 license from Paper I © 2020 Authors).**

Material	t slag or PG/t product <sup>1</sup>	Product [Mt/a] <sup>2</sup>	Slag or PG [Mt/a] <sup>3</sup>
AOD slag	0.27	0.53	0.15
Fayalitic slag	4.5	0.032	0.14
Jarosite	0.5–0.9	0.315	0.16–0.28
Ladle slag	0.012–0.015	2.1	0.025–0.0315
Phosphogypsum	4–6	0.3 <sup>c</sup>	1.2–1.8
Total	9.3–11.7	3.28	1.7–2.4

<sup>1</sup>AOD slag [53], fayalitic slag [102], jarosite slag [103], [104], ladle slag [105], and phosphogypsum [106] <sup>2</sup> [107] <sup>3</sup> [108]

### 2.5.1 AOD slag

AOD slag is a byproduct from the stainless steelmaking process, where steel melt is refined in an AOD converter. It has the potential to be used as a raw material for cement manufacture because of its high CaO and SiO<sub>2</sub> content, which is similar to PC cement. The major mineral phase of AOD slag is dicalcium silicate C<sub>2</sub>S [3],

[102]. If the slag is boron stabilized,  $C_2S$  exists as  $\beta-C_2S$ . Stabilization with borax prevents the disintegration of  $\beta-C_2S$  to  $\gamma-C_2S$  during cooling, which leads to the volume expansion of dicalcium silicate, causing dusting and making the slag very challenging to store [45]. Other minerals present in AOD slag are cuspidine ( $C_4S_2(F,OH)_2$ ), bredigite ( $C_7MS_4$ ), merwinite ( $C_3MS_2$ ), periclase (MgO), fluorite ( $CaF_2$ ), magnetite ( $Fe_3O_4$ ), free lime (CaO), and spinel [54], [102]–[104]. The cuspidine content can be quite high and originate in fluorite ( $CaF_2$ ) addition during the steelmaking process to decrease the slag's viscosity [105]. The problems associated with the direct use of AOD slag as a binder are a high MgO content and impurities such as chromium, fluorine, and boron [104]. Excess MgO content may cause unsoundness in concrete [3], and chromium may leech or oxidize to hexavalent chromium [45], [106].

### **2.5.2 Ladle slag (LS)**

Ladle slag originates in a secondary metallurgical process, ladle treatment, in which the final composition of the steel melt is adjusted before the continuous casting of steel slabs. The chemical composition and therefore the mineral phase composition vary among steel plants. Adesanya (2019) presents a good review of different compositions [107]. Generally, the major crystal phases of dry ladle slag are gamma belite ( $\gamma-C_2S$ ), alite ( $C_3S$ ), tricalciumaluminate ( $C_3A$ ), mayenite ( $C_{12}A_7$ ), and periclase (MgO) [82]. Along the mentioned phases, recent findings suggest that 50 wt.% ladle slag consists of the pleochroite/Q-phase ( $Ca_{20}Al_{26}Mg_3Si_3O_{68}$ ) [81].

### **2.5.3 Burned jarosite slag (BJA) – Fe slag**

The burned jarosite slag (BJA) is also called Fe slag in this study due to its high iron content. Jarosite is a byproduct from zinc production, with the general formula  $ZFe_3(SO_4)_2(OH)_6$ , where Z represents  $Ag^+$ ,  $H_3O^+$ ,  $K^+$ ,  $Li^+$ ,  $Na^+$ ,  $NH_4^+$ , or  $\frac{1}{2} Pb^{2+}$  [108]. The slag used for the cement production in this study was a pyrometallurgically treated jarosite residue (Fe slag), which was produced in a novel process [109] to recover valuable metals and obtain an inert glass structure for safe storage and applications such as aggregates. The process to burn jarosite slag is in the pilot stage. The slag used in this study was water-granulated, consisting of an amorphous Ca-Fe silicate with crystalline phases such as periclase, magnetite, spinel (Cr), and some traces of metals (Zn, Cu etc.).

#### **2.5.4 Fayalitic slag**

Fayalitic slag consist of crystalline fayalite mineral and amorphous iron-silicate glass (~60 wt.%), with very similar chemistry to fayalite. Magnetite exists as a minor phase [110]. The chemical composition consists of iron and silicon. The most common minor elements are Mg and metals such as Ni, Cu, and Cr. Fayalitic slag is a byproduct of the flash smelting furnace process of nickel or copper production [111]. In this study, the slag originated in nickel production and is sometimes referred to as granulated nickel slag because it is water-granulated to granules.

#### **2.5.5 Phosphogypsum (PG)**

Phosphogypsum (PG) is similar to natural gypsum but also contains traces of phosphoric acid, phosphates, fluoride, and organic matter. PG is a byproduct of the production of phosphoric acid fertilizer, which is extracted from phosphate rock. In some locations, phosphate rock has radioactive elements that makes the utilization of phosphogypsum very challenging or impossible [112]. In Finland, PG is not radioactive and its utilization is therefore possible for earth construction and other applications, with certain limitations.

### **2.6 Utilization of metallurgical slags as raw materials for CSA-based cements and other applications**

Industrial byproducts have unique impurities and mineralogy, depending on the product, raw materials, and process. Industry produces huge volumes of inorganic byproducts that contain beneficial ingredients for the production of cement clinker:  $\text{Al}_2\text{O}_3$ ;  $\text{CaO}$ ;  $\text{SiO}_2$ ; and  $\text{Fe}_2\text{O}_3$  [113]. Currently, the vast majority of the byproducts is landfilled instead of utilized as raw materials, which could enhance resource efficiency. For CSA cement manufacture, a major obstacle is that CSA binders require aluminum, that is much scarcer and more expensive than other natural raw materials for cement manufacture, such as clays and limestone. The utilization of local industrial byproducts as raw materials for CSA manufacture could reduce the cost of manufacture and make CSA a more feasible product.

In this thesis the focus was on less utilized slags: AOD slag, ladle slag, Fe slag/BJA, and fayalitic slag. The metallurgical industry generates large amounts of inorganic residues that contain the necessary ingredients to produce cement clinkers. The replacement of limestone ( $\text{CaCO}_3$ ) in a raw mix with calcium-rich

slags in which CO<sub>2</sub> has been burned in the original process is a very efficient way to reduce the CO<sub>2</sub> emissions of cement manufacture. Currently, the most used slag type for cement manufacture is GGBFS (ground granulated blast furnace slag), which is standardized and easy to use as a raw material and SCM's (supplementary cementitious materials) [3]. The future availability of GGBFS may be reduced due to the steel industry's ambition to move toward carbon neutrality, which will lead to the replacement of the blast furnace with direct reduction (DR) using electric arc furnaces (EAF). In this route, hydrogen is used in the direct reduction process to produce a sponge iron that is further refined in EAF [114].

When industrial byproducts are planned as raw materials for cement, it is important to ensure the effect of impurities on clinkering parameters, phase formation, cement hydration, and the leaching of hazardous elements from the concrete/cement. Various studies about the use of different kinds of byproducts in various ye'elimite-based clinker systems such as fly ash [115]–[117], blast furnace slag [115], red mud [13], [118], [119], jarosite [120], AOD slag [121], ladle slag [122]–[124] EAFs [125] etc. exist.

AOD slag remains an underused byproduct because of the environmental concerns and high content of non-hydraulic crystalline phases compared to GGBFS, which makes it challenging to use as an SCM [126]. The applications studied for AOD slag have been use as aggregate [102], [127], a precursor in the alkali activation [128] and carbonation of slag [129]. AOD slag was used as raw material for ye'elimite clinker types [121] at a laboratory scale. In Paper I, AOD slag was used as a raw material, and it was found that if fluorine was present in AOD slag, it caused melting, which limited the maximum content of AOD slag to CSAB cement clinker. Therefore, in Papers II and IV, the clinker type was changed from a CSAB to an AYF (alite-ye'elimite-ferrite) clinker system, in which fluorine could be used as a mineralizer for alite formation. The goal of Paper II was to produce AYF clinker at a laboratory scale using AOD slag as a fluorine source, and in Paper IV, the results were scaled to a pilot-scale demonstration.

Dry ladle slag (LS) can be used as an alkali-activated material, a sole binder, or a co-binder with calcium sulfate [81], [107], [130]. However, the weathered slag needs thermal activation. Because of the low proportion of heavy metals in LS, it can be used to improve soil basicity in agriculture [131] and construction applications that do not require standardization. LS has also been used as a filler material in construction applications [132], [133] and asphalt [134]. LS could be a good source of aluminum to produce ye'elimite in CSA clinkers locally [122], [123]. However, the low production volumes compared to blast furnace and other

metallurgical slags (Table 5) and already high use for other applications may restrict its availability.

The high iron content of fayalitic and Fe slag/BJA slags restricts their use as raw materials for PC clinkers. The use of iron-rich slags can be increased by developing novel clinkers with a higher ferrite phase content [20] [110]. The studies of fayalitic slags consist of use as SCMs to replace PC [135], [136] and as alkali-activated materials [137]–[140]. In Papers I and III, AOD slag, fayalitic slag, and Fe slag/BJA slag were used for CSA cement manufacture in a sole mix with RGC chemicals. In Paper III, Fe slag could be used with LS, PG, and natural raw materials in a semi-industrial trial to produce CSABF clinker. In Paper IV, fayalitic slag was used with AOD slag, PG, LS, and natural raw materials to produce AYP clinker. In these studies, it was found that iron-rich raw materials were suitable for the formation of the cement phase when mixed with CaO-, Al<sub>2</sub>O<sub>3</sub>-, SO<sub>3</sub>-, and SiO<sub>2</sub>-bearing raw materials. For further reading, a good table of properties of Fe-rich byproducts and residues can be found in a review study [20].

## **2.7 Applications of CSA-based concretes**

CSA-based concretes offer superior properties compared to PC, but the production cost is significantly higher, which restricts the reasonable applications. CSA cements should be considered for applications where extended worktime or closure is impossible, such as the critical infrastructure of civilian and government organizations (nuclear, military, and transportation).

The hydration product of CSA cements, namely ettringite, is known to be able to stabilize and/or encapsulate heavy metals, sulfates, and hazardous components [11], [141]–[143]. Locally, if sufficient raw materials to produce CSA are available, the applications could be mine backfilling or waste stabilization [10], [144], [145].

The curing of PC concrete becomes challenging when the temperature drops below 10 °C. In cold regions, the faster hydration time (higher early heat of hydration) of the CSA type of cements is beneficial for overcoming the deceleration of the hydration reaction due to the cold environment. CSA has been used in China for cold weather concreting from the very beginning of its development [4]. Recently, there have been studies especially of CSA ad PC blends for cold concreting [25], [26], [31], [146].



## 3 Materials and Methods

### 3.1 Materials

The industrial byproduct materials used as raw materials for CSA and AYF cement in this study were AOD slag, LS, PG, Fe slag, and fayalitic slag. Limestone and clay were the natural raw materials. Reagent grade chemicals were used in the laboratory clinkers as raw materials in the preliminary testing and to balance the oxide composition. In the preparation of concrete mortars, gypsum and standard sand were used. In hydration studies of AYF, citric acid was used as a retarder. The properties of the various materials are described in the following subsections.

#### 3.1.1 Reagent-grade chemicals (RGC)

The reagent-grade chemicals for clinker production in Papers I–IV were:

- Aluminum oxide ( $\text{Al}_2\text{O}_3$ ; metal basis fine powder; 99%; CAS: 1344-28-1)
- Calcium oxide ( $\text{CaO}$ ; reagent-grade powder; 98%; CAS:1305-78-8)
- Calcium sulfate ( $\text{CaSO}_4$ ; anhydrous powder; 99%; CAS:7778-18-1)
- Iron (III) oxide ( $\text{Fe}_2\text{O}_3$ ; metals basis powder; 98%; CAS: 1309-37-1)
- Silicon dioxide ( $\text{SiO}_2$ ; mesh-fused amorphous powder; 99%; CAS: 7631-86-9)

Gypsum ( $\text{CaSO}_4 \cdot 2\text{H}_2\text{O}$ ; powder, 99%; CAS: 10101-41-4) was used to make mortars in Papers I and IV with deionized water. In Papers III and IV, calcium fluoride ( $\text{CaF}_2$ ; reagent-grade powder; 99%; CAS: 7789-75-5) was used as a mineralizer to introduce fluorine to raw mixes. Calcium carbonate ( $\text{CaCO}_3$ ; metal basis, 99.5%; CAS: 471-34-1) was used in some of the laboratory-scale clinkers in Paper IV. The hydration rate was controlled in Paper IV by adding citric acid ( $\text{C}_6\text{H}_8\text{O}_7$ ; crystals; 99.5%; CAS: 77-92-9) to water.

In Paper I,  $\text{CaO}$  was calcined at  $800\text{ }^\circ\text{C}$  for 4 h to remove possible moisture and/or  $\text{CO}_2$  that may have interacted with it. Calcium sulfate was dried at  $250\text{ }^\circ\text{C}$  for 2 h, and all the sidestream raw materials were ground with a ball mill and dried at  $105\text{ }^\circ\text{C}$  for 24 h. In Paper II, all reagent-grade chemicals—except  $\text{CaF}_2$ —were dried in a  $500\text{ }^\circ\text{C}$  muffle furnace for 12 h. In Papers III and IV prior to weighting, all reagent-grade chemicals were dried at  $500\text{ }^\circ\text{C}$  in a muffle furnace for 12 h, except for  $\text{CaCO}_3$  and  $\text{CaF}_2$  in Paper IV.

### 3.1.2 Industrial sidestreams

In Paper I, the Finish industrial sidestreams used as raw materials were Argon Oxygen Decarburization (AOD) slag resulting from the stainless-steel refining process at Outokumpu Stainless Oy (Tornio), fayalitic slag from the nickel flash furnace process at Boliden Harjavalta, and Fe slag (BJA) from the pyrometallurgically treated jarosite at Kokkola Boliden. In Paper I, the idea was to maximize the quantity of each raw material within the limitations of target oxide and phase composition. The chemical composition of raw materials are presented in Table 6.

**Table 6. Chemical composition of raw materials obtained through the XRF (X-ray fluorescence) analysis and LOI (loss on ignition) (adapted under CC BY 4.0 license from Paper I © 2020 Authors).**

Paper	I&IV <sup>1</sup>	I	I
Raw material	AOD	BJA	Fayalitic
Oxide	wt.%	wt.%	wt.%
Al <sub>2</sub> O <sub>3</sub>	1.7	5.1	2.3
CaO	55.4	16.8	1.8
Fe <sub>2</sub> O <sub>3</sub>	0.7	39.5	58.8
K <sub>2</sub> O	0.3	0.5	0.5
MgO	8.7	3.1	6.2
MnO	0.2	0.7	0.1
Na <sub>2</sub> O	0	2.8	0.4
P <sub>2</sub> O <sub>5</sub>	0	0.2	0.3
SiO <sub>2</sub>	28.1	29.9	33.5
SO <sub>3</sub>	0.4	0.8	0.2
SrO	0	0.1	0
TiO <sub>2</sub>	0.3	0.5	0.2
Cr <sub>2</sub> O <sub>3</sub>	0.5	0.1	0.2
F	1.5 <sup>2</sup>	0	0
Others	0.1	1.4	1.1
Sum	98	101.5	105.5
LOI (950 °C, 3 h)	-0.4	-4.8	-4.3

<sup>1</sup>Paper IV laboratory studies <sup>2</sup>close to detection limit



The chemical composition of industrial byproducts and natural materials utilized in the semi-industrial trials of Papers III and IV are presented in Table 7. The AOD slag, BJA/Fe slag, and fayalitic slag used in Papers III and IV were similar to the raw materials in Paper I, with slight differences in chemical composition. The differences in chemical composition are due to different production batches. The ladle slag was from steel production at SSAB Europe (Raahe), and phosphogypsum from fertilizer production at Yara Suomi (Siilinjärvi). In Papers III and IV, to balance the composition, Parfill 500 limestone from Nordkalk (Parainen, Finland) and a high alumina-containing clay originating in China were used when necessary.

**Table 7. Chemical composition of raw materials obtained through the XRF (X-ray fluorescence) analysis and LOI (loss on ignition) (adapted under CC BY 4.0 license from Paper I © 2020, Paper III © 2022 Authors).**

Paper	I&III	IV	I&IV	III&IV	III&IV	III&IV	III&IV
Raw material	BJA	AOD	Fayalitic	LS	PG	Clay	Limestone
Oxide	wt.%	wt.%	wt.%	wt.%	wt.%	wt.%	wt.%
Al <sub>2</sub> O <sub>3</sub>	6.8	1.7	2.9	22.9	0.1	38.7	0.8
CaO	12.2	55.6	2.1	37.6	29.1	0.6	50.5
Fe <sub>2</sub> O <sub>3</sub>	49.3	0.8	51.3	1.6	0.1	6.1	0.5
K <sub>2</sub> O	0.4	0	0.64	0.1	0	0	0
MgO	1.5	8.9	6.9	6.1	0.1	0.4	3.1
MnO	0.6	0.3	0.1	0.7	0	0	0
Na <sub>2</sub> O	4.8	0	0.5	0.1	0	0.1	0.1
P <sub>2</sub> O <sub>5</sub>	0.5	0	0	0	0.5	0.1	0
SiO <sub>2</sub>	20.6	29.7	34.4	8.5	0.3	38.8	3.6
SO <sub>3</sub>	0.7	0.5	0.5	0.5	39.8	0	0
SrO	0.3	0	0	0	0.5	0	0
TiO <sub>2</sub>	0.2	0.5	0.2	0.9	0	0.6	0
Cr <sub>2</sub> O <sub>3</sub>	0.1	0.7	0.2	0	0	0	0
F	0	1 <sup>1</sup>	0	0	0	0	0
Others	1.6	1.0	1.2	0.2	0.6	0	0.2
Sum	99.6	99.7	100.9	79.2	71.1	85.4	58.8
LOI (1000 °C, 1h)	-4.9	-0.4	-4.5	19.2	29.3	12.8	41.5

<sup>1</sup>close to detection limit

The particle size distribution (PSD) of raw materials for the semi-industrial trial (Papers III and IV) is presented in Fig. 2. The analysis method for PSD is described in Section 3.2. Prior to particle size analysis and piloting, fayalitic slag and Fe slag

were ground. The median particle sizes  $d_{50}$  for AOD slag, fayalitic slag, Fe slag, ladle slag, phosphogypsum, and limestone were 22  $\mu\text{m}$ , 36  $\mu\text{m}$ , 55  $\mu\text{m}$ , 334  $\mu\text{m}$ , 99  $\mu\text{m}$ , and 232  $\mu\text{m}$  respectively.

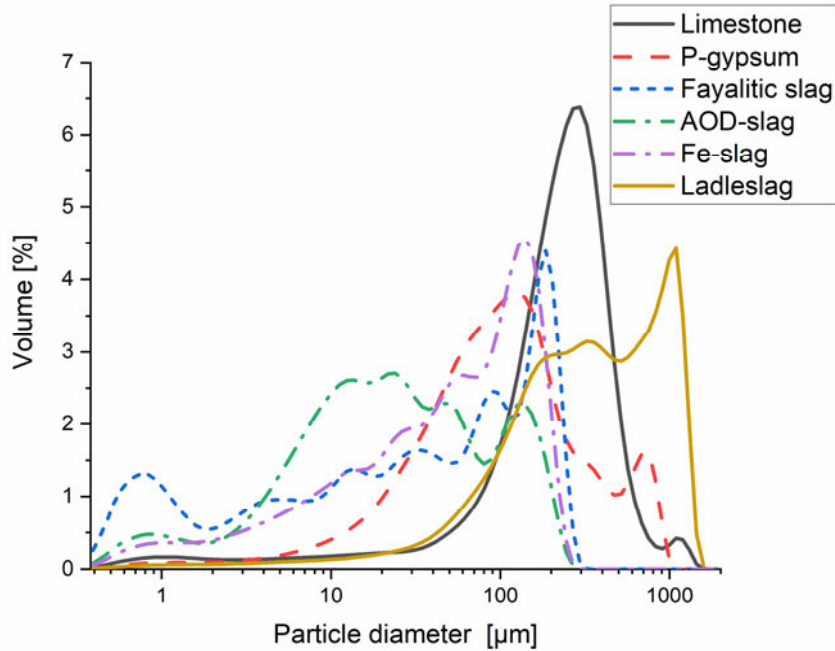


**Fig. 2. PSD of raw materials: Limestone, P-Gypsum, Fayalitic slag, AOD-slag, Fe-slag and Ladleslag. (adapted under CC BY 4.0 license from Paper III © 2022 Authors).**

### **3.1.3 Aggregates and cements**

CEN standard sand supplied by Normensand GmbH and conforming to EN 196-1 [147] was used in Papers I and IV to make mortars.

Cement I in Table 8 refers to the Portland cement type, CEM II/B-M (S-LL) 42.5 N (Plussementti 2019, Finnsementti), which was used in the reference samples to compare the quality of produced CSA clinkers in Paper I and AYW clinkers in Paper IV. That cement type contains 10–25% blast furnace slag and 6–15% limestone in addition to clinker. Cement II is a commercial rapid setting and

hardening CSA cement (Calumex Belicem, Caltra Nederland B.V.) that consists of roughly 40% ye'elimite, 35% belite, and 25% anhydrite.

**Table 8. The commercial cements used as references for comparison. Cement I CEM II/B-M (S-LL) 42,5 N (Plussementti 2019, Finnsementti) and Cement II CSA cement (Calumex Belicem, Caltra Nederland B.V.).**

Paper	I & IV	III
Raw material	Cement I	Cement II
Oxide	wt. %	wt. %
Al <sub>2</sub> O <sub>3</sub>	5.4	25.6
CaO	58.4	46.1
Fe <sub>2</sub> O <sub>3</sub>	3.3	2.2
K <sub>2</sub> O	0.7	0.3
MgO	3.9	1.4
Na <sub>2</sub> O	0.6	0.2
P <sub>2</sub> O <sub>5</sub>	0.1	0.5
SiO <sub>2</sub>	21.7	7.1
SO <sub>3</sub>	3.5	18.1
TiO <sub>2</sub>	0.6	1.1
LOI 950 °C	3.4	<3
Blaine cm <sup>2</sup> /g	4800	4500

## 3.2 Methods

### 3.2.1 Pretreatment and characterization of materials

#### *Grinding and particle size distribution (PSD)*

In Paper I, AOD slag and fayalitic slag were ground with a stainless-steel jar mill (10 L) (Germatec, Germany) for 1 h using 120 stainless-steel balls (d = 30 mm). Fe slag was crushed/ground using a vibratory disc mill (RS 200, Retsch, Germany) with the following settings: 1000 rpm for 1 min 30 sec. The PSD of clinkers in Paper I was measured using a laser diffraction technique with the wet system module of Beckman Coulter LS 13 320 and the Fraunhofer model [148]. Isopropanol was used instead of water to avoid the hydration of the clinker.

In Papers III & IV, AOD slag, phosphogypsum, and ladle slag were not pretreated for the semi-industrial trials, but prior to the PSD analysis, they were sieved with a 2 mm sieve, and 100%, 95.5%, and 86% passed through respectively.

Prior to the pilot demonstration, 90kg of Fe slag and fayalitic slag were ground in 30 kg batches using a stainless-steel jar mill (TPR-D, Germantec, Germany) with a jar diameter of  $d = 0.6$  m and  $h = 0.6$  m. The grinding media consisted of stainless-steel balls of  $d = 10$  mm (20 kg),  $d = 25$  mm (10 kg), and 50 mm (10 kg). The grinding time was 4 h until all the ground material passed through a 200  $\mu\text{m}$  sieve.

In Papers III & IV, clinker ground with the same configuration as Fe slag and fayalitic slag. Here the grinding was operated for 2–3 h until >85% of the material passed through the 45  $\mu\text{m}$  sieve. The total mass of clinkers ground was 240 kg of CSA clinker and three different types of AYF clinkers, A: 31 kg, B: 20 kg, and C: 27 kg. After grinding, the clinkers were mixed using the quartering method, in which samples for PSD, density, XRD, and XRF analyses were collected to represent the whole batch of each clinker. After sample collection, the quartering was continued until all the clinkers were stored in airtight plastic buckets (~20 kg each). The PSD of the byproducts and the ground clinker was measured with a laser diffraction technique using the dry powder system module of Beckman Coulter LS 13 320 with the Fraunhofer model.

### *Chemical composition*

Prior to X-ray fluorescence (XRF) analysis, loss on ignition (LOI) was measured from the raw materials presented in Section 3.1.2. For Paper I, LOI was measured using 42 ormal-gravimetric analysis (TGA) (Prepash, Precisa Gravimetrics, Switzerland). The heating cycle in TGA was 30 min ramp to 105 °C/4 h hold, 2 h 30 min ramp to 525 °C/3 h hold, and 1 h ramp to 950 °C/3 h hold. For Papers III and IV, the loss on ignition (LOI) was determined by weight change: 1.5 g of sample material was placed in a preheated corundum crucible and heated to 1000 °C for 1 h.

Two different X-ray fluorescence (XRF) configurations were used in this research work to determine the chemical composition of raw materials and clinkers. At the University of Oulu, Finland, the melt-fused beads were prepared with Eagon 2 fluxer (Malvern Panalytical, USA), and beads were analyzed with an Omnian Pananalyticals Axiosmax 4 kV (Malvern Panalytical, UK) X-ray fluorescence (XRF) spectrometer. At Bauhaus-University of Weimar, Germany, the melt-fused beads were prepared using an automatic electric furnace (xrfuse2, XRF Scientific, Australia), and the beads were analyzed with a wavelength Dispersive X-ray Fluorescence spectrometer S8 Tiger (Bruker, USA). In Oulu, 1.5 g of each material mixed separately in a Pt/Rh crucible with 7.5 g of X-ray flux (Spectromelt A12)

type 66:34 (66%  $\text{LiB}_4\text{O}_7$  and 34%  $\text{LiBO}_2$ ), and in Weimar, 1 g of the preheated sample material was mixed with 8 g of flux. The melting was conducted at 1150–1200 °C.

All the clinkers (Papers I, III, & IV), granules, kiln inlet material, and byproducts; AOD slag (Paper I); Fe slag (Papers I, III, & IV), and fayalitic slag (Papers I, III, & IV) were analyzed at the University of Oulu. Raw materials and granules for semi-industrial pilot AOD slag (Paper IV), ladle slag (Papers III & IV), phosphogypsum (Papers III & IV), natural clay (Papers III & IV), and limestone (Papers III & IV) were analyzed with the configuration at the University of Weimar.

In Paper I, trace elements of industrial sidestream materials were measured with inductively coupled plasma atomic emission spectroscopy (ICP-OES). The microwave-assisted wet digestion was performed using a 3:1 ratio of  $\text{HNO}_3$  and an HCl acid mixture for 0.5 g of AOD slag, Fe Slag, and fayalitic slag at 175 °C according to EPA3051A.

### *X-ray diffraction measurement*

The XRD diffractometers and operating parameters of Papers I–IV are presented in Table 9. In Paper I, all the clinkers were analyzed with a Rigaku SmartLab 9 kW, and in Paper II, with a Bruker D2 PHASER. The laboratory scale experiments in paper III and IV were analyzed with Rigaku SmartLab 9 kW and ground and mixed clinkers from the semi-industrial pilot and reference clinkers were analyzed using a Siemens D5000.

**Table 9. XRD diffractograms and parameters for Papers I–IV.**

Paper/ parameter	XRD	Detector	X-ray source	Voltage (kV)	Current (mA)	Step (deg.)	2 $\theta$ (deg.)	Counts
Paper I	Rigaku SmartLab 9 kW	D/teX Ultra 250	Co	40	135	0.02	5–120	5750
Paper II	Bruker D2 PHASER	LYNXEYE XE- T	Cu	0.03	10	0.02	10–70	3000
Paper III	Rigaku SmartLab 9 kW	D/teX Ultra 250	Cu	45	200	0.02	5–130	6251
	Siemens D5000	SolX, Bruker (EDX)	Cu	40	40	0.02	5–70	3250
Paper IV	Rigaku SmartLab 9 kW	D/teX Ultra 250	Co	40	135	0.02	5–130	6251
	Siemens D5000	SolX, Bruker (EDX)	Cu	40	40	0.02	5–70	3250

The crystalline mineralogy of the clinkers was measured with X-ray diffraction. Prior to the analysis with Rigaku SmartLab and Bruker D2 PHASER, the samples were ground to a fine powder by hand using an agate mortar and then loaded into sample holders. For Siemens D5000 the samples were ground to fine powders using McCrone micronizing mill. The phases from the XRD patterns obtained with the Rigaku SmartLab and Bruker D2 PHASER (Papers I–IV) were identified by a Whole Powder Pattern Fit (WPPF) analysis using Rigaku PDXL 2 software with the PDF-4+ RDB database. In Paper II, the phases were initially identified from diffraction patterns using EVA software (Bruker, USA). The amorphous content in Paper III was conducted using an internal standard method by mixing 80–20 clinker–Rutile (TiO<sub>2</sub>) mix with the McCrone micronizing mill, and the XRD pattern was then collected with the Siemens D5000.

### *Scanning electron microscopy (EDX)*

In Paper I, crushed pieces of clinkers and hydrated samples were cast to epoxy resin then cut to polished sections, cast again to optical-grade epoxy resin (Struers Epofix, Denmark) and polished using a wheel polisher (Struers, LaboPol-6, Denmark). A more detailed description of the procedure can be found in Paper I. The field emission scanning electron microscope FESEM (Zeiss Ultra Plus, Oxford

Instruments, UK) equipped with an energy-dispersive X-ray spectroscopy (EDX) analysis system, and back-scattered electron detector (BSE) was used in Paper I to analyze phase distribution in CSAB clinkers. The acceleration voltage was 15 kV, the current 3.2–4.8 nA, and the working distance between 7.3 and 8.0 mm. Analysis software (Aztec 4.3, Oxford Instruments, UK) was used to analyze the BSE pictures and the elemental chemical composition of the selected EDX points.

In Papers III & IV, ground clinker was pressed into a tablet and embedded in epoxy resin. The polishing of the polished sections was operated with an automatic polishing device (TF250, JeanWirtz, Germany) and diamond oil paste sizes of 15, 9, 3, 1, and 0.25  $\mu\text{m}$  (MetaDi II, Buehler, US). All the polished sections were coated with approx. 8–10 nm carbon to achieve electric conductivity. Imaging, elemental mapping, and analysis of the chemical composition of the major phases in Papers III and IV was conducted using a high-resolution field emission SEM (Helios G4UX, ThermoScientific, USA). The BSE imaging and EDX analysis in Paper III were acquired using a 12 kV acceleration voltage and 0.8 nA electron current. In Paper IV, the values for imaging and analysis were a 7 kV acceleration voltage and 0.8 nA electron current respectively. The detector(s) for the acquisition of EDX data in Paper III was a silicon drift detector (X-Max80, Oxford Instruments, UK) and in Paper IV, two silicon drift detectors were used in parallel (UltimExtreme and X-Max80, Oxford Instruments, UK). The detectors allowed the collection of elemental distribution maps at a high resolution (450nmali. 0.1  $\mu\text{m}$  pixel resolution) and high-count number. The EDX data acquisition and analysis were conducted with analysis software (Aztec 4.3, Oxford Instruments, UK), and the phase maps were calculated with a different version of the same software (Aztec 5.0, Oxford Instruments, UK). SEM-EDX was calibrated with a pure cobalt standard. An Fe-L line was used to determine the iron content, and the rest of the elements were quantified using K-alpha lines.

### *Density and specific surface area of clinkers*

To determine the specific surface area, the density of clinkers was analyzed using a gas pycnometer (AccuPyc II 1340, Micromeritics, USA) from the samples with masses of around 6 g at 22.9–23.1  $^{\circ}\text{C}$ . Helium was used as a probe gas, the run pressure was set to 19.5 psig, and the pressure was 0.005 psig/min. Two samples from each clinker were run for 10 cycles to improve accuracy. The standard deviations were between 0.0012 and 0.002, and the average density of the clinkers was calculated from these 20 runs. The specific surface area for clinkers produced

in Papers I, III, and IV were determined according to Blaine analysis (EN 196-6), which was obtained with Blaine's apparatus, and the density data from the pycnometer.

### *Thermal analysis of granules*

In Papers III and IV, to determine the gases emitted at certain temperatures during clinkering, a simultaneous differential thermal analysis (DTA), thermogravimetric analysis (TG), and mass spectrometry (MS) were conducted for the granules. The granule sample was ground with agate mortar, and 25.22 mg of the sample was placed on an alumina crucible. The heating ramp for DTA-TG-MS (STA449 F3 Jupiter, Netzsch, Germany and QMS403D Aëolos Quadro, Netzsch, Germany) was set to 10 °C/min from room temperature to 1300 °C. The test was run in an argon atmosphere with a gas flow of 60 ml/min. For mass spectrometry, the selected ions to be analyzed were  $m/z = 17$  (OH), 18 (H<sub>2</sub>O), 28 (CO), 44 (CO<sub>2</sub>), 48 (SO), 64 (SO<sub>2</sub>), and 80 (SO<sub>3</sub>), where  $m/z$  is the mass to charge ratio. In the mass spectrometer analysis, OH/H<sub>2</sub>O, CO<sub>2</sub>, and SO<sub>2</sub> were detected.

### **3.2.2 Design of the clinker recipes**

CSABF clinker recipes in Papers I and III were calculated using the so-called modified Bogue calculation, where the molar mass of clinker oxides and molar masses of each phase were used to calculate the target compositions for the final clinker. Due to the high iron content of industrial byproducts, it was decided that the target phase composition of all the clinkers prepared in this research should have relatively high iron, i.e., ferrite phase, content. The equations and molar masses for phase calculations for CSA clinkers are presented in Table 10. In Papers II and IV, similar calculations were used to calculate target phase compositions for AYF clinkers, but the belite C<sub>2</sub>S was replaced with alite C<sub>3</sub>S (228.32 g/mol). The equations used are presented in Table 11. The fluoride content was adjusted according to the equation Ca<sub>3</sub>Si<sub>1-x</sub>Al<sub>x</sub>O<sub>5-x</sub>F<sub>x</sub>, and hence the target alite content changed the fluorine content required.



**Table 10. Molar masses and equations used to calculate the target phase composition (under CC BY 4.0 license from Paper III © 2022 Authors).**

Oxide	Molar mass oxide [g/mol]	Phase	Molar mass phase [g/mol]
Al <sub>2</sub> O <sub>3</sub>	101.96	C <sub>4</sub> AF	485.96
CaO	56.08	C <sub>2</sub> S	172.24
Fe <sub>2</sub> O <sub>3</sub>	159.69	C <sub>4</sub> A <sub>3</sub> S	610.26
SiO <sub>2</sub>	60.08	C\$	136.34
SO <sub>3</sub>	80.06	-	-

Equations

$$\text{Al}_2\text{O}_3 = [\text{C}_4\text{A}_3\text{S} (\text{wt.}\%) / (\text{C}_4\text{A}_3\text{S} (\text{g/mol}) / 3 * \text{Al}_2\text{O}_3 (\text{g/mol}))] + [\text{C}_4\text{AF} (\text{wt.}\%) / (\text{C}_4\text{AF} (\text{g/mol}) / \text{Al}_2\text{O}_3 (\text{g/mol}))]$$

$$\text{CaO} = [\text{C}_4\text{A}_3\text{S} (\text{wt.}\%) / (\text{C}_4\text{A}_3\text{S} (\text{g/mol}) / 4 * \text{CaO} (\text{g/mol}))] + [\text{C}_4\text{AF} (\text{wt.}\%) / (\text{C}_4\text{AF} (\text{g/mol}) / 4 * \text{CaO} (\text{g/mol}))] + [\text{C}_2\text{S} (\text{g/mol}) / (2 * \text{CaO} (\text{g/mol}))] - \text{C\$} (\text{wt.}\%) * 0.41$$

$$\text{Fe}_2\text{O}_3 = [\text{C}_4\text{AF} (\text{wt.}\%) / (\text{C}_4\text{AF} (\text{g/mol}) / \text{Fe}_2\text{O}_3 (\text{g/mol}))]$$

$$\text{SiO}_2 = [\text{C}_2\text{S} (\text{wt.}\%) / (\text{C}_2\text{S} (\text{g/mol}) / \text{SiO}_2 (\text{g/mol}))]$$

$$\text{SO}_3 = [\text{C}_4\text{A}_3\text{S} (\text{wt.}\%) / (\text{C}_4\text{A}_3\text{S} (\text{g/mol}) / \text{SO}_3 (\text{g/mol}))] + [\text{C\$} (\text{wt.}\%) / (\text{C\$} (\text{g/mol}) / \text{SO}_3 (\text{g/mol}))]$$

**Table 11. Equations used to calculate the target phase composition in Papers II & IV (under CC BY 4.0 license from Paper II © 2021 Authors).**

Oxide	Equations
Al <sub>2</sub> O <sub>3</sub>	$[\text{C}_4\text{A}_3\text{S} (\text{wt.}\%) / (\text{C}_4\text{A}_3\text{S} (\text{g/mol}) / 3 * \text{Al}_2\text{O}_3 (\text{g/mol}))] + [\text{C}_4\text{AF} (\text{wt.}\%) / (\text{C}_4\text{AF} (\text{g/mol}) / \text{Al}_2\text{O}_3 (\text{g/mol}))]$
CaO	$[\text{C}_4\text{A}_3\text{S} (\text{wt.}\%) / (\text{C}_4\text{A}_3\text{S} (\text{g/mol}) / 4 * \text{CaO} (\text{g/mol}))] + [\text{C}_4\text{AF} (\text{wt.}\%) / (\text{C}_4\text{AF} (\text{g/mol}) / 4 * \text{CaO} (\text{g/mol}))] + [\text{C}_3\text{S} (\text{g/mol}) / (3 * \text{CaO} (\text{g/mol}))]$
Fe <sub>2</sub> O <sub>3</sub>	$[\text{C}_4\text{AF} (\text{wt.}\%) / (\text{C}_4\text{AF} (\text{g/mol}) / \text{Fe}_2\text{O}_3 (\text{g/mol}))]$
SiO <sub>2</sub>	$[\text{C}_3\text{S} (\text{wt.}\%) / (\text{C}_3\text{S} (\text{g/mol}) / \text{SiO}_2 (\text{g/mol}))]$
SO <sub>3</sub>	$[\text{C}_4\text{A}_3\text{S} (\text{wt.}\%) / (\text{C}_4\text{A}_3\text{S} (\text{g/mol}) / \text{SO}_3 (\text{g/mol}))]$

### 3.2.3 Production of clinkers in laboratory

In Papers I–IV the laboratory scale clinkering (firing) was conducted according to heating procedures presented in Fig. 3.

The target phase compositions were:

- CSAB clinker in Paper I was 41% C<sub>4</sub>A<sub>3</sub>S, 35% C<sub>2</sub>S, 17% C<sub>4</sub>AF, 6% C\$, and 1% C
- In Paper III, the composition of CSABF clinker was 45% C<sub>4</sub>A<sub>3</sub>S, 36% C<sub>2</sub>S, 15% C<sub>4</sub>AF, 2% C\$, and 2 C. Additionally, in Paper III, a total of six different compositions was tested to analyze the limitations of the chemical composition of clinker.

- In Paper II, a total of 24 AYF clinkers was produced. First, seven clinkers with target 50 wt.%  $C_3S$ , 30 wt.%  $C_4A_3S$ , and 20 wt.%  $C_4AF$  with a fluorine content between  $0 < X < 0.3$ . Then eight clinkers with fixed alite content of 50 wt.% (fixed fluorine content  $X = 0.15$ ),  $C_4A_3S$  content was between 32.5 and 50 wt.%, and the  $C_4AF$  was between 0 and 17.5 wt.%. Finally, nine clinkers were prepared with target  $C_3S$  of 28–66 wt.% and a target  $C_4AF$  of 0–37 wt.%, and the  $SO_3$  was kept constant with a target  $C_4A_3S$  of 28 wt.% and  $C_2S$  of 6 wt.%.
- In Paper IV, the target composition for AYF clinker was 30%  $C_4A_3S$ , 30%  $C_3S$ , 30%  $C_2S$ , 10%  $C_4AF$ , and 1%  $C_2S$ . 1 wt.%  $CaF_2$  was added to reach an adequate fluorine content for the mineralization effect.

<b>Heating procedure Paper I CSAB(F)</b>			
Decarbonation	Heating ramp 10 °C/min	Dwell	Quench
Preheat for 0.5 h at preheated furnace 800 °C	to 1300°C in 60 min	at 1300 °C for 4 h	Copper table with water circulation

<b>Heating procedure Paper II AYF</b>			
Decarbonation	Heating ramp 5 °C/min	Dwell	Quench
Preheat for 0.5 h at preheated furnace 800 °C	to 1250°C in 90 min	at 1250 °C for 90 min	Air cooled on a ceramic plate

<b>Heating procedure Paper III &amp; IV CSABF</b>			
Decarbonation	Heating ramp 7.6 °C/min	Dwell	Quench
Preheat for 0.5 h at preheated furnace 800 °C	to 1260°C in 60 min	at 1260 °C for 1 h	Air cooled on a copper table

Fig. 3. Heating procedure in Papers I–IV. Heating procedure for CSAB(F) in Paper I to 1300 °C for 60 min, Paper 2 to 1250 °C for 90 min and Paper III&IV to 1260 °C for 60 min.

#### *Sidestream incorporation to clinkers*

The corresponding oxide composition of pure CSAB clinker in Paper I was 49 wt.% CaO, 20 wt.%, 10 wt.%, Al<sub>2</sub>O<sub>3</sub>, 12 wt.% SiO<sub>2</sub>, 10 wt.% Fe<sub>2</sub>O<sub>3</sub>, and 9 wt.% SO<sub>3</sub>. Table 12 presents the recipes with maximum byproduct incorporation to each clinker until the limitation of certain oxide was reached.

**Table 12. Recipes for CSAB clinker in Paper I (under CC BY 4.0 license from Paper I © Authors).**

Sample	RG_C	AOD_C	Fay_C	Fe_C
AOD slag		43.3		
Fayalitic slag			17	
Fe slag				25.3
Al <sub>2</sub> O <sub>3</sub>	20.3	19.5	19.9	19
SiO <sub>2</sub>	12.2	Limit	6.5	4.6
CaSO <sub>4</sub>	15.3	15	15.2	15
CaO	42.3	18.4	42	38.2
Fe <sub>2</sub> O <sub>3</sub>	10	9.7	Limit	Limit

In Paper II, no sidestreams were used. To analyze the effect of the particle size of raw materials on the clinker produced in the pilot demonstration, a reference clinker (Paper III) was produced in the laboratory with the procedure presented in Fig. 3, using the granules presented in Section 3.2.4. Prior to firing, the granules were ground ( $d_{50} = 8 \mu\text{m}$ ) using a disc mill (RS 200, Retsch, Germany).

In Paper IV, a reference clinker was prepared from industrial byproducts and natural materials to confirm that AOD slag could be used as a fluorine source to replace CaF<sub>2</sub>. The AOD slag for pre-tests was the same as in Paper I (Table 6). The target phase composition, chemical composition, and recipe for clinker is shown in Table 3. The AOD slag used in the pilot is presented in Table 7. According to XRF analysis, the composition was very similar to that in the pre-tests. However, in the AYW pilot, we could not produce alite. After the pilot, the laboratory tests were therefore repeated with both AOD slags, using the recipe presented in Table 13. In Appendix 8 it was shown that alite was forming also with phosphogypsum present.

**Table 13. The target phase composition, oxide content, and recipes for laboratory-scale pre-testing (Paper IV) with industrial byproducts and natural raw materials.**

Target phases						
Phase	C <sub>3</sub> S	C <sub>2</sub> S	C <sub>4</sub> A <sub>3</sub> S	C <sub>4</sub> AF	CS (anhydrite)	
wt. %	30	30	29	10	1	
Target oxide composition and required fluorine content						
Oxide	Al <sub>2</sub> O <sub>3</sub>	CaO	F <sup>1</sup>	Fe <sub>2</sub> O <sub>3</sub>	SiO <sub>2</sub>	SO <sub>3</sub>
wt. %	16.6	57.3	0.37	3.3	18.4	4.4
Pre LAB & After LAB						
Raw material	Kaolin	AOD slag <sup>2</sup>	CaCO <sub>3</sub>	CaSO <sub>4</sub>	Fayalitic slag	Ladle slag
wt. %	9.4	20	45.5	10.4	3.8	42.9

<sup>1</sup>Target, <sup>2</sup>Pre-test Table 6 & After Table 7

The effect of the particle size of raw materials on the results of the pilot demonstration (Paper IV) was tested by grinding a small batch of granules ( $d_{50} = 6 \mu\text{m}$ ) using a disc mill (RS 200, Retsch, Germany) and refiring them in a muffle furnace according to Fig. 3.

### 3.2.4 Production of clinkers in pilot kiln

The CSABF clinker in Paper III and AYF clinker in Paper IV were produced in a 48-hour semi-industrial-scale pilot in a rotary cement kiln. The first 24 hours of production was for CSABF clinker, and the second 24 hours of the trial with AYF clinkers was divided to be undertaken with three different clinker recipes PIL A, PIL B, and PIL C.

The process parameters in the kiln are presented in Table 14, and the simplified flowsheet of the rotary kiln and the configuration is shown in Fig. 4. The configuration consisted of a mixer/granulator, a belt feeder, a kiln tube, a cyclonic kiln dust separator, a dust baghouse filter, an exhaust extractor fan, a burner, and an oxygen feeding system. The burner of the kiln was operated with natural gas. The consumption of natural gas was about 20.1 Nm<sup>3</sup>/h. Oxidizing conditions were ensured by blowing 5 vol.% secondary air into the kiln when the oxygen volume was measured to be  $4.9 \pm 0.7$  vol.% at the kiln inlet head. The heat in the kiln was measured/controlled with thermocouples presented in Fig 3., and the temperature at the burning zone was measured hourly with a digital pyrometer (CellaPort PT 140, Keller, Germany). The exhaust gases (CO<sub>2</sub>, CO, SO<sub>3</sub>, and SO<sub>2</sub>) were analyzed with near infrared analyses (NIR) every 2 h from the kiln inlet and after the baghouse filter. The average exhaust SO<sub>2</sub> content throughout the 48-hour trial was

60 ppm at the kiln inlet. The amount of CO<sub>2</sub> exhaust gas flow was 10.5 ± 0.5 vol.%, and the amount of CO was constantly below 0.1 vol.%.

**Table 14. Process parameters of the pilot kiln trial (adapted under CC BY 4.0 license from Paper III © 2022 Authors).**

Operation	Paper III	Paper IV
Kiln length	7.4 m (7.0 m heated)	7.4 m (7.0 m heated)
Kiln inner diameter	0.3 m	0.3 m
Refractory thickness	5 cm	5 cm
Kiln inclination	1.0°	1.0°
Kiln rotation speed	2 rpm	2 rpm
Heating method	Direct heating	Direct heating
Operating configuration	Counter current flow	Counter current flow
Residence time	3 h	3 h
Raw meal feed (wet)	20–25 kg/h	20 kg/h
Raw meal feed (dry)	15–19 kg/h	~18.5 kg/h
Natural gas flow rate	20.1 ± 0.6 m <sup>3</sup> /h	20.1 ± 0.6 m <sup>3</sup> /h
Oxygen flow rate (burner)	5 m <sup>3</sup> /h	5 m <sup>3</sup> /h
Oxygen volume kiln inlet	4.9 ± 0.7 vol.%	4.9 ± 0.7 vol.%
Clinkering zone temperature	1260 ± 6.5 °C	1260 ± 6.5 °C
Exhaust cleaning	dust filter, cyclone	dust filter, cyclone

Prior to firing in Papers III and IV, the raw materials used in the trials were weighted, mixed, and granulated to achieve a homogenous mix and prevent material losses that might occur due to high gas velocity from the burner during firing. It was found in laboratory scale granulation with a mixer (R02, Eirich, Germany) that a 5 wt.% water addition was adequate for the granulation for CSABF (Paper III), and AYW granules (Paper IV) required 7–8 wt.% water addition. The granule size in both was between 1 mm and 5 mm. The granulation for the pilot was operated with a mixer equipped with a star pin rotor (R11, Eirich, Germany). The granulation was conducted according to the batches presented in Table 15, and the following steps were used.

1. Weighting and loading to mixer
2. Dry mixing 1 min with 700 rpm
3. Addition of tap water according to the recipe and mixing 700 rpm for 6 min
4. Granulation with 600 rpm for 5 min
5. Discharging of wet granules to 200 l steel drums

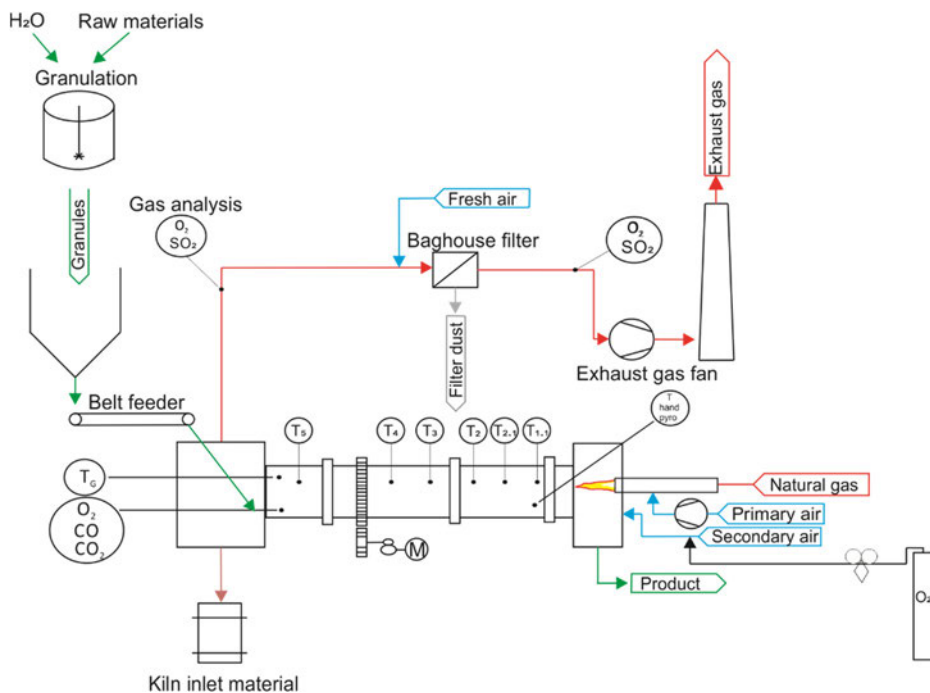


**Fig. 4. Simplified flowsheet/description of the rotary kiln configuration used in the pilot plant trials (adapted under CC BY 4.0 license from Paper III © 2022 Authors).**

**Table 15. Semi-industrial pilot granule recipes for CSABF and AYF clinkers in Papers III and IV (adapted under CC BY 4.0 license from Paper III © 2022 Authors).**

Recipe/clinker	CSABF (Paper III)	PIL A (Paper IV)	PIL B (Paper IV)	PIL C (Paper IV)
Unit	kg wt. %	kg wt. %	kg wt. %	kg wt. %
LS	106.5 68.1	39.8 24.4	49.5 28.1	58.5 36.3
AOD slag		18 11.0	24 13.6	28.5 17.7
Fayalitic		2.3 1.4	2.3 1.3	3 1.9
Fe slag	6 3.8			
PG	18 11.5	11.3 6.9	11.3 6.4	12 7.5
Clay	6 3.8	18 11.0	13.5 7.7	9 5.6
Limestone	13.5 8.6	60.8 37.3	63.3 35.9	39 24.2
Added water	6.5 4.2	13 8.0	12.5 7.1	11 6.8
Weight of mix	150 100	163 100	176 100	161 100

The firing procedure in the pilot kiln is presented in Fig. 5. In Paper III, the feeding speed of the wet granules was adjusted from 25 kg/h to 20 kg/h because material was lost due to the airflow from the burner. In Paper IV, the feeding speed was 20 kg/h. The total residence time in the kiln was 3 hours, from which around 40 minutes was in a burning zone consisting of 1.5 m of the kiln. After the loss of material to the kiln inlet material and evaporation of i.e., CO<sub>2</sub>, H<sub>2</sub>O, and SO<sub>2</sub>, the total production rate of clinker with 20 kg/h feed was around 10 kg/h of clinker. The cooling of the clinker started at a 0.4 m zone after the burner, where it is estimated that clinker cools to ~1000 °C over a 10 min timescale before discharging onto a metal tray, where it was quenched to room temperature in air. The cooling was assumed to be fast due to low throughput (~10 kg/h), and the tray was emptied occasionally. The robustness of the pilot was controlled by making an XRD analysis of the produced clinker on the site every 1 hour. It was found that the XRD patterns were constant throughout the pilot (Appendix 1).

<b>Heating procedure pilot kiln</b>			
<b>Feeding with belt feeder</b>	<b>Material loss because of air flow</b>	<b>Firing</b>	<b>Quench</b>
20-25 kg/h	Around 20% material was lost to kiln inlet material	0.7h at burning zone 1260 °C and total 3h in kiln	to 1000 °C in kiln and discharged on a metal tray




Fig. 5. Firing procedure in the pilot kiln.

### **3.2.5 Preparation of samples for hydration studies: Workability, setting time and compressive strength**

In Paper I, the cement pastes to analyze hydration products after 7 days of curing were prepared by mixing 15% of gypsum with RG\_C clinker (reagent grade chemicals only), water addition with water to cement ratio 0.5, and cured in a humidity chamber (22 °C ± 2 °C and 99% humidity). After 7 days of curing, the hydration was stopped by immersing a crushed (d < 4 mm) sample in acetone for two days and then filtered and dried in a 40 °C furnace. The polished section was prepared and analyzed with FESEM-EDX as described in Section 3.2.1.



Compressive strength samples were prepared according to the EN 196-1 cement standard [147] with some slight modifications. In Paper I,  $2 \times 2 \times 8$  cm prisms were used instead of  $4 \times 4 \times 16$  cm prisms because of the limited amount of clinker. In Papers III and IV, the prism size was  $4 \times 4 \times 16$  cm. The cement mixtures for the mortars were mixed using 85% clinker and 15% gypsum (Paper I), 15% anhydrite (Paper III), and 87.5% clinker and 12.5% anhydrite (Paper IV). All mortars (Papers I, III, and IV) were prepared using a laboratory-scale cement mixer (65-L0006/AM AUTOMIX) using prepared cement mixes (clinker + gypsum/anhydrite), standard sand, and tap water/DI-water, with a cement to water ratio of 0.5.

In Paper I, the mortars were left to cure for 24 hours in the molds, which were sealed in airtight plastic bags and then unmolded and stored in a humidity chamber to cure for 1, 7, and 28 days. The  $2 \times 2 \times 8$  cm mortars were cut in half and then tested with unconfined compressive strength tests, totaling six measurements for each type of mortar. The tests were operated using a Zwick testing machine with a maximum load of 100 kN, employing a loading force of 2.4 kN/s. The reference sample from commercial PC was mixed according to the EN 196-1 standard and tested after 7 and 28 days of curing.

In Papers III and IV, cement dry mixes for setting time testing and the mortars for compressive strength testing were prepared by mixing each clinker with 15 wt.% (Paper III) and 12.5 wt.% (Paper IV) anhydrite. The anhydrite content was selected to achieve maximum ettringite gain according to equation  $C_4A_3S + 2CSH_2 + 34H \rightarrow C_3A \cdot 3CS \cdot 32H + 2AH_3$ . The ye'elimite content of the clinkers was obtained from XRD-analysis. Anhydrite was mixed with clinkers using a stainless-steel jar mill (10 L) with the grinding media consisted of 120 stainless-steel balls ( $d=30$  mm) for 20 minutes. For the pastes and mortars, 0.5 water/binder ratio was used. In Papers III and IV, citric acid (CA) -deionized water solution was used to retard the hydration speed of cements. The solutions were 0.5 vol.% (Papers I and IV: sample PIL C) and 2 vol.% (Paper IV: samples PIL A and PIL C). The reference PC (Portland cement, CEM II/B-M (S-LL) 42.5 N) cement was prepared without CA and analyzed to compare the performance of the prepared clinkers.

The workability and setting times of the pilot clinkers—pilot CSA (Paper III) and AYP clinkers, namely PIL A, PIL B and PIL C (Paper IV)—were determined from cement paste samples (with citric acid additions) using an automated Vicat apparatus (Matest E044 N, Italy) at  $22 \pm 1$  °C according to the EN196-3 standard. The pastes were filled into a cylindrical mold (inner  $d = 80$  mm and  $h = 40$  mm). The initial setting time was reported when the needle failed to pierce the sample

beyond  $6 \pm 3$  mm from the bottom, and the final setting time was reported when the distance from the needle to the bottom was 39.5 mm.

The mortars for compressive strength were prepared like pastes for setting time tests. The compressive strength of PIL A, PIL B, and PIL C was tested according to the EN 196-1:2005 standard. The tests were conducted after 1, 3, 7, and 28 days of curing. 40 mm x 40 mm x 160 mm prisms were prepared in molds fitting one 2,025 g batch of cement mix, resulting in 3 prisms per mold. Four batches were prepared using 450 g clinker-anhydrite mix (Paper III: pilot CSA; Paper IV: PIL A, PIL B, and PIL C) or 450 g commercial PC, 1350 g CEN standard sand for each mix, and 225 g DI water (with citric acid). The reference PC was prepared without CA addition to water. The mortar mixes were prepared with automatic cement mixer. The prisms were casted as determined in the standard, including the use of a jolting apparatus. After casting, the prisms were cured for 24 hours in molds sealed in plastic bags to avoid moisture loss. After 24 hours of curing, the prisms were demolded and submerged in water at 20 °C. The compressive strength testing was conducted using a Dartec 1992 (modernized in 2009 by Zwick/Roell) testing machine with a testing range of 0–400 kN. The testing machine was calibrated by Eurofins to reach the required accuracy for an accredited testing laboratory. The loading speeds for the compressive strength test were 2400 N/s until fracture. The compressive strength was calculated using the equation  $R_c = F_c/1600$ , where  $R_c$  is the compressive strength in megapascals (Mpa),  $F_c$  is the maximum load at fracture in newtons (N), and 1600 is the area of the platens or auxiliary plates (40 x 40 mm) in square meters (1600 m<sup>2</sup>).

## 4 Results and discussion

The general idea in this research was to directly replace the maximum amount of natural raw materials with industrial byproducts without expensive pretreatments (grinding and heating, etc.) to produce alternative cements.

The mineralogy of the byproduct materials is discussed in Section 2.5. The chemical composition of the raw materials obtained through XRF (X-ray fluorescence) analysis and LOI (loss on ignition) is presented in Tables 6 (Paper I) and 7 (Papers III & IV). It was found that the industrial byproducts were rich in the oxides required for clinker manufacture. In Paper III, 85% of the typical raw materials (clay and limestone) of CSABF clinker could be replaced with byproducts in a pilot-scale demonstration. In Paper IV, the replacement of natural raw materials was between 48% and 68%. In Papers I, III, and IV, it was found that the byproducts contained a wide variety of impurities that might affect the mineralogy of the clinkers, changing their clinkering properties and final mineralogy.

### 4.1 Laboratory-scale CSAB clinker production

CSAB (Paper I) and CSABF (Paper III) clinkers were produced at laboratory scale using a muffle furnace. In Paper I, the idea was to test the suitability of a single industrial byproduct to produce CSAB cement clinker. The clinker recipes for CSAB (Paper I) are shown in Table 12. Four clinkers with the same phase target composition were prepared from pure reagent-grade chemicals that were incorporated with byproducts AOD slag, fayalitic slag, and Fe slag.

In Paper III, prior to the pilot demonstration, a sensitivity analysis was conducted according to the recipes shown in Table 16. The analysis was conducted to see how the clinker phases changed if the original target composition of C1, 45 wt.% ye'elimite ( $C_4A_3S$ ), 38 wt.% belite ( $C_2S$ ), 15 wt.% ferrite ( $C_4AF$ ). And 2 wt.% anhydrite  $C\$,$  was modified. The clinkers produced for sensitive analysis were analyzed with XRD, and it was found that if the CaO content in the raw mix was too low, it led to the formation of gehlenite. The formation of gehlenite is unwanted since it has poor hydraulic properties. In the pilot recipe (C6 in Table 16), 2 wt.% belite  $C_2S$  was therefore replaced by 2 wt.% CaO in the target composition compared to C1. After the pilot demonstration of CSABF clinker (Paper III), a reference clinker was made in a laboratory furnace from ground CSABF pilot

granules (Table 16) to show if the PSD of raw materials had an impact on the final clinker.

**Table 16. XRD results for a sensitivity analysis on raw meal fluctuations conducted for C2–C6 (under CC BY 4.0 license from Paper III © 2022 Authors).**

$\Delta$ target composition $\pm$ g	C1	C2	C3	C4	C5	C6
CaO	0	+5	-5	+5	+5	+0.7
SiO <sub>2</sub>	0	0	0	0	+1.5	-0.7
Al <sub>2</sub> O <sub>3</sub>	0	0	0	+2.5	0	0
Result XRD [wt. %]						
C <sub>4</sub> A <sub>3</sub> S [73]	40	35.1	49.1	36.6	38.5	38.6
C <sub>2</sub> S [147]	44.8	48.1	42.4	48.8	45.4	42.6
C <sub>2</sub> (A,F) [2]	9.8	14.1	3.6	12.7	13	15
C\$ [148]	1.2	0.8	0	1.2	1.4	1.2
C <sub>12</sub> A <sub>7</sub> [149]	4.1	1.9	0	0.7	1.7	2.7
C <sub>2</sub> AS [150]	0	0	4.9	0	0	0
R <sub>wp</sub> [%]	4.19	4.91	4.08	4.28	4.62	4.55

#### 4.1.1 Mineralogy

The mineralogical composition of clinkers prepared in Paper I is presented in Table 17. The phase composition of CSAB clinkers produced from RGC, fayalitic slag, and Fe slag were close to the designed target composition. The major phases (ye'elimite,  $\beta$ -belite, and ferrite) of RG\_C clinker were detected from the FESEM-BSE image shown in Fig. 6. The phase identification was made using an EDX detector to quantify the chemical composition of each phase. The phases exist mainly as mono-mineral clusters composed of at least ten individual mineral grains. The grain size of the phases was small, which is typical of CSA clinkers. With EDX analysis, it was quantified that the iron and alumina content of ferrite phase were C<sub>2</sub>(A<sub>x</sub>F<sub>1-x</sub>) with  $0.2 < x < 0.3$  ( $X_{RG\_C} = 0.24$ ,  $X_{AOD\_C} = 0.2$ ,  $X_{Fay\_C} = 0.28$ , and  $X_{Fe\_C} = 0.3$ ). The minor phases present were periclase, anhydrite, mayenite, and unreacted SiO<sub>2</sub>. It was found that fluorine originating in AOD slag led to the formation of a poorly hydraulic phase, fluorellestadite. AOD slag is therefore unsuitable for producing CSAB clinker at 1300 °C.

**Table 17. XRD results of the produced clinkers. The values are given in %. The quality of analysis is given as a weighted profile R-factor ( $R_{wp}$ ) and the goodness of fit as S (adapted under CC BY 4.0 license from Paper I © 2020 Authors).**

Phase name	Formula	RG_C [%]	AOD_C [%]	Fay_C [%]	Fe_C [%]
Ye'elimite, cubic [58]	$Ca_4Al_6(SO_4)O_{12}$	19.7	26.2	23.8	27.2
Ye'elimite, orthorhombic [56]	$Ca_4Al_6(SO_4)O_{12}$	19.7	14	16.6	12.5
Ye'elimite total	$Ca_4Al_6(SO_4)O_{12}$	39.4	40.2	40.4	39.7
Belite, $\beta$ ([149])	$Ca_2(SiO_4)$	32.6	19.7	26.4	32.9
Belite, $\alpha'$ [150]	$Ca_2(SiO_4)$	1.8	3.2	7.5	1.2
Belite total	$Ca_2(SiO_4)$	34.4	22.9	33.9	34.1
Ferrite [66]	$Ca_2(Fe_2)O_5$	18.8	12.3	18.9	19.9
Anhydrite [151]	$Ca(SO_4)$	6.7	1.1	5.3	3.9
Mayenite [152]	$Ca_{12}Al_{14}O_{33}$	0.2	2.9	0	1.6
Fluorellestadite [44]	$Ca_5(SiO_4)_{1.5}(SO_4)_{1.5}F$	0	14	0	0
Periclase [153]	MgO	0.2	3.7	1	0.7
Silicon Dioxide [154]	$SiO_2$	0.3	0.4	0.5	0.2
Iron (III) oxide [155]	$Fe_2O_3$	0	2.3	0	0
Total		100	100	100	100
$R_{wp}$ [%]		5.3	4.4	5	5
S value		2.7	3.6	3.9	3.9

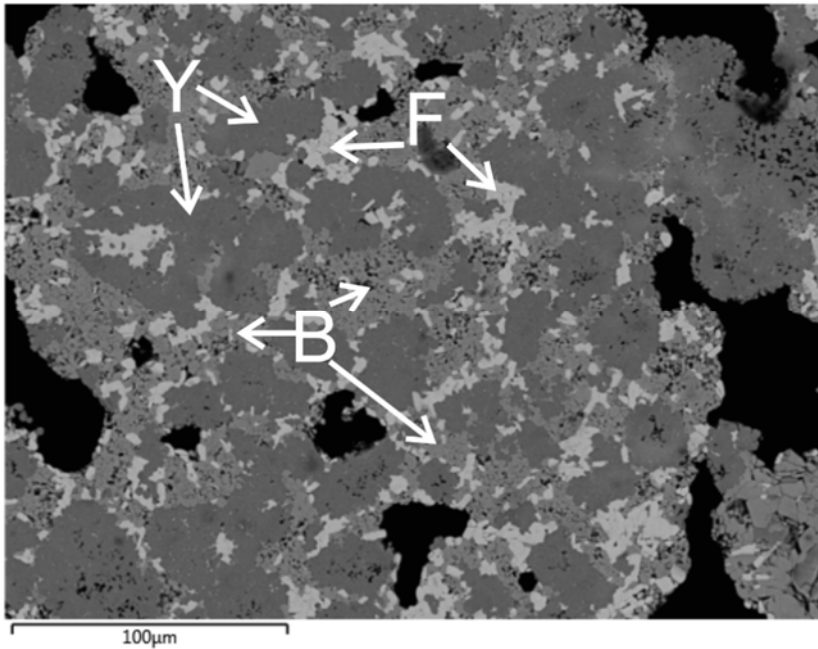


**Fig. 6.** FESEM-BSE image of reference clinker (RG\_C). F: ferrite, Y: ye'elimite, and B: belite (adapted under CC BY 4.0 license from Paper I © 2020 Authors).

#### **4.1.2 Chemical composition**

The chemical composition of the clinkers produced in Paper I were analyzed with XRF, and the results are presented in Table 18. The original target oxide composition was 48.6 wt.% CaO, 20.3 wt.% Al<sub>2</sub>O<sub>3</sub>, 12.2 wt.% SiO<sub>2</sub>, 10 wt.% Fe<sub>2</sub>O<sub>3</sub>, and 9 wt.% SO<sub>3</sub>. The clinkers produced from industrial byproducts had various impurities, of which MgO was the most notable.

**Table 18. XRF of clinkers produced in Paper I.**

Oxides	RG_C	AOD_C	Fay_C	Fe_C
CaO	47.97	45.82	47.33	46.67
Al <sub>2</sub> O <sub>3</sub>	19.56	18.86	19.44	19.18
SiO <sub>2</sub>	12.22	11.95	12.56	12.60
Fe <sub>2</sub> O <sub>3</sub>	10.46	9.79	10.25	10.57
SO <sub>3</sub>	8.39	8.31	8.16	8.25
MgO	0.26	3.59	1.28	0.98
BaO	0.00	0.00	0.01	0.09
Cl	0.06	0.12	0.13	0.11
Cr <sub>2</sub> O <sub>3</sub>	0.02	0.23	0.09	0.09
CuO	0.00	0.02	0.06	0.10
K <sub>2</sub> O	0.00	0.06	0.10	0.13
MnO	0.00	0.12	0.02	0.19
Na <sub>2</sub> O	0.00	0.09	0.17	0.80
NiO	0.01	0.05	0.12	0.07
P <sub>2</sub> O <sub>5</sub>	0.01	0.00	0.02	0.07
SrO	0.05	0.05	0.05	0.08
TiO <sub>2</sub>	0.01	0.17	0.01	0.10
ZnO	0.03	0.04	0.03	0.19
ZrO <sub>2</sub>	0.00	0.01	0.01	0.02
Total	99.06	99.27	99.83	100.29

#### **4.1.3 Effect of impurities**

The impurities of each phase present in the produced clinkers in Paper I were analyzed with FESEM-EDX, and the impurities found are listed in Table 19. It was found that all the phases had impurities present. The impurities are known to stabilize high temperature forms of C<sub>2</sub>S ( $\beta$ -C<sub>2</sub>S,  $\alpha$ -C<sub>2</sub>S, or  $\alpha'$ -C<sub>2</sub>S) over  $\gamma$ -C<sub>2</sub>S [18], [48], [50], [156]–[158]. In the present study, it was found that larnite (C<sub>2</sub>S) was the most abundant. Na, Mg, K, Ti, Mn, and Cr were present in the ferrite phase, which are typical impurities in ferrite phases appearing in cements [70], [159]. Ye’elimite had iron as an impurity, which is known to stabilize the cubic or pseudocubic structure of ye’elimite [57], [160]. However, in XRD analysis, the orthorhombic form of ye’elimite was also present. Fluorine originating in AOD slag led to melting during the firing and formation of the fluorellestadite phase, which is related to the fluxing effect of fluorine [85], [87].

**Table 19. Impurities detected with FESEM-EDX in the clinkers produced from sidestreams.**

Phase/clinker	AOD_C	Fay_C	Fe_C
Ye'elimite (C <sub>4</sub> A <sub>3</sub> S)	Mg, K, Fe	Mg, K, Fe	Na, Fe
Larnite (β-C <sub>2</sub> S)	Al, Mg, Fe, S	Al, Mg, Fe, S	Al, P, Na, Mg, Fe, S
Ferrite C <sub>2</sub> (AF)	Mg, K, Ti, Mn, Cr	Na, Mg, K	Mg, Na, Ti, Mn
Periclase (MgO)	Fe, Ni	Fe, Ni, Co	Zn, Ni

## 4.2 CSAB(F) clinker production in pilot demonstration

In Paper I, it was proven that industrial byproducts can be used as alternative raw materials for CSAB clinker. Additionally, ladle slag and phosphogypsum as raw materials for CSAB cement production were studied in [122]. It was unclear whether the weighting and mixing led to the correct chemical composition, and whether some of the material might be lost in the airflow caused by the burner in the pilot kiln. A sensitivity analysis was therefore conducted at laboratory scale to find a target recipe with safe limits to prevent the formation of unwanted phases such as gehlenite. The target phase composition (45 wt.% C<sub>4</sub>A<sub>3</sub>S, 36 wt.% C<sub>2</sub>S, 15 wt.% C<sub>2</sub>(A,F), 2 wt.% C<sub>S</sub> and 2 C) was selected through the results obtained from the sensitivity analysis described in Section 4.2. The mixing and granulation of raw materials (Fe slag, ladle slag, phosphogypsum, limestone, and clay) were conducted with a mixer equipped with a star pin rotor (R11, Eirich, Germany) in 150 kg batches. The pilot demonstration was conducted in a directly heated 7-meter rotary kiln with a counter current flow described in Section 3.2.4. Virgin raw materials for CSABF cement, such as limestone, clay, and bauxite, were 85% replaced by industrial sidestreams. The CO<sub>2</sub> emissions associated with the raw mix in the produced CSAB(F) were only 51 kg/t of CO<sub>2</sub>, which is 90% lower than that of Portland cement made from virgin raw materials. A total of 240 kg of clinker was produced in the demonstration. After the pilot demonstration, a small quantity of granules was ground and refired in a muffle furnace and analyzed with XRD and SEM analysis to ensure that the PSD of raw materials did not affect the final clinker mineralogy.

### 4.2.1 Granules

The chemical composition required to form the target phase composition is 49.7 wt.% CaO, 25.7 wt.% Al<sub>2</sub>O<sub>3</sub>, 12.5 wt.% SiO<sub>2</sub>, 7.1 wt.% SO<sub>3</sub>, and 4.9 Fe<sub>2</sub>O<sub>3</sub>. The



XRF analysis presented in Table 20 shows that impurities, mostly MgO, from the byproducts diluted the quantity of oxides required for cementitious phase formation. To show the ratio of cement oxides without impurities, the major oxides were also normalized to 100%.

**Table 20. Oxide composition obtained by the XRF analysis of dried granules. LOI of the granules at 950 °C was 17.5 wt.% (adapted under CC BY 4.0 license from Paper III © 2022 Authors).**

Major oxides [wt.%]	Granules	Granules normalized to major oxides
CaO	43.3	45.2
Al <sub>2</sub> O <sub>3</sub>	21.5	22.4
SiO <sub>2</sub>	12.3	12.8
Fe <sub>2</sub> O <sub>3</sub>	6.6	6.9
SO <sub>3</sub>	7.2	7.5
MgO	4.9	5.1
TiO <sub>2</sub>	0.8	0
MnO	0.7	0
Na <sub>2</sub> O	0.4	0
P <sub>2</sub> O <sub>5</sub>	0.2	0
Sum	98.41	100

<sup>1</sup>The oxides/elements with quantities <0.1 were Cr<sub>2</sub>O<sub>3</sub>, K<sub>2</sub>O, SrO, Cl, BaO, Nb<sub>2</sub>O<sub>5</sub>, NiO, CuO, ZrO<sub>2</sub>, ZnO, and Co<sub>3</sub>O<sub>4</sub>.

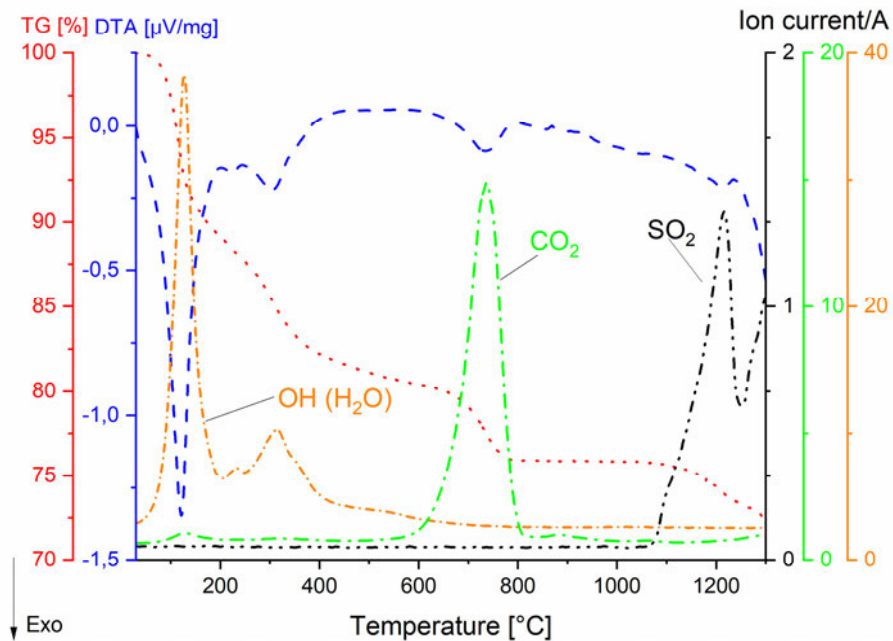


**Fig. 7. DTA-TG curves from raw meal granules with a mass spectrometry analysis of H<sub>2</sub>O, CO<sub>2</sub>, and SO<sub>2</sub> gases. Argon atmosphere and a heating ramp of 10 °C/min between 30–1300 °C were used (under CC BY 4.0 license from Paper III © 2022 Authors).**

DTA-TG-MS was conducted to analyze/simulate the behavior of granules during clinkering, and the DTA-TG and mass spectrometer curves are presented in Fig. 7. According to the mass spectrometer ( $m/z = 17(\text{OH})$ ), the endothermic peaks in the DTA curve below 200 °C are associated with water loss as H<sub>2</sub>O and later hydrates (OH). Part of the mass loss through water evaporation is associated with the decomposition of gypsum, first to hemihydrate and then to anhydrite [161]. The total mass loss associated with moisture and crystalline water below 500 °C was 20 wt.%. The decomposition of limestone can be detected as CO<sub>2</sub> ( $m/z = 44(\text{CO}_2)$ ) loss between 600 °C and 800 °C, with the highest intensity at around 700 °C. The total mass loss through CO<sub>2</sub> loss was around 5 wt.%. The decomposition of anhydrite (from phosphogypsum) can be detected as sulfur loss ( $m/z = 64(\text{SO}_2)$ ), which starts at 1100 °C and has the highest intensity at 1215 °C [161]. The second peak of sulfur loss was detected at 1250 °C, which may indicate the start of partial melting and decomposition of ye'elite, which releases SO<sub>2</sub> and O<sub>2</sub> [90], [162].

The total mass loss of raw meal according to the TG curve (30–1300 °C) was around 25 wt.%.

#### **4.2.2 Ground and mixed clinker**

The granules were fired in a pilot kiln according to the procedure explained in Section 3.2.4, and the grinding and mixing with the quartering method is explained in Section 3.2.1. The grinding of pilot clinker was continued until 87.5% of the particles passed through a 45 µm sieve, and the median particle size value ( $d_{50}$ ) of the pilot clinker was measured with laser diffraction at 6.78 µm. The density of the produced clinker was measured with a pycnometer at 3.155 g/cm<sup>3</sup>, and Blaine fineness at 3300 cm<sup>2</sup>/g. The ground clinker was stored in closed plastic buckets at normal room temperature.

#### **4.2.3 Chemical composition of clinker**

The chemical composition of the clinker was measured using XRF, and the results were compared with the XRF analysis of the granules in Table 21. The Rietveld analysis was also back-calculated to oxide abundances, and it was found that the phases and their content in Rietveld analysis were adequate. A comparison of the XRF results of granules and clinker showed that the sulfur content of clinker was reduced compared to the granules. The sulfur content can be explained by the decomposition of anhydrite (gypsum) during the firing and decomposition of ye'elimite, which can be demonstrated in the DTA-TG-MS analysis in Section 4.3.1. The iron content increased in the final clinker compared to the granules, this can be explained with the airflow in the kiln that carries some of the lighter component to the kiln inlet material, which leads to a concentration of heavier iron-bearing raw materials in the final clinker. As was previously mentioned, 20% of the raw material feed was carried to the kiln inlet. MgO was the highest impurity in the clinker, but the clinker otherwise contained only a small quantity of impurities.

**Table 21. Comparison of the normalized amount of target oxides between the granules and the clinker based on XRF analysis (under CC BY 4.0 license from Paper III © 2022 Authors).**

Oxide	Rietveld [wt.%]	Granules [wt.%]	Clinker [wt.%]
CaO	42	43.3	42.3
Al <sub>2</sub> O <sub>3</sub>	24.7	21.5	20.9
SiO <sub>2</sub>	13.9	12.3	12.5
Fe <sub>2</sub> O <sub>3</sub>	5.6	6.6	9.7
SO <sub>3</sub>	6.5	7.2	5.2
MgO	4.8	4.9	4.8
TiO <sub>2</sub>	1.1	0.8	0.8
MnO		0.7	0.8
Na <sub>2</sub> O		0.4	0.3
Sum		98.41	98.1

<sup>1</sup>The oxides/elements with quantities <0.1 were P<sub>2</sub>O<sub>5</sub>, Cr<sub>2</sub>O<sub>3</sub>, K<sub>2</sub>O, SrO, Cl, BaO, Nb<sub>2</sub>O<sub>5</sub>, NiO, CuO, ZrO<sub>2</sub>, ZnO, and Co<sub>3</sub>O<sub>4</sub>.

#### 4.2.4 Mineralogy of clinker

The phase composition of the ground and mixed clinker (pilot clinker) was determined with XRD analysis, and the composition was compared to a clinker (reference clinker) prepared from ground granules and fired in the laboratory furnace. The results of the Rietveld analysis are shown in Table 22. The XRD diffractograms with phase identification are presented in Fig. 8.

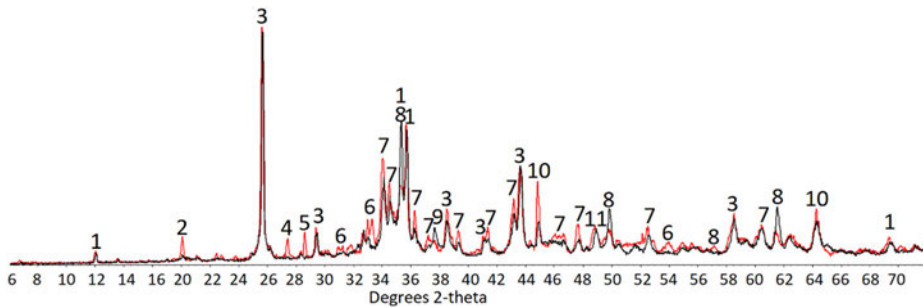


**Fig. 8. XRD pattern of CSABF pilot clinker (red line) with phase identification and the reference sample prepared in a laboratory furnace from ground granules (black line). 1: C<sub>2</sub>(A,F), 2: C<sub>12</sub>A<sub>7</sub>, 3: C<sub>4</sub>A<sub>3</sub>\$, 4: C\$, 5: SiO<sub>2</sub>, 6: C<sub>2</sub>AS, 7: C<sub>2</sub>S, 8: C<sub>3</sub>A, 9: Al<sub>2</sub>O<sub>3</sub>, 10: MgO, 11: K<sub>2</sub>SO<sub>4</sub> (under CC BY 4.0 license from Paper III © 2022 Authors).**

**Table 22. Phase composition of mixed pilot clinker analyzed with the Rietveld method. The error of analysis and quality of the analysis  $R_{wp}$  were obtained from analysis software (under CC BY 4.0 license from Paper III © 2022 Authors).**

Phase	Reference	Pilot Clinker [wt.%]	Target phases [wt.%]	Reference clinker [wt.%]
$C_4A_3\$$	[58]	31.3	45.0	34.4
$C_2S$	[163]	28.9	36.0	25.9
$C_2(A,F)$	[66]	8.7	15.0	9.1
$C\$$	[151]	1.7	2.0	1.7
$C_{12}A_7$	[152]	2.0	0.0	0.1
$C_2AS$	[164]	6.1	0.0	1.9
M	[165]	4.4	0.0	3.4
S	[154]	1.4	0.0	1.4
$Ca_3Ti(Fe,Al)$	[166]	0.6	0.0	0.2
$C_3A$	[167]	5.3	0.0	9.3
$K_2SO_4$	[168]	2.6		2.6
A	[169]	0.2		0.1
$C_2F$	[66]	2.7		4.2
CT	[170]	0.2		0.4
Spinel (TF)	[171]	1.6		3.5
$C_3MS_2$	[172]	2.4		4.6
C		0.0	2.0	0.0
Amorphous		2.7 <sup>1</sup>	0.0	n.d.
$R_{wp}$ [%]		14		17

<sup>1</sup>Amorphous content was analyzed with a separate sample with an internal standard.

The analysis indicates that in the pilot clinker some more unreacted or intermediate phases are present, i.e., mayenite, gehlenite, anhydrite, and quartz, but the major phase composition is not drastically affected by the large particle size of the raw materials. The amorphous content of pilot clinker was analyzed with an internal standard and was found to be very low. The major phases of the clinker were identified to be ye'elimite  $C_4A_3\$$ , belite  $C_2S$ , and ferrite  $C_2(A,F)$ , and the minor phases were gehlenite  $C_2AS$ , tricalcium aluminate  $C_3A$ , anhydrite  $C\$$ , mayenite  $C_{12}A_7$ , periclase  $MgO$ , quartz  $SiO_2$ , potassium sulfate  $K_2SO_4$ , Spinel (TF), and åkermanite  $C_3MS_2$ . The target oxides needed to form hydraulic cement phases consisting of around 90 wt.% of all the produced phases.

In the diffractogram presented in Fig. 8, ye'elimite ( $C_4A_3\$$ ) was identified as having an orthorhombic structure [58]. The orthorhombic structure can only have a minor iron substitution [57], [160]. The finding of ye'elimite's low iron content was confirmed with EDX analysis (Table 23). Belite ( $C_2S$ ) was present as  $\beta$ -

polymorph (larnite). The  $\beta$ - $C_2S$  is stabilized by minor elements from industrial byproducts [156], which prevents the existence of low-temperature  $\gamma$ - $C_2S$ . The ferrite phase was found to have the best fit with the iron-rich variable of the brownmillerite-srebrodolskite series [66]. The major transitory phases and artifacts from raw materials were gehlenite, mayenite, and tricalcium aluminate ( $C_3A$ ). The only MgO-bearing phase formed was åkermanite ( $C_3MS_2$ ), and with EDX, it could be detected that Mg was substituted for cement phases in minor amounts, but most of the MgO from raw materials did not incorporate and was present as periclase (free MgO). Tricalcium aluminate in final clinker is partly artifacts from unreacted ladle slag, and part of it may have formed during firing. In the EDX analysis (Fig. 9), it was seen that  $C_3A$  was directly intergrown with ye'elimite and belite, which indicates it was part of the formed clinker phases. Mayenite was clearly detected with XRD but was not found by the EDX analysis.

The confirmation of the phases in the XRD analysis was conducted with FESEM-EDX analysis, which is shown in Fig. 8. The sizes of the individual clinker phases were small—below 5–10  $\mu\text{m}$  in diameter—which required high-resolution EDX mapping data to determine the composition of the individual phases.

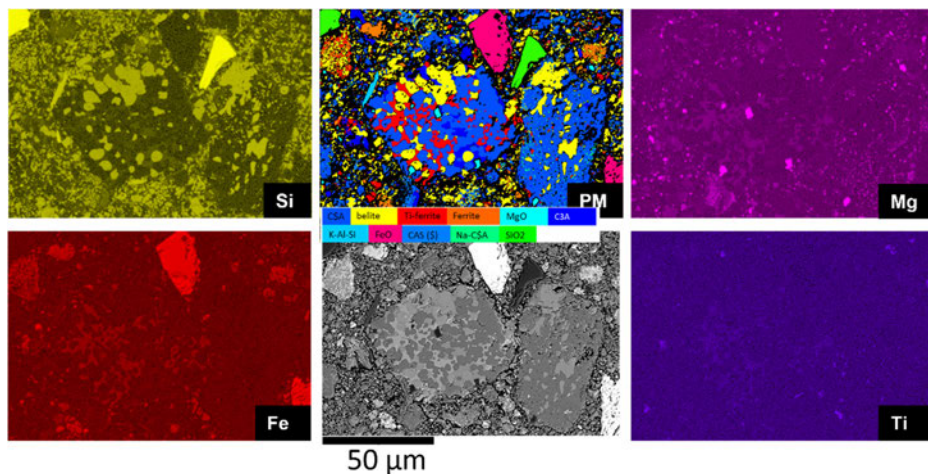


**Fig. 9. Results of the EDX mapping analysis at an acceleration voltage of 7 kV: Elemental distribution maps were used to segment the phase maps (PM) of each major phase's ye'elimite, belite, Ti-ferrite, ferrite,  $C_3A$ , and MgO. The phase distribution maps shown have a pixel resolution of 100 nm (under CC BY 4.0 license from Paper III © 2022 Authors).**

The phase map was gathered using the phase clustering algorithm implemented in the software (Aztec 4.3, Oxford Instruments, UK). The amount of the phase was reduced by merging similar phases into one phase. The major phases were ye'elimite, belite, ferrite, and periclase. Ferrite was also detected with a variable with an increased titanium content, which is part of a brownmillerite-perovskite ( $\text{Ca}_2(\text{Fe}_{1-x}, \text{Al}_x)_2\text{O}_5 - \text{CaTiO}_2$ ) series.  $\text{C}_3\text{A}$  and Ca-Al-Si-S phase (CAS(\$)) were detected intergrowth with ye'elimite and belite. (CAS(\$)) is probably a transitory phase, and due to its small crystal size, the determination of its chemical composition may have been disrupted because of neighboring phases. The unreacted or partially reacted artifacts/impurities from raw materials were FeO, K-Al-Si-oxide,  $\text{C}_3\text{A}$ , and  $\text{SiO}_2$ . To acquire the chemical composition of the phases, a spot analysis was conducted for the analysis area presented in Fig. 9. The results of the analysis are presented in Table 23. The data were collected from 10 spots of each major phase from the middle of the crystal to prevent overlapping with neighboring phases. Additionally, sum spectra were collected from ferrite, Ti-ferrite, and ye'elimite with Na substitution. The sum spectra from all areas are segmented and therefore have more X-ray counts than spot analysis, thus providing a quantification of the minor elements.

**Table 23. Average chemical composition (given in oxide wt.%) of the clinker phases from EDX spot analyses (7 kV acceleration voltage using a cobalt standard for calibration). The spot analysis was deduced from Fig. 9 (adapted under CC BY 4.0 license from Paper III © 2022 Authors).**

Phase/oxide	Al	Ca	Fe	Mg	Mn	Na	P	S	Si	Ti
Point spectra										
Ye'elimite	49.9	35.4	0	0	0	0	0	14.6	0	0
Std. deviation	0.7	0.8	0	0	0	0	0	0.7	0	0
Belite	2.4	63.3	0.8	0.0	0	0.3	0.04	3.1	30.0	0
Std. deviation	0.3	0.8	1.03	0.06	0	0.14	0.1	0.6	1.1	0
Ferrite	6.5	37.25	52.59	0.77	0	0.04	0	0	2.8	0
Std. deviation	1.2	1.88	2.48	0.44	0	0.09	0	0	0.8	0
Ti-Ferrite	20.31	43.82	25.99	2.76	0	0.08	0.02	0.15	1.7	5.67
Std. deviation	3.84	1.21	8.31	0.95	0	0.15	0.07	0.51	0.53	6.71
$\text{C}_3\text{A}$	40.17	52.1	4.68	0.74	0	0.06	0	0.2	2.12	0
Std. deviation	7.83	6.59	2.98	0.83	0	0.09	0	0.46	1.31	0
Sum spectra										
Na-Ye'elimite	49.03	35.28	1.88	0.12		0.28	0.99	12.38	0	0
Ferrite	7.56	36.05	48.99	1.08	0	0.1	0.00	0.60	2.95	2.66
Ti-Ferrite	21.67	39.90	23.31	2.26	4.92	0.06	0.07	1.55	1.63	4.63

The chemical composition analysis (Table 23) shows that in addition to major elements, all the clinker phases contained minor elements causing deviation from an ideal phase composition.

#### 4.2.5 Effect of minor elements on phases

The XRD and FESEM-EDX analyses in the previous chapter introduced the fact that minor elements from industrial byproducts led to the formation of phases outside the target phase composition. The effect of minor elements on phases is discussed in more detail in this chapter.

According to EDX spot analysis, in general ye'elimite did not have a significant substitution of minor elements, and this indicates that most of the ye'elimite in the clinker was orthorhombic. Minor quantities of Na-, Fe-, and S-enriched ye'elimite could be detected. Iron substitution in ye'elimite leads to a pseudocubic structure [57]. Impurities are known to stabilize high temperature forms  $\beta$ -C<sub>2</sub>S,  $\alpha$ -C<sub>2</sub>S, or  $\alpha'$ -C<sub>2</sub>S over the low-temperature form  $\gamma$ -C<sub>2</sub>S [48], [50], [156]–[158], which is beneficial for hydration properties, as  $\gamma$ -C<sub>2</sub>S is known to have poor hydraulic properties. The detected impurities in belite were Al, Fe, S, P, and Na. Three different types of belite could be determined with the EDX spot analysis presented in Table 24. It was found that the single crystals had different quantities of substitutions than the average compositions presented in Table 23. Belite-1 had a high sulfur content, which slightly exceeded the reported maximum solubility of sulfur for belite (2 wt.% as SO<sub>3</sub>) [42]. Belite-2 had much less substitution than belite-1. P-belite had a rather high phosphorus content, which indicates that most of the phosphorus from phosphogypsum is included in belite.

**Table 24. SEM EDX spot analyses of belite-a and belite-2 and P-belite (under CC BY 4.0 license from Paper III © 2022 Authors).**

Phase/oxide	Na <sub>2</sub> O	MgO	Al <sub>2</sub> O <sub>3</sub>	SiO <sub>2</sub>	P <sub>2</sub> O <sub>5</sub>	SO <sub>3</sub>	CaO	Fe <sub>2</sub> O <sub>3</sub>	CaO/SiO <sub>2</sub>
Belite-1	0.3		2.4	30		3.1	63.3		2.1
Std. deviation	0.1		0.3	1.1		0.7	0.8		
Belite-2			0.6	35.2			63.6		1.8
Std. deviation				1.1			0.5		
P-belite		1.2	0.3	32.5	2.8		63.2		1.9



The chemical composition obtained with EDX analysis was used to calculate an empirical formula for the ferrite phase that was most abundant in the clinker. The calculation showed that ferrite had a formula of  $C_2(A_{0.19}, F_{0.81})$ , which is close to  $C_6AF_2$ . The ferrite phase (brownmillerite) was enriched with impurities (Si, Na, Mn, and Mg) that are common for the ferrite phase in cements [159], [173]. The Ti-ferrite had higher alumina content than ferrite, and iron was substituted with titanium giving the formula  $C_2(A_{0.59}, F_{0.41})$ . It was found that Ti-ferrite was an intermediate phase, which is a mixture of perovskite-brownmillerite ( $CaTiO_3$ – $Ca_2(Fe,Al)_2O_5$ ) [174]. The minor elements found in titanium-rich ferrite phases were similar to the ferrite phase.

EDX analysis (Fig. 10) also confirmed gehlenite formation with other transitional phases. Mg-rich gehlenite is åkermanite, which could also be detected with XRD. Such assemblages with multiple non-cementitious phases originate as unreacted or partly reacted raw materials.

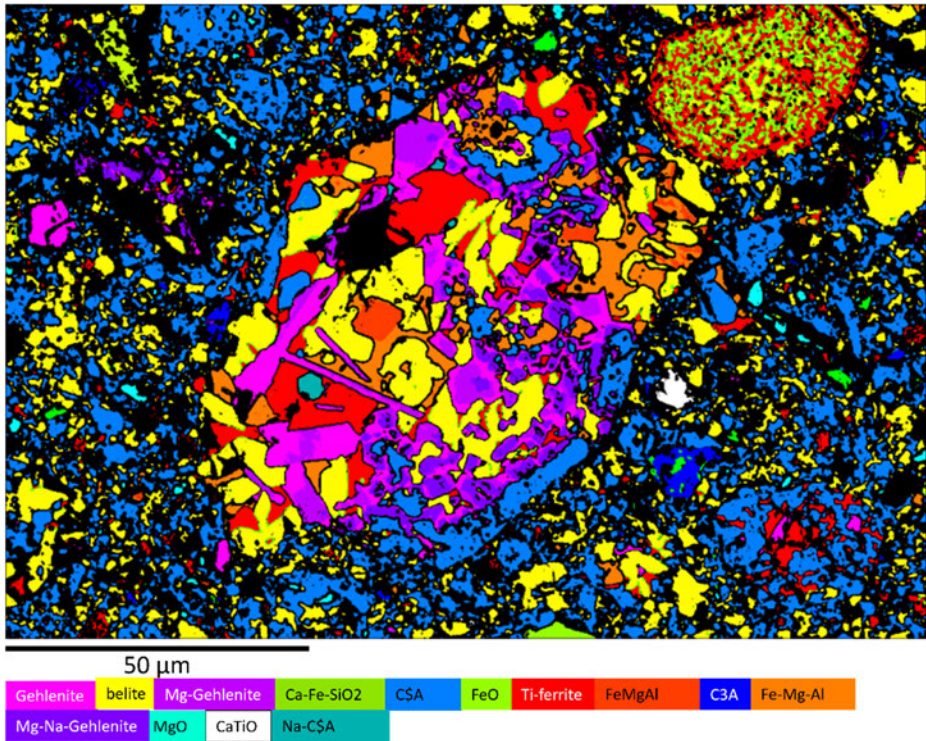


**Fig. 10.** Phase map from pilot clinker showing an area with transitional phases, i.e., gehlenite, Mg-rich gehlenite, and Ca-Fe-silicate (under CC BY 4.0 license from Paper III © 2022 Authors).

### 4.3 AYF clinker production in laboratory scale

In Paper I, it was proven that AOD slag was challenging to use to produce CSAB clinker. The reason was found to be fluorine, which causes the melting of the clinker and formation of fluorellestadite. A new approach was therefore taken in Papers II and IV to produce AYF clinker at 1260 °C, which is around 200 °C lower than the typical production temperature of alite. The production temperature was chosen for two reasons.

1. To prevent poorly hydraulic fluorellestadite. Fluorellestadite is reported to decompose at ~1250°C into C<sub>2</sub>S, SO<sub>2</sub>, O<sub>2</sub>, and a liquid phase [17], [85]–[87]. The temperature must therefore be above 1250 °C.

2. Ye'elinite decomposes in normal processing conditions at temperatures above 1300°C [61], [90], [175]. The production of AYF is therefore limited to a temperature range of 1250–1300 °C

The target phase compositions and raw material mix chemical compositions are presented in Table 25. The idea was first to test how different fluorine content affected the phase formation of target composition 50 wt.% C<sub>3</sub>S, 30 wt.% C<sub>4</sub>A<sub>3</sub>Ŝ, and 20 wt.% C<sub>4</sub>AF. The effect of altering the target ferrite (C<sub>4</sub>AF) and alite (C<sub>3</sub>S) and C<sub>4</sub>AF and C<sub>4</sub>A<sub>3</sub>\$ content was then tested with fixed fluorine content. Fluoride content was adjusted according to the formula (Ca<sub>3</sub>Si<sub>1-x</sub>Al<sub>x</sub>O<sub>5-x</sub>F<sub>x</sub>) by changing the value of X. The formula was adapted from the study, in which it was found that alite could be produced at low temperatures if fluorine and alumina were present [39]. The selected range of XRD patterns from test series 1 to show the peaks of alite (C<sub>3</sub>S) and free lime (CaO) (Fig. 11 a&b).

**Table 25. The target phase compositions and raw material mix chemical compositions of test series 1–3. X presents fluoride content in the formula ( $\text{Ca}_3\text{Si}_{1-x}\text{Al}_x\text{O}_{5-x}\text{F}_x$ ) (adapted under CC BY 4.0 license from Paper II © 2021 Authors).**

Series /sample	Target compositions			Raw material mix compositions						
	C <sub>3</sub> S	C <sub>4</sub> A <sub>3</sub> \$	C <sub>4</sub> AF	C	S	A	F	C\$	CaF <sub>2</sub>	X
Series 1										
X = 0	50	30	20	54.36	13.16	19.23	6.57	6.68	0.00	0.00
X = 0.025	50	30	20	54.24	13.13	19.19	6.56	6.67	0.21	0.025
X = 0.0375	50	30	20	54.18	13.12	19.17	6.55	6.66	0.32	0.0375
X = 0.075	50	30	20	54.01	13.08	19.1	6.53	6.64	0.64	0.075
X = 0.15	50	30	20	53.66	12.99	18.98	6.49	6.6	1.29	0.15
X = 0.225	50	30	20	53.31	12.91	18.86	6.45	6.55	1.93	0.225
X = 0.3	50	30	20	52.95	12.82	18.73	6.4	6.51	2.58	0.30
Series 2										
0 C <sub>4</sub> AF	50	50	0	50	12.99	24.73	0	10.99	1.29	0.15
2.5 C <sub>4</sub> AF	50	47.5	2.5	50.45	12.99	24.01	0.81	10.44	1.29	0.15
5 C <sub>4</sub> AF	50	45	5	50.91	12.99	23.29	1.62	9.89	1.29	0.15
7.5 C <sub>4</sub> AF	50	42.5	7.5	51.37	12.99	22.57	2.43	9.35	1.29	0.15
10 C <sub>4</sub> AF	50	40	10	51.83	12.99	21.86	3.25	8.8	1.29	0.15
12.5 C <sub>4</sub> AF	50	37.5	12.5	52.28	12.99	21.14	4.06	8.25	1.29	0.15
15 C <sub>4</sub> AF	50	35	15	52.74	12.99	20.42	4.87	7.7	1.29	0.15
17.5 C <sub>4</sub> AF	50	32.5	17.5	53.2	12.99	19.7	5.68	7.15	1.29	0.15
Series 3										
0 C <sub>4</sub> AF	70	30	0	53.89	17.45	14.23	0	13.11	1.32	
5 C <sub>4</sub> AF	65	30	5	52.59	16.2	15.23	1.56	13.11	1.32	
10 C <sub>4</sub> AF	60	30	10	51.29	14.95	16.22	3.11	13.11	1.32	
15 C <sub>4</sub> AF	55	30	15	49.98	13.71	17.21	4.67	13.11	1.32	
20 C <sub>4</sub> AF	50	30	20	48.68	12.46	18.21	6.22	13.11	1.32	
25 C <sub>4</sub> AF	45	30	25	47.38	11.21	19.2	7.78	13.11	1.32	
30 C <sub>4</sub> AF	40	30	30	46.07	9.97	20.19	9.34	13.11	1.32	
35 C <sub>4</sub> AF	35	30	35	44.77	8.72	21.19	10.89	13.11	1.32	
40 C <sub>4</sub> AF	30	30	40	43.46	7.48	22.18	12.45	13.11	1.32	

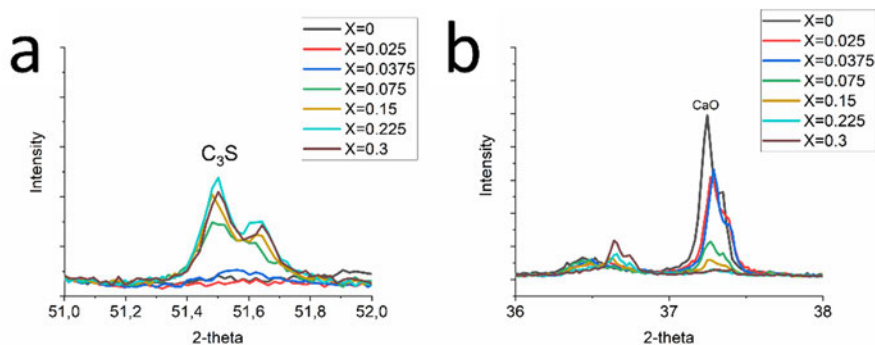


**Fig. 11.** XRD-patterns (51–52° and 36–38°) of a) 2-theta 51.4–51.6° alite ( $C_3S$ ), and b) 2-theta 37–37.5° CaO of test series 1. (Adapted under CC BY 4.0 license from Paper II © 2021 Authors)

It is observed that alite forms at 1250 °C only if there is enough fluorine (Fig. 11a) as mineralizer ( $X < 0.075$ ), and with insufficient fluorine in the raw mix, there is no mineralization effect leading to unreacted free CaO (Fig. 11b) in clinker. It was detected that fluorellestadite content increased with increasing fluorine content  $X < 0.15$  (see Appendix 3), and the formation of fluorellestadite consumed sulfur designed for ye'elimite. With increasing fluorine content, ye'elimite content in final clinker therefore decreased and led to the formation of mayenite instead. It was observed that with increasing fluorine content, the samples were denser, which indicates at least partial melting in the samples. The optimization of fluorine content is important to avoid melting in the kiln because melting is harmful in the kiln and makes the clinker stick to kiln refractories, which may block the kiln. It was found in test series 2 and 3 that without iron in the raw mix, alite can form, but there was free lime because burnability was too low (Appendix 3). The adequate iron content in the raw mix was achieved when  $C_4AF$  content was 10 wt.% or more in the raw mix. Sulfur was found to stabilize belite over alite [42], and the formation of belite could therefore not be avoided. To summarize the optimal amount of fluorine with a target composition of 50 wt.%  $C_3S$ , 30 wt.%  $C_4A_3S$ , and 20 wt.%  $C_4AF$  was between  $0.075 < X < 0.15$  in  $Ca_3Si_{1-x}Al_xO_{5-x}F_x$ .

#### 4.3.1 Effect of industrial byproducts

Prior to the pilot demonstration, a clinker was prepared at laboratory scale according to the target phase composition presented in Table 13. The target phase

composition was acquired through the findings of Paper II that fluorine content should be targeted at  $X=0.15$  in the equation  $(Ca_3Si_{1-x}Al_xO_{5-x}F_x)$ ,  $C_4AF$  should be at least 10 wt.%, and belite cannot be avoided because of sulfur. It was thereby added to the target phases to avoid unreacted raw materials. The phase composition was selected to be 30 wt.%  $C_3S$ , 30 wt.%  $C_2S$ , 29 wt.%  $C_4A_3S$ , 10 wt.%  $C_4AF$ , and 1 wt.%  $CS$ . The recipe was tested with 20 wt.% of AOD slag in the raw mix with natural raw materials and other industrial byproducts. It was assumed that 20 wt.% AOD slag (Table 6) has enough fluorine for the mineralizing effect. Moreover, some pre-testing was conducted with AOD slag content between 15 and 25 wt.%, which is not reported in this study. The XRD analysis results of clinker prepared prior to pilot is presented in Table 26.

**Table 26. XRD Rietveld results of laboratory-scale pre-testing (Paper IV). The error of analysis and quality of the analysis  $R_{wp}$  was 3.1%. The XRD pattern is presented in (Appendix 4 Fig. A5).**

Phase	C <sub>4</sub> A <sub>3</sub> \$	C <sub>3</sub> S	C <sub>2</sub> S	C <sub>2</sub> (A,F)	C <sub>12</sub> A <sub>7</sub>	M	C <sub>2</sub> AS	F-ell
Reference	[58]	[176]	[163]	[66]	[152]	[165]	[164]	[44]
Pre LAB	12.1	24	28.8	13.7	6.2	5	3.6	6.7

The XRD analysis proved that major-phase alite (C<sub>3</sub>S), belite (C<sub>2</sub>S), ye'elimite (C<sub>4</sub>A<sub>3</sub>\$), and ferrite C<sub>2</sub>(A,F) could be produced, but the minor phases C<sub>12</sub>A<sub>7</sub> periclase (M) and fluorellestadite (F-ell) were also present. The pre-test results indicated that fluorine from AOD slag could be used to achieve a mineralizing effect to form alite (C<sub>3</sub>S) similar to when pure CaF<sub>2</sub> is used. Because fluorellestadite was forming, it was decided that the pilot would be started with recipe PIL A (Table 15), which had an AOD slag content of 17.5 wt.% in a “dry mix” (i.e., without LOI, moisture, and added water). As is explained in Section 4.5, alite did not form in the pilot demonstration, and the results of the pilot demonstration were therefore not in line with the pre-testing at laboratory scale. The laboratory testing was repeated after piloting with the same raw mix presented in Table 13, but this time the AOD slag was the same as in the pilot demonstration (Table 7). The XRD analysis of clinker produced after piloting using the same AOD slag as in pilot is presented in Table 27. It was clearly seen that C<sub>3</sub>S was not detected, so it was concluded that there was an inadequate amount of fluorine in the AOD slag, or some other properties of the slag differed, as with the slag used for the pre-testing.

**Table 27. XRD Rietveld results of clinker prepared in the laboratory from AOD slag used for the pilot (Paper IV). The error of analysis and quality of the analysis  $R_{wp}$  were obtained from analysis software and was 3.5%. The XRD pattern is presented in Appendix 4.**

Phase	C <sub>4</sub> A <sub>3</sub> \$	C <sub>3</sub> S	C <sub>2</sub> S	C <sub>2</sub> (A,F)	C <sub>12</sub> A <sub>7</sub>	M	C <sub>2</sub> AS	F-ell
Reference	[58]	[176]	[163]	[66]	[152]	[165]	[164]	[44]
After LAB	7.3	0	39	12.6	17.2	6.5	8.8	8.6

#### 4.4 AYF clinker production in pilot demonstration

Because fluorine played a crucial role for AYF clinkers in Paper IV, an EDX analysis was conducted for the AOD slag presented in Table 7 to determine the existence of fluorine-bearing and other major phases. The identification of major phases of AOD slag and major impurities is shown in Fig. 12. An XRD analysis

was conducted to show that the XRD patterns of AOD slags in Table 6 (Papers I & pre-test Paper III) and Table 7 (Paper III pilot) were very similar (Appendix 5). The phases shown in the phase mapping were identified through the chemical composition acquired with the EDX analysis (Appendix 5). In Fig. 12, it is shown that fluorine is present in AOD slag in two different phases, cuspidine ( $C_4S_2(F,OH)_2$ ) and fluorite ( $CaF_2$ ). It was challenging to analyze the actual fluorine content in Tables 6 and 7 with the XRF analysis because the total content was low and close to the analysis method's detection limit.

It was shown in the pre-lab experiments that industrial byproducts could be used to produce clinker with the target phases 30 wt.% alite, 30 wt.% belite, 30 wt.% ye'elinite, and 10 wt.% ferrite. In the pilot demonstration, AOD slag, ladle slag, fayalitic slag, and phosphogypsum were used to produce three clinkers with increasing AOD slag content according to the recipes shown in Table 15. The clinkers were named PIL A, PIL B, and PIL C. Mixing, granulation, and firing were conducted similarly as for CSAB clinker, described in Section 4.3.



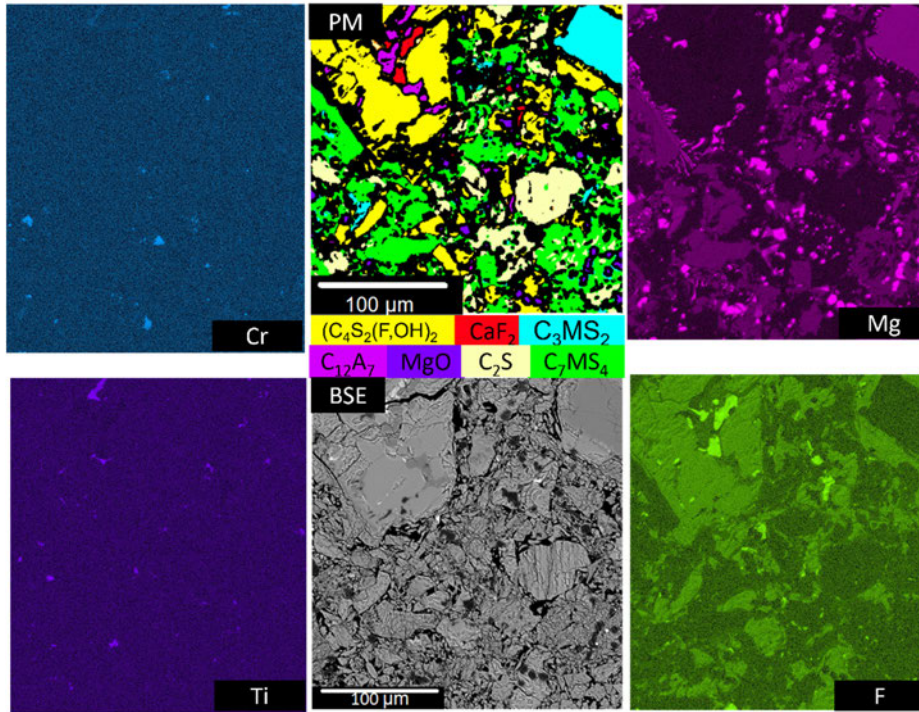


Fig. 12. SEM-BSE image and EDX mapping analysis of AOD slag (Paper IV). Elemental distribution maps were used to segment the phase maps (PM) of each major phase. The phase map (PM) reveals the following phases: yellow – cuspidine ( $C_4S_2(F,OH)_2$ ), red – fluorite ( $CaF_2$ ), cyan –merwinite ( $C_3MS_2$ ), magenta – mayenite ( $C_{12}A_7$ ), purple – periclase (MgO), cream –  $C_2S$  (belite), and green – bredigite ( $C_7MS_4$ ).

#### 4.4.1 Chemical composition of granules and clinker

The chemical composition of granules and fired clinkers are shown in Table 28. The most notable impurities from industrial byproducts were Mg, Ti, Mn, and Cr. Fluorine was only detected in PIL C granules, but it is noted that other granules and clinkers also contain fluorine, as was proven in Fig. 12 and in Section 4.5.3. The concentration of iron increased in all the clinkers during firing when compared to the granules. CaO and  $SO_3$  were lost during firing. The loss of CaO can be explained by the airflow in the kiln, and  $SO_3$  loss is explained through the decomposition of gypsum, which is shown in the DTA-TG-MS analysis (Fig. 13).

**Table 28. XRF analysis of granules and clinker (Paper IV). The original elemental wt.% obtained from the analysis was converted to oxides and normalized. The LOI of the granules was A: 24 wt.%; B: 21.6 wt.%, and C: 18 wt.% at 950 °C, and the LOI of clinkers was negligible.**

Analysis/oxide	Target		PIL A		PIL B		PIL C	
	Target	Target	XRF	XRF	XRF	XRF	XRF	XRF
	MgO		granules	clinker	granules	clinker	granules	clinker
CaO	56.9	53.7	53.6	51.3	52.8	49.5	50.5	50
Al <sub>2</sub> O <sub>3</sub>	16.5	15.6	14.1	15.1	13.5	14.7	14.3	14.6
SiO <sub>2</sub>	18.2	17.2	17.5	17.3	17.4	17.4	17.8	17.5
Fe <sub>2</sub> O <sub>3</sub>	3.3	3.1	3.5	5.5	4.7	7.2	4	5.7
SO <sub>3</sub>	4.4	4.1	4.3	3.7	4.4	3.7	5	3.8
MgO	0	5.6	5.1	5.1	5.4	5.3	5.9	6
BaO					<0.1		<0.1	
CaF <sub>2</sub>	0.76	0.7	0	0	0	0	0.82	0
Cl			0	0	0	0.1	0.1	0.1
Co <sub>3</sub> O <sub>4</sub>			0	<0.1	0	<0.1	<0.1	0
Cr <sub>2</sub> O <sub>3</sub>			0.2	0.2	0.2	0.2	0.2	0.3
CuO			<0.1	<0.1	<0.1	<0.1	<0.1	<0.1
K <sub>2</sub> O			0.2	0.2	0.2	0.1	0.1	0.1
MnO			0.3	0.5	0.4	0.5	0.5	0.6
Na <sub>2</sub> O			0.2	0.1	0.1	0.1	0.1	0.1
Nb <sub>2</sub> O <sub>5</sub>			<0.1	<0.1	<0.1	<0.1	<0.1	<0.1
NiO			<0.1	0.1	<0.1	0	<0.1	0.1
P <sub>2</sub> O <sub>5</sub>			0.1	0.1	0.1	0.1	0.1	0.1
SrO			0.1	0.1	0.1	0.1	0.1	0.1
TiO <sub>2</sub>	0	0	0.7	0.7	0.7	0.7	0.7	0.7
V <sub>2</sub> O <sub>5</sub>			0	0.1	0	0.1	0	0.2
ZnO			<0.1	0	0	<0.1	0	0
ZrO <sub>2</sub>			<0.1	<0.1	<0.1	<0.1	<0.1	<0.1
Total	100	100	100	100	100	100	100	100
F	0.5	0.4	0	0	0	0	0.4	0

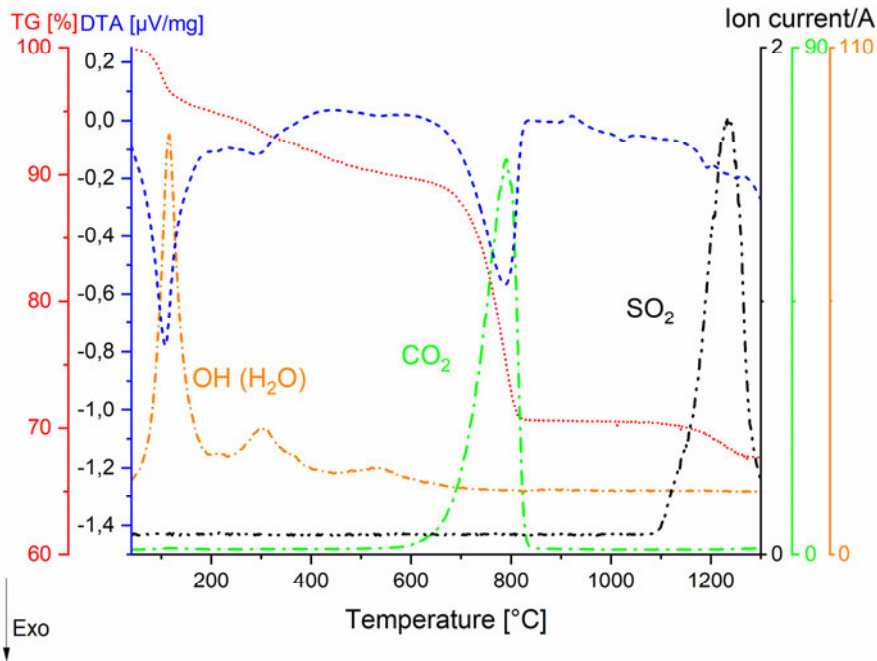


**Fig. 13.** DTA-TG-MS curves from the raw meal granules of PIL B with mass spectrometry analysis of H<sub>2</sub>O, CO<sub>2</sub>, and SO<sub>2</sub> gases (Paper IV). Argon atmosphere, 10 °C/min 30–1300 °C.

The peaks detected with mass spectrometry ( $m/z = 17(\text{OH})$ ) below 200 °C are associated with the evaporation of moisture and decomposition of gypsum first to hemihydrate and then to anhydrite (~170 °C) [161]. Because water was added to the granules, the existence and decomposition of hydrates such as C-S-H, monosulfate, and ettringite was also possible. The peaks at 300 °C and 530 °C are the decomposition temperatures of Al(OH)<sub>3</sub> [177] and kaolin[178] respectively. Limestone (CaCO<sub>3</sub>) decomposes at 800 °C ( $m/z = 44(\text{CO}_2)$ ). The sulfur loss at 1233 °C ( $m/z = 64(\text{SO}_2)$ ) is associated with the decomposition of anhydrite (phosphogypsum) [161]. The total mass loss between 30 and 1300 °C was 32 wt.%, of which H<sub>2</sub>O (OH) and CO<sub>2</sub> consisted of 10 wt.% and 20 wt.% respectively. It was noteworthy that the second sulfur loss peak was not observed as for CSAB clinker in Fig. 7. It is discussed that less iron in AYF compared to the CSAB clinker allows ye'elimite to remain stable at higher temperatures [12], [74], [162].

#### 4.4.2 Ground and mixed clinker

The grinding and mixing of AYF clinkers produced in the pilot kiln was conducted similarly as for CSAB clinker. The median particle sizes  $d_{50}$  for PIL A, PIL B, and PIL C were 5.5  $\mu\text{m}$ , 5.6  $\mu\text{m}$ , and 3.7  $\mu\text{m}$  respectively. The measured average densities for the PIL A, PIL B, and PIL C samples were 3.141  $\text{g}/\text{cm}^3$ , 3.165  $\text{g}/\text{cm}^3$ , and 3.181  $\text{g}/\text{cm}^3$  respectively.

#### 4.4.3 Mineralogy

The phase composition of PIL A, PIL B, and PIL C (Table 15) produced in the pilot kiln was determined with XRD analysis. XRD patterns of clinkers with phase identifications are shown in Fig. 14, and the phase quantities obtained with Rietveld analysis are shown in Table 29.

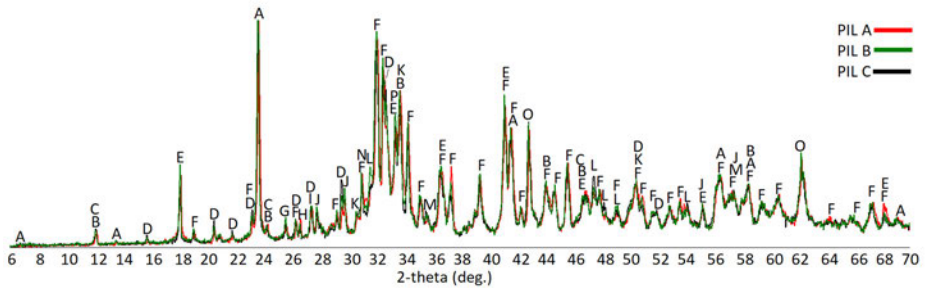


Fig. 14. XRD pattern of PIL A (red line), PIL B (green line), and PIL C (black line) pilot clinkers with phase identification (Paper IV). A:  $\text{C}_4\text{A}_3\text{S}$ , B:  $\text{C}_2(\text{A},\text{F})$ , C:  $\text{C}_2\text{F}$ , D:  $\gamma\text{-C}_2\text{S}$ , E:  $\text{C}_{12}\text{A}_7$ , F:  $\beta\text{-C}_2\text{S}$ , G:  $\text{C}\text{S}$ , H:  $\text{SiO}_2$ , I:  $\text{C}_2\text{AS}$ , J:  $\text{C}_3\text{A}$ , K:  $\text{C}_5\text{S}_2\text{S}$ , L:  $\text{CaF}_2$ , M: FT, N:  $\text{C}_2\text{MS}_2$ , O: MgO, and P: CT.

**Table 29. XRD analysis of reference clinkers produced in the laboratory furnace and pilot clinkers after firing, grinding, and mixing (Paper IV). The error of analysis and quality of the analysis  $R_{wp}$  were obtained from the analysis software.**

Phase	Ref.	Target phases	Pil A	Pil B	Pil C	After LAB
$\beta$ -C <sub>2</sub> S	[150]	30	42.8	41.3	39.5	49.1
C <sub>4</sub> A <sub>3</sub> \$	[56]	29	17.2	16.7	16.6	13.9
C <sub>2</sub> (A,F)	[66]	10	6.9	6.7	7.2	9.4
C <sub>3</sub> S	[176]	30	0.0	0.0	0.0	0.0
$\gamma$ -C <sub>2</sub> S	[149]	0	4.2	6.4	10.3	3.7
C <sub>12</sub> A <sub>7</sub>	[152]	0	8.0	7.5	6.5	7.9
M	[165]	0	4.5	4.6	5.6	5.3
CaF <sub>2</sub>	[179]	0	0.8	0.9	0.9	1.5
C <sub>5</sub> S <sub>2</sub> \$	[180]	0	3.6	4.2	3.3	2.9
C <sub>2</sub> AS	[164]	0	1.3	1.6	0.8	0.8
C <sub>3</sub> A	[167]	0	1.8	2.4	2.2	0.7
C <sub>2</sub> F	[66]	0	1.4	0.8	1.0	0.1
C <sub>2</sub> MS <sub>2</sub>	[164]	0	3.2	2.4	2.0	0.7
C\$	[151]	1	0.8	1.3	1.0	1.3
S	[154]	0	0.5	0.2	0.2	0.0
CT	[170]	0	2.0	2.0	1.9	2.2
FT	[181]	0	0.9	1.0	1.0	0.6
C		0	0.0	0.0	0.0	0.0
$R_{wp}$ [%] <sup>1</sup>			9.98	9.78	9.02	9.05

<sup>1</sup>The high  $R_{wp}$  is due to a rutile addition to the sample and the high background of a detector.

The target was to produce clinker containing 30 wt.% alite (C<sub>3</sub>S), 30 wt.% (C<sub>2</sub>S), 29 wt.% C<sub>4</sub>A<sub>3</sub>\$, 10 wt.% C<sub>2</sub>(A,F), and 1 wt.% C\$. The XRD analysis showed that the produced clinker lacked any alite and was instead belite clinker, with ye'elimite and ferrite as major phases. Major phases detected were larnite ( $\beta$ -C<sub>2</sub>S), ye'elimite (C<sub>4</sub>A<sub>3</sub>\$), ferrite C<sub>2</sub>(A,F), mayenite (C<sub>12</sub>A<sub>7</sub>), and periclase (MgO). The minor phases were gamma-belite ( $\gamma$ -C<sub>2</sub>S), fluorite (CaF<sub>2</sub>), ternesite (C<sub>5</sub>S<sub>2</sub>\$), gehlenite (C<sub>2</sub>AS), tricalcium aluminate (C<sub>3</sub>A), an iron-rich solution of ferrite (C<sub>2</sub>F), åkermanite (C<sub>2</sub>MS<sub>2</sub>), anhydrite (C\$), quartz (S), perovskite (CT), and titanomagnetite (FT). The increase of AOD slag in clinker mixes (PIL A < PIL B < PIL C) increased the content of  $\gamma$ -C<sub>2</sub>S and MgO in the final clinker, but all the produced clinkers otherwise had a similar mineral composition. The clinker that was produced in the laboratory furnace from ground granules (PIL B) had a slightly higher content of belite (C<sub>2</sub>S) and fewer transitory phases/unreacted raw materials such as  $\gamma$ -C<sub>2</sub>S, C<sub>2</sub>AS, C<sub>3</sub>A, and C<sub>2</sub>MS<sub>2</sub>. However, the composition was generally very similar to

PIL B.  $\text{CaF}_2$  could be analyzed, which indicates that there was fluorine in the granules and clinker, but somehow it did not lead to the desired mineralization effect of alite.

The major and minor phases were analyzed with the SEM-EDX analysis in Fig. 15 (PIL B), and the average chemical compositions of each phase are presented in Table 30 (PIL B). It was found that clinker phases formed clusters, with the size of individual phases below  $10\ \mu\text{m}$ . Different phases originating in raw materials were detected such as CA, CSMA, CaO, S-A-C-K, etc. The unreacted raw materials had much larger particle size than in the clinker phases.

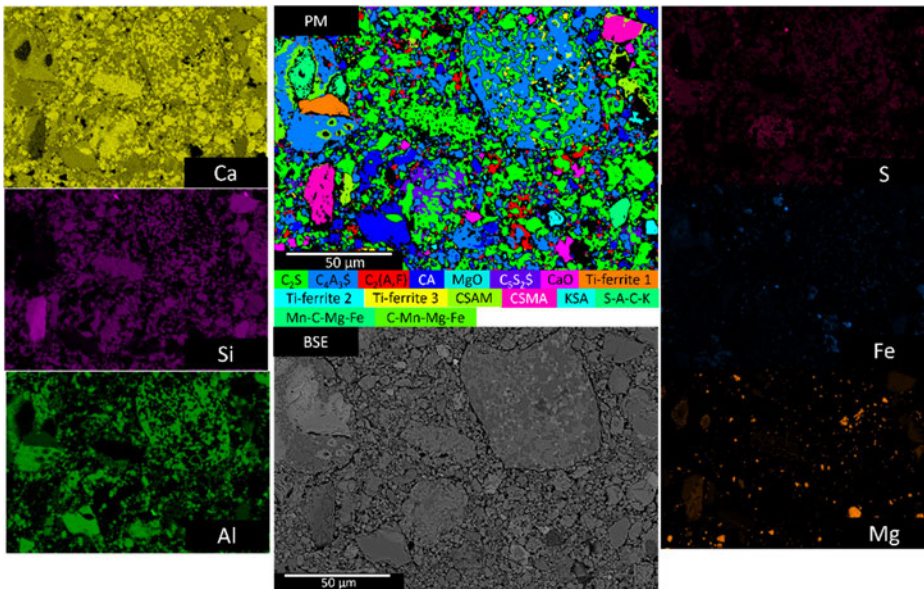


**Fig. 15. Results of the EDX mapping analysis of PIL B clinker (Paper IV):** Elemental distribution maps were used to calculate phase maps (PM). PM shows the major phases of belite ( $\text{C}_2\text{S}$ ), ye'elimite ( $\text{C}_4\text{A}_3\text{S}$ ), four different types of ferrite  $\text{C}_2(\text{A},\text{F})$ , calcium aluminate (CA), and periclase (MgO). The minor phases were ternesite ( $\text{C}_5\text{S}_2\text{S}$ ), free lime (CaO), and CSAM-CSMA are associated with gehlenite ( $\text{C}_2\text{AS}$ ) – åkermanite ( $\text{C}_2\text{MS}_2$ ) series. KSA, S-A-C-K, Mn-C-Mg-Fe, and C-Mn-Mg-Fe are probably residues from raw material. Elemental distribution maps for minor elements are presented in the Appendix, Fig. A8.

**Table 30. Average chemical composition (given in %) of the PIL B clinker phases from EDX analyses (Paper IV).**

Phase/oxide	O	Ca	Si	Al	Mg	S	Fe	Na	Ti	Mn	F	K
Belite	57.4	26.6	13.3	1.4	0.5	0.4	0.2	0.1	0.0	0.0	0.0	0.0
Ye'elimite	59.1	15.6	1.7	19.1	0.3	3.3	0.6	0.1	0.0	0.2	0.0	0.0
Ferrite	56.6	20.7	2.4	9.9	1.2	0.9	6.1	0.0	1.1	1.0	0.0	0.0
CA	55.7	17.8	1.2	21.8	0.8	0.3	0.5	0.1	0.0	0.0	1.6	0.0
Ternesite	58.5	23.2	8.4	1.3	0.2	5.3	0.0	0.2	0.2	0.0	2.6	0.0
Ti-ferrite 1	58.3	19.9	1.2	8.1	0.5	0.0	1.0	0.0	8.3	0.9	0.0	0.0
Ti-ferrite 2	58.0	18.3	2.6	11.0	0.6	1.3	4.1	0.0	3.1	0.9	0.0	0.0
Ti-ferrite 3	57.3	20.0	3.0	5.2	1.2	0.3	6.8	0.0	4.7	1.2	0.0	0.0
CSAM	58.3	17.3	13.1	5.7	4.3	0.2	0.6	0.3	0.0	0.1	0.0	0.0
CSMA	59.3	12.3	18.2	1.0	7.9	0.0	0.5	0.4	0.0	0.0	0.0	0.3
KSA	56.5	2.4	12.7	11.8	0.6	0.0	1.6	1.2	0.5	0.0	0.0	12.8
S-A-C-K	60.1	11.2	16.0	6.5	0.3	0.0	2.6	0.8	0.4	0.0	0.0	1.7
Mn-C-Mg-Fe	52.0	10.9	0.2	1.2	9.8	0.0	6.6	0.0	0.0	19.4	0.0	0.0
C-Mn-Mg-Fe	55.0	20.5	0.8	10.7	1.3	0.7	3.5	0.0	0.7	6.4	0.0	0.0

In the EDX analysis, it was finally confirmed that no alite was present. Fluorine was designed as a mineralizer, and its fate in the pilot clinker was therefore tracked in the EDX analysis. The presence of fluorine in AOD slag was confirmed in Fig. 12, and it could be detected in all the clinkers through the EDX analysis, mostly as  $\text{CaF}_2$ . In the EDX analysis of PIL C (with the most AOD slag in the mix), it was shown (Fig. 16) that the clinker contained  $\text{CaF}_2$ , but calcium silicate with fluorine was also present. Through the EDX spot analysis shown in Table 30, it was also observed that fluorine was substituted for the ternesite ( $\text{C}_5\text{S}_2$ ) and calcium aluminat phase (CA), which was identified as mayenite or tricalcium aluminat originating in the slags. From the EDX analysis, it was detected that ferrite was present in at least four different phases/variatiions with different Fe, Al, and Ti.



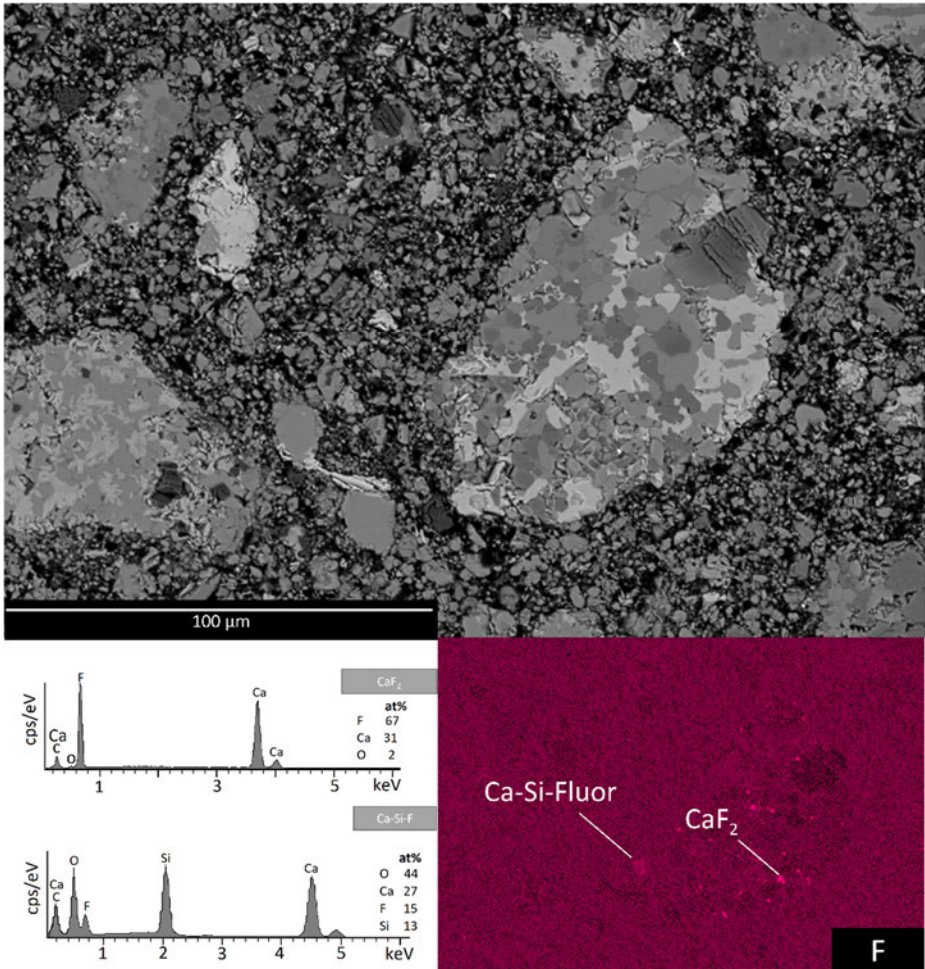


**Fig. 16. Results of the EDX mapping analysis of PIL 2C (Paper IV): elemental distribution maps of calcium (Ca) and fluorine (F) are shown. The fluorine-bearing calcium silicate and fluorite (CaF<sub>2</sub>) are marked in the figure.**

The effect of the particle size of raw materials on microstructure and phase formation was analyzed from the sample, which was ground from the granules (PIL B) and fired in the laboratory furnace at 1260 °C. The EDX analysis of the clinker is shown in Fig. 17, and the average chemical composition of each phase can be found in Appendix 6, Table A2.



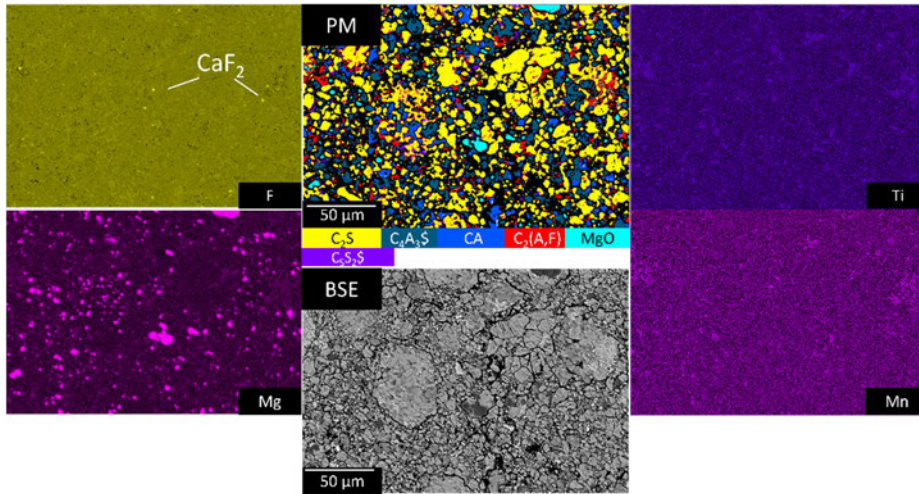


**Fig. 17. Results of the EDX mapping analysis of ground LAB B clinker (Paper IV): Phase map (PM) differentiates the following phases: belite ( $C_2S$ ), ye'elimite ( $C_4A_3S$ ), ferrite  $C_2(A,F)$ , calcium aluminate (CA), periclase (MgO), and ternesite ( $C_5S_2S$ ).  $CaF_2$  is identified because of its small size only in the elemental distribution map of fluorine (F) as light dots.**

Grinding led to a more heterogenous distribution of clinker phases, and much fewer unreacted raw materials were detected. The major phase composition consisted of the same major ( $C_2S$ ,  $C_4A_3S$ , and  $C_2(A,F)$ ) and minor (CA, MgO, and ternesite) phases as in the pilot kiln demonstration. It was detected with the elemental distribution mapping that fluorine was present as  $CaF_2$ . The production of clinker in optimal laboratory conditions proved that the conditions in the pilot kiln were not the reason for the lack of alite in the clinker. It could therefore be concluded from laboratory tests with two different AOD slags that the reason for the lack of alite in the pilot demonstration was the properties of AOD slag. The reason the fluorine from the AOD slag used in the pilot did not interact with the phase formation remains unknown. The results show that a very specific and detailed analysis is required when industrial byproducts are used.

## 4.5 Hydration of cement pastes and mortars

### 4.5.1 CSAB

The preparation of hydrated CSAB cement samples (Paper I) after 7 days of curing for FESEM-EDX is described in Section 3.2.5, and the BSE image with the phase identification is presented in Fig. 18. It was detected that ye'elinite with gypsum and water had formed ettringite ( $\text{Ca}_6\text{Al}_2(\text{SO}_4)_3(\text{OH})_{12}\cdot 26\text{H}_2\text{O}$ ). After 7 days of hydration, ferrite and belite could still be observed mostly unreacted.

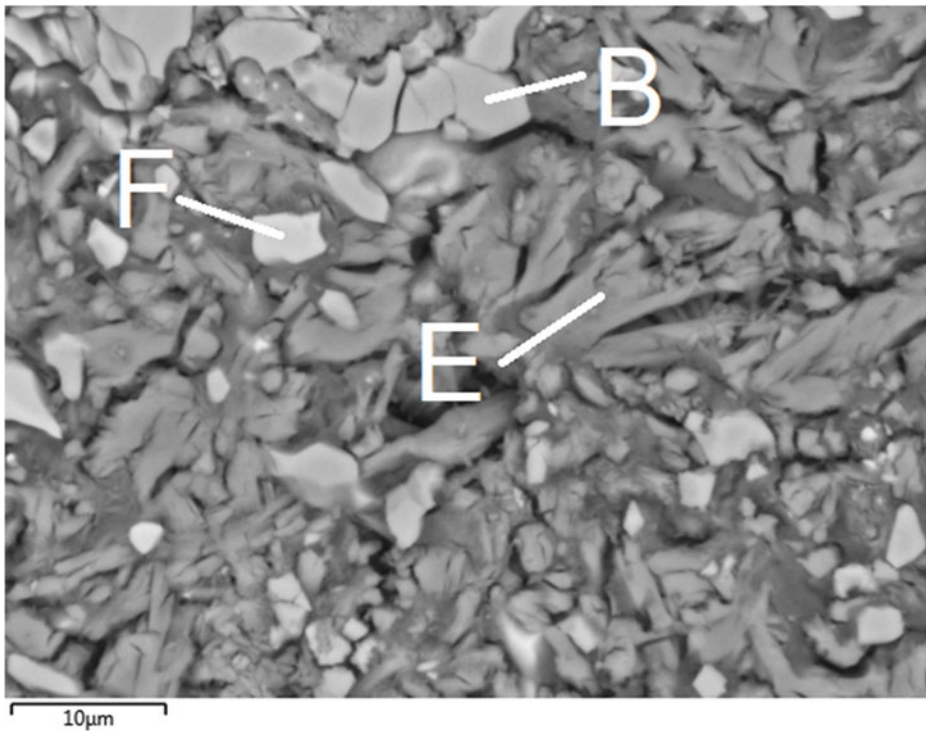


**Fig. 18. FESEM-BSE image of CSAB prepared from reagent-grade chemicals (RGC\_C) after 7 days of curing and stop of hydration, where E: ettringite, F: ferrite, and B: belite (adapted under CC BY 4.0 license from Paper I © 2020 Authors).**

The clinkers and reference PC cement were ground prior to the compressive strength testing. The Blaine fineness, PSD, and density are presented in Table 31.

The preparation of samples and compressive strength testing is described in Section 3.2.5, and the results are presented in Fig. 19.

**Table 31. The Blaine fineness, PSD, and density of clinkers produced in Paper I.**

Clinker or cement	Blaine fineness	PSD	Density
	cm <sup>2</sup> /g	d <sub>50</sub> [μm]	g/cm <sup>3</sup>
RG_C	2720	6.42	3.10
AOD_C	3378	5.43	3.09
Fay_C	3026	6.37	3.10
FE_C	3292	6.37	3.12
CEM II/B-M (S-LL) 42.5 N	3161	n.d	3.15

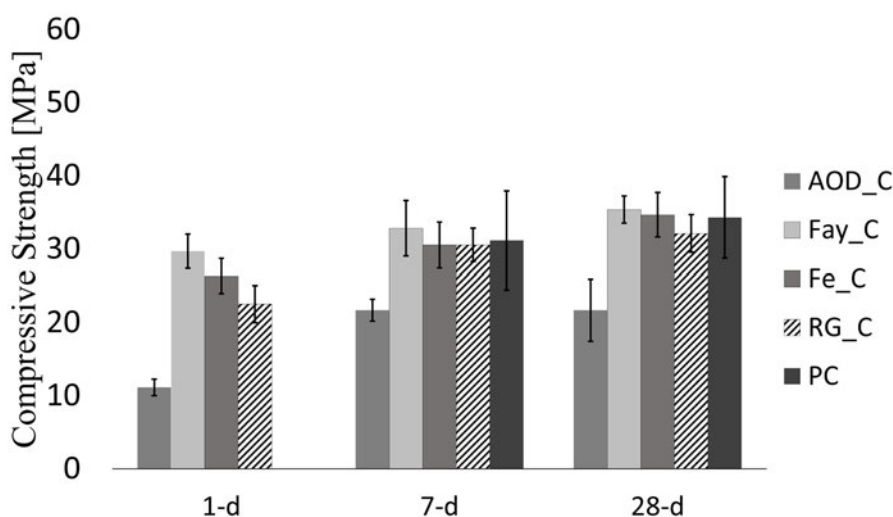


**Fig. 19. Compressive strength test results (1,7 and 28 d) of AOD\_C, Fay\_C, Fe\_C, RG\_C, and PC (adapted under CC BY 4.0 license from Paper I © 2020 Authors).**

The average values of six tests from each sample showed that the strength of the samples produced from fayalitic slag, Fe slag, and reagent-grade chemicals had very similar strength properties after 7 and 28 days of curing as the commercial PC cement. The strength after 28 days of curing was between 30 and 35 MPa. It should be noted that the small sample size may have affected the strength, and the results can only be compared with each other. The clinker prepared with 43% AOD slag in the raw mix had a very low strength because of the formation of poorly hydraulic fluorellestadite.

#### 4.5.2 CSAB(F)

The hydration studies of CSAB(F) (Paper III) are presented in more detail in Appendix 7. Setting the time of CSAB(F) was measured with Vicat, and it was found that without an addition of citric acid, the initial and final setting times were 39 min and 77 min respectively. With a 0.5 vol.% citric acid–water solution, the initial and final setting times improved to 87 min and 182 min respectively. The main hydration product was ettringite, which was responsible for most of the strength development. The hydration of belite and ferrite was very limited in the first 28 days. The compressive strength was measured for the pilot clinker and the reference PC (CEM II/B-M (S-LL) 42.5 N) according to the EN 196-1 standard, and the results are shown in Fig. 20.

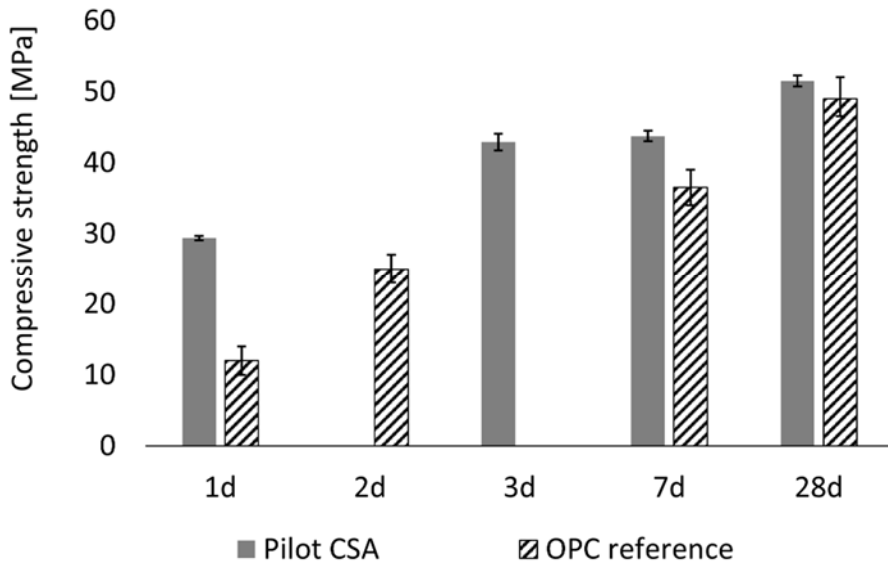


**Fig. 20. The compressive strength results (1 - 28d aging) of pilot CSAB cement with 15 wt.% anhydrite and citric acid and OPC reference CEM II/B-M (S-LL) 42.5 N.**

The compressive strength data show that CSA cement has a much higher initial strength after 1 day of curing, but the final strength is like PC after 28 days. This indicates that the clinker produced can compete with a commercial product on final strength but also has a higher initial strength. The strength after 28 days of curing reached around 50 MPa.

According to the XRD and EDX analyses, periclase (MgO) was present in the clinker (as seen in Fig. 20). Free MgO is known to be harmful for the cement matrix because it may hydrate to brucite  $Mg(OH)_2$ , which causes expansion, leading to cracking of the cement/concrete. At normal pressure and temperature, the reaction takes a long time [76], [77]. The presence of MgO is a factor that needs to be considered and tested when the clinker produced in this study is used.

### 4.5.3 AYF

The setting time of three pilot AYF clinkers and reference commercial PC cement pastes was tested with VICAT apparatus, and the results are shown in Table 32. The AYF clinkers were mixed with 12.5 wt.% anhydrite and citric acid, as described in Section 3.2.5. The setting time was increased with more AOD slag in the raw mix. This is probably due to the increasing content of poorly hydrating  $\gamma$ -C<sub>2</sub>S, which was observed with the XRD analysis.

**Table 32. Setting times of tested PIL A, PIL B, PIL C, and reference PC cement pastes.**

Sample/ Setting time	PIL A	PIL B	PIL C	PC
Initial [min]	47	54	158	242
Final [min]	87	167	685	385

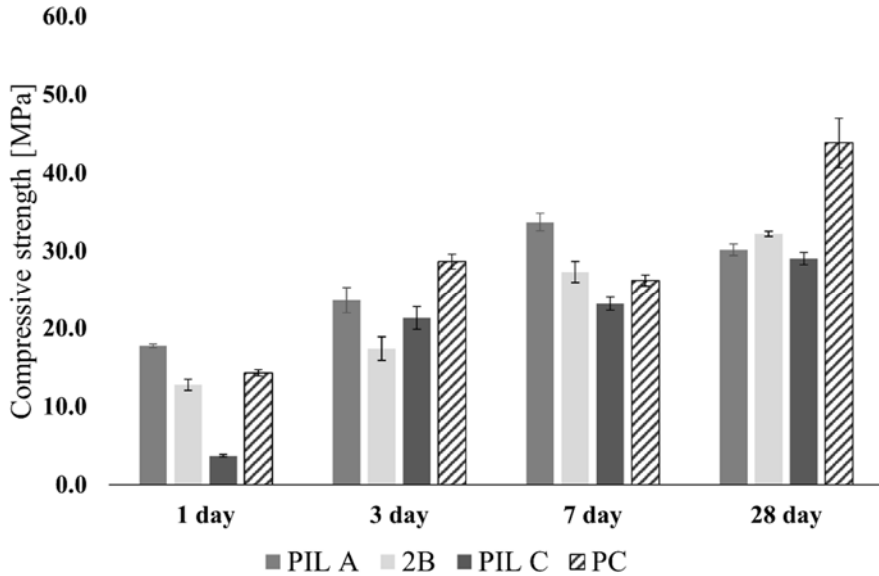


**Fig. 21. Compressive strength of A: PIL A, B: PIL B, C: PIL C, and reference Portland cement CEM II/B-M (S-LL) 42.5 N.**

The compressive strength data show that the best performance from the prepared pilot clinkers was achieved with PIL A and PIL B. PIL C showed slow strength development. The 28-day performance of the clinkers was roughly between 30 and 35 MPa. None of the prepared clinkers failed to reach the 28-day performance of the reference PC cement (CEM II/B-M (S-LL) 42.5 N). The low strength was due to the fact that the prepared clinkers were BYF (belitic calcium sulfoaluminate) clinkers instead of AYF (alite calcium sulfoaluminate) clinkers, as was designed.

#### **4.6 Brief sustainability assessment**

Table 33 shows that the clinkers composed in the pilot kiln had raw-material-based CO<sub>2</sub> emissions that were much lower than that of Portland cement made from virgin raw materials.

**Table 33. Comparison of the reduction of CO<sub>2</sub> emissions of clinkers produced in the pilot demonstrations. The top three rows present pure raw mixes produced from limestone and other raw materials, and the bottom four rows present the clinkers produced with industrial byproducts.**

Clinker type	CaO [kg/t]	CaCO <sub>3</sub> [kg/t clinker]	CO <sub>2</sub> [kg/t]	CO <sub>2</sub> reduction [%]
Without industrial byproducts				
PC	670	1327	584	
Paper III CSAB(F)	464	919	404	31
Paper IV AYF	571	1131	497	15
With industrial byproducts				
Paper III CSAB(F)	464	120	50	91
Paper IV PIL A	571	586	243	56
Paper IV PIL B	571	472	196	64
Paper IV PIL C	571	356	148	73

It is shown that shifting the phase composition of PC clinker to less calcium-bearing phases can reduce CO<sub>2</sub> emissions associated with the burning of limestone 31% and 15% for CSAB(F) and AYF clinkers respectively. When the clinker raw meal is composed of industrial byproducts, the CO<sub>2</sub> emissions associated with limestone can be further reduced to 91% in the case of CSAB(F) clinker and 56–73% for AYF clinkers. AYF and CSAB(F) clinkers can be produced at a temperature 200 °C lower than conventional PC clinker. The estimation of CO<sub>2</sub> reduction of the firing in the pilot kiln needs exact information about the kiln setup and energy sources. However, a sintering temperature around 200 °C lower is beneficial because less energy needs to be consumed, there is less wearing of the kiln refractories, and lower NO<sub>x</sub> emissions [6].

The annual production of PC cement in Finland was 1.02 Mt/a in 2018 [182]. When this is compared with the availability of industrial byproducts used in Papers III and IV in Fig. 22, it is obvious that the volume of slags is insufficient to cover natural raw materials like cement raw materials, but the utilization of byproducts can promote waste valorization and circularization.

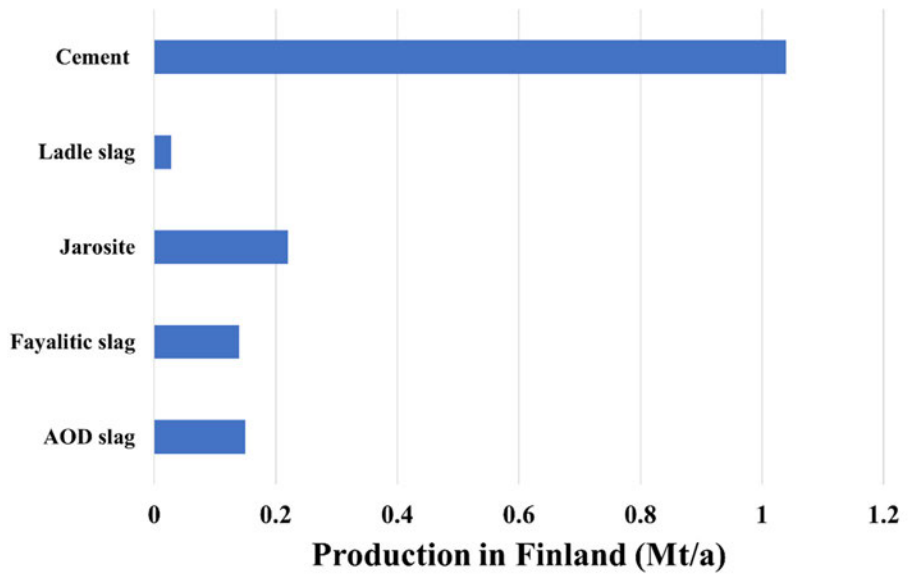


Fig. 22. Annual production of cement (PC) and slags (Papers III and IV) in Finland.



## 5 Summary and concluding remarks

The aim of this study was to utilize Finnish industrial byproducts for the manufacture of the CSA and AYF types of cement clinkers. The study was conducted first at laboratory scale and then scaled to a semi-industrial kiln. The main concern about utilizing byproducts as raw materials was the impurities that could lead to the formation of intermediate/transitory phases and incorporation to clinker phases.

In the laboratory-scale experiments, CSAB clinker could be produced first using only Fe slag, fayalitic slag, and AOD slag to produce three clinkers in a muffle furnace at 1300 °C. The target phase composition was 40 wt.% ye'elimite ( $C_4A_3S$ ), 35 wt.% belite ( $C_2S$ ), 20 wt.% ferrite ( $C_2F$ ), and 5 wt.% anhydrite ( $CS$ ). The replacement of pure raw materials with Fe slag and fayalitic slag led to only minor changes in the designed target composition. The use of AOD slag was found to be challenging because of fluorine, which led to partial melting of the clinker and the formation of fluorellstadite. The utilization of ladle slag and phosphogypsum was tested with a similar recipe at the laboratory scale [122]. After proving the concept in the laboratory-scale experiments, the target phase composition for a semi-industrial trial was adjusted to 45 wt.%  $C_4A_3S$ , 36 wt.%  $C_2S$ , 15 wt.%  $C_2(AF)$ , 2 wt.%  $CS$ , and 2 C. The clinker with a new recipe was first prepared at laboratory scale and then scaled to a semi-industrial pilot demonstration with a 7 m rotary kiln at 1260 °C, where the raw mix consisted of ladle slag, Fe slag, phosphogypsum, and natural raw materials.

Prior to the pilot demonstration, there were uncertainties about how the accuracy of XRF analysis and LOI with factors such as the weighting of materials and the possible loss of material to ring formation or airflow in the kiln might affect the chemical composition of raw feed and clinker during manufacture. A sensitivity study was therefore undertaken to demonstrate how minor changes of  $Al_2O_3$ - $SiO_2$ - $CaO$  quantities changed the phase composition of clinker. It was found that too little  $CaO$  might lead to the formation of gehlenite, and therefore in the target phase composition, 2 wt.% of  $C_2S$  was replaced with 2 wt.% free  $CaO$ . Excess anhydrite was added to ensure sufficient sulfur for ye'elimite formation because it was known that some sulfur was lost during firing.

The  $CO_2$  emissions based on  $CaCO_3$  decomposition of pilot CSAB(F) were 90% lower than that of OPC cement made with virgin raw materials. The results of the pilot demonstrated that even with minimal raw material homogenization, the clinker phase composition was robust and remained similar throughout the trial.

Because some of the raw materials were lost to the kiln inlet material and the impurities from industrial byproducts, the final clinker had 25 wt.% of minor phases that were not targeted. CSAB(F) clinker mixed with anhydrite had similar compressive strength to commercial PC cement and good workability.

The limitations and optimization for the AYF clinkers were first studied at laboratory scale with a total of 24 different raw mixes. It was found that AYF clinker could be produced at 1260 °C when the raw mix had enough fluorine as a mineralizer. Iron was found to improve burnability to avoid free lime. Sulfur was found to stabilize belite, and it was thus present in all the clinkers with alite, ye'elimite, and ferrite phases as major phases. Too much fluorine in raw mix was found to lead to the formation of mayenite and fluorellestadite instead of designed clinker phases. The target phase composition of AYF clinker in the semi-industrial trial was adjusted to 30 wt.% C<sub>3</sub>S, 30 wt.% C<sub>2</sub>S, 29 wt.% C<sub>4</sub>A<sub>3</sub>F, 10% C<sub>4</sub>AF, and 1% C<sub>3</sub>S, and the target fluorine content was set to X=0.15 in the formula of alite Ca<sub>3</sub>Si<sub>1-x</sub>Al<sub>x</sub>O<sub>5-x</sub>F<sub>x</sub>. In the pilot demonstration, the idea was to utilize fluorine-bearing AOD slag as a source of fluorine mineralizer instead of using CaF<sub>2</sub>. The utilization of AOD slag as a fluorine source to produce alite was successful in laboratory experiments from the first batch of AOD slag, where clinker with alite and ye'elimite could be produced at 1260 °C. However, the AOD slag from the second batch that was used in the pilot demonstration did not lead to the designed mineralization effect to form the alite phase, and the clinkers produced in the pilot demonstration were belitic CSA clinkers with ferrite (BYF) instead. After the pilot demonstration, it was proven that the AOD slag utilized at pilot scale did not have a mineralization effect either in the laboratory-scale tests.

One of the major concerns of CSAB production is the availability of alumina-rich raw materials. One way to tackle this problem would be to use kaolin clays to produce belitic CSA clinker with a low ye'elimite content. Suggested applications for belitic CSA could be standalone binders, mixes with PC to improve working time and utilization as an activator in cold concreting, or blends with calcined clays (metakaolin), which are known to have low initial strength development. Typically, the PC-CSA blends come with high ye'elimite content, but there exist commercial applications using PC-belitic CSA blends as well. In CSA cements there is also a potential for stabilization of sulfate and heavy metal containing solid waste and waste waters.

The different behavior of two batches of AOD slag during clinkering shows that if it is desired to utilize the AOD slag to produce AYF clinker, the chemical and mineralogical properties of the slag need to be quantified very precisely. The

best scenario would be that the properties of slag could be adjusted already in the AOD process at the steel plant to fit the limitations of AYF clinker manufacture. Further investigation for the properties of hydration mechanism and kinetics, mechanical properties and durability for the AYF and CSA cements produced in this work are necessary to prove their usability for practical applications.

The steelmaking industry aims for zero CO<sub>2</sub> steel production by replacing the blast furnace with a direct hydrogen reduction. The new process route means less GGBFS (ground granulated blast furnace slag) will be available for the cement industry in some locations in the future. The lack of GGBFS may increase the cement industry's industry in alternative cement grades. Future studies to improve the knowledge of how to utilize high iron-containing slags such as steelmaking slags (EAF and AOD) in cement manufacture and how to improve the reactivity of iron-bearing cement phases are suggested. The possible utilization of steelmaking slags and other byproducts can include altered PC (Portland cement), ye'elimate, and belite cements with increasing ferrite (C<sub>4</sub>AF) content. When industrial byproducts are utilized as raw materials, it is very important that the raw materials are available locally to avoid long and expensive logistics, valuable compounds are removed from the byproducts before use, and environmental risks are assessed.



## References

- [1] J. S. J. van Deventer, J. L. Provis, P. Duxson, and D. G. Brice, “Chemical Research and Climate Change as Drivers in the Commercial Adoption of Alkali Activated Materials,” *Waste and Biomass Valorization* 2010 1:1, vol. 1, no. 1, pp. 145–155, Feb. 2010, doi: 10.1007/S12649-010-9015-9.
- [2] K. L. Scrivener, V. M. John, and E. M. Gartner, “Eco-efficient cements: Potential economically viable solutions for a low-CO<sub>2</sub> cement-based materials industry,” *Cem Concr Res*, vol. 114, pp. 2–26, Dec. 2018, doi: 10.1016/J.CEMCONRES.2018.03.015.
- [3] P. Hewlett, M. Liska, and F. M. Lea, *Lea’s Chemistry of Cement and Concrete*, 5th ed. Oxford: Butterworth-Heinemann, 2019.
- [4] L. Zhang, M. Su, and Y. Wang, “Development of the use of sulfo- and ferroaluminate cements in China,” *Advances in Cement Research*, vol. 11, no. 1, pp. 15–21, Jan. 1999, doi: 10.1680/adcr.1999.11.1.15.
- [5] E. Bescher, K. Vallens, and J. Kim, “Belitic calcium sulfoaluminate cement: Hydration chemistry, performance, and use in the United States,” *15th International Congress on the Chemistry of Cement Prague*, 2019. [https://www.researchgate.net/publication/335830876\\_Belitic\\_calcium\\_sulfoaluminate\\_cement\\_Hydration\\_chemistry\\_performance\\_and\\_use\\_in\\_the\\_United\\_States](https://www.researchgate.net/publication/335830876_Belitic_calcium_sulfoaluminate_cement_Hydration_chemistry_performance_and_use_in_the_United_States) (accessed Feb. 25, 2021).
- [6] M. ben Haha, F. Winnefeld, and A. Pisch, “Advances in understanding ye’elimite-rich cements,” *Cement and Concrete Research*, vol. 123. Elsevier Ltd, p. 105778, Sep. 01, 2019. doi: 10.1016/j.cemconres.2019.105778.
- [7] T. Hanein, J. L. Galvez-Martos, and M. N. Bannerman, “Carbon footprint of calcium sulfoaluminate clinker production,” *J Clean Prod*, vol. 172, pp. 2278–2287, Jan. 2018, doi: 10.1016/j.jclepro.2017.11.183.
- [8] G. Álvarez-Pinazo, I. Santacruz, M. A. G. Aranda, and Á. G. de La Torre, “Hydration of belite–ye’elimite–ferrite cements with different calcium sulfate sources,” <http://dx.doi.org/10.1680/jadcr.16.00030>, vol. 28, no. 8, pp. 529–543, Aug. 2016, doi: 10.1680/JADCR.16.00030.
- [9] F. P. Glasser and L. Zhang, “High-performance cement matrices based on calcium sulfoaluminate-belite compositions,” *Cem Concr Res*, vol. 31, no. 12, pp. 1881–1886, Dec. 2001, doi: 10.1016/S0008-8846(01)00649-4.
- [10] J. Kiventerä, K. Piekkari, V. Isteri, K. Ohenoja, P. Tanskanen, and M. Illikainen, “Solidification/stabilization of gold mine tailings using calcium

- sulfoaluminate-belite cement,” *J Clean Prod*, vol. 239, p. 118008, Dec. 2019, doi: 10.1016/j.jclepro.2019.118008.
- [11] M. Chrysochoou and D. Dermatas, “Evaluation of ettringite and hydrocalumite formation for heavy metal immobilization: Literature review and experimental study,” *J Hazard Mater*, vol. 136, no. 1, pp. 20–33, Aug. 2006, doi: 10.1016/J.JHAZMAT.2005.11.008.
- [12] F. Bullerjahn, “Characterisation and hydration of ye’elinite containing cements,” EPFL, Lausanne, 2018. doi: 10.5075/EPFL-THESIS-7953.
- [13] T. Duvallet, “Influence of ferrite phase in alite-calcium sulfoaluminate cements,” PhD dissertation, University of Kentucky University of Kentucky, Kentucky, 2014. Accessed: Feb. 25, 2021. [Online]. Available: [https://uknowledge.uky.edu/cme\\_etds/27](https://uknowledge.uky.edu/cme_etds/27)
- [14] J. D. Zea-Garcia, I. Santacruz, M. A. G. Aranda, and A. G. de la Torre, “Alite-belite-ye’elinite cements: Effect of dopants on the clinker phase composition and properties,” *Cem Concr Res*, vol. 115, pp. 192–202, Jan. 2019, doi: 10.1016/j.cemconres.2018.10.019.
- [15] V. Isteri *et al.*, “The Effect of Fluoride and Iron Content on the Clinkering of Alite-Ye’elinite-Ferrite (AYF) Cement Systems,” *Front Built Environ*, vol. 7, p. 89, Jul. 2021, doi: 10.3389/FBUIL.2021.698830/BIBTEX.
- [16] T. Hanein *et al.*, “Alite calcium sulfoaluminate cement: chemistry and thermodynamics,” *Advances in Cement Research*, vol. 31, no. 3, pp. 94–105, Mar. 2019, doi: 10.1680/jadcr.18.00118.
- [17] D. Londono-Zuluaga, J. I. Tobón, M. A. G. Aranda, I. Santacruz, and A. G. de la Torre, “Clinkering and hydration of belite-alite-ye’elinite cement,” *Cem Concr Compos*, vol. 80, pp. 333–341, Jul. 2017, doi: 10.1016/j.cemconcomp.2017.04.002.
- [18] M. A. G. Aranda and A. G. de la Torre, “Sulfoaluminate cement,” *Eco-Efficient Concrete*, pp. 488–522, Jan. 2013, doi: 10.1533/9780857098993.4.488.
- [19] S. Nagataki and H. GOMI, “EXPANSIVE ADMIXTURES (MAINLY ETTRINGITE),” *Cem Concr Compos*, vol. 20, no. 2/3, 1998.
- [20] A. Peys *et al.*, “Sustainable iron-rich cements: Raw material sources and binder types,” *Cem Concr Res*, vol. 157, p. 106834, Jul. 2022, doi: 10.1016/J.CEMCONRES.2022.106834.
- [21] L. Black, C. Breen, J. Yarwood, J. Phipps, and G. Maitland, “In situ Raman analysis of hydrating C3A and C4AF pastes in presence and absence of

- sulphate,” <https://doi.org/10.1179/174367606X120179>, vol. 105, no. 4, pp. 209–216, Aug. 2013, doi: 10.1179/174367606X120179.
- [22] A. Klein, “Studies of calcium sulpho aluminate admixtures for expansive cements,” *Proceedings of ASTM*, vol. 58, pp. 968–1008, 1958, Accessed: Jul. 04, 2022. [Online]. Available: <https://cir.nii.ac.jp/crid/1571980074493205760.bib?lang=en>
- [23] ASTM International, “ASTM C845-04,” 2004
- [24] China Building Materials Academy, “Sulphoaluminate cement GB 20472-2006,” 2006. Accessed: Jul. 27, 2022. [Online]. Available: <https://www.chinesestandard.net/PDF/English.aspx/GB20472-2006>
- [25] G. Huang, D. Pudasainee, R. Gupta, and W. V. Liu, “Hydration reaction and strength development of calcium sulfoaluminate cement-based mortar cured at cold temperatures,” *Constr Build Mater*, vol. 224, pp. 493–503, Nov. 2019, doi: 10.1016/J.CONBUILDMAT.2019.07.085.
- [26] P. Li, X. Gao, K. Wang, V. W. Y. Tam, and W. Li, “Hydration mechanism and early frost resistance of calcium sulfoaluminate cement concrete,” *Constr Build Mater*, vol. 239, p. 117862, Apr. 2020, doi: 10.1016/J.CONBUILDMAT.2019.117862.
- [27] European Technical Assessment, “ETA-19/0458,” Berlin, Jun. 2020.
- [28] K. Quillin, “Performance of belite–sulfoaluminate cements,” *Cem Concr Res*, vol. 31, no. 9, pp. 1341–1349, Sep. 2001, doi: 10.1016/S0008-8846(01)00543-9.
- [29] “Use of calcium sulfoaluminate cement to improve strength of mortars at low temperature,” *Concrete Repair, Rehabilitation and Retrofitting II*, pp. 343–344, Nov. 2008, doi: 10.1201/9781439828403-136.
- [30] G. Zhang, Y. Yang, H. Yang, and H. Li, “Calcium sulphoaluminate cement used as mineral accelerator to improve the property of Portland cement at sub-zero temperature,” *Cem Concr Compos*, vol. 106, p. 103452, Feb. 2020, doi: 10.1016/J.CEMCONCOMP.2019.103452.
- [31] A. Alzaza *et al.*, “Blending eco-efficient calcium sulfoaluminate belite ferrite cement to enhance the physico–mechanical properties of Portland cement paste cured in refrigerated and natural winter conditions,” *Cem Concr Compos*, vol. 129, p. 104469, May 2022, doi: 10.1016/J.CEMCONCOMP.2022.104469.
- [32] F. Winnefeld and S. Barlag, “Calorimetric and thermogravimetric study on the influence of calcium sulfate on the hydration of ye’elimite,” *J Therm*

- Anal Calorim*, vol. 101, no. 3, pp. 949–957, Sep. 2010, doi: 10.1007/S10973-009-0582-6/FIGURES/9.
- [33] E. M. Gartner and D. E. MacPhee, “A physico-chemical basis for novel cementitious binders,” *Cem Concr Res*, vol. 41, no. 7, pp. 736–749, Jul. 2011, doi: 10.1016/J.CEMCONRES.2011.03.006.
- [34] C. W. Hargis, A. P. Kirchheim, P. J. M. Monteiro, and E. M. Gartner, “Early age hydration of calcium sulfoaluminate (synthetic ye’elinite,  $C_4A_3S^-$ ) in the presence of gypsum and varying amounts of calcium hydroxide,” *Cem Concr Res*, vol. 48, pp. 105–115, Jun. 2013, doi: 10.1016/J.CEMCONRES.2013.03.001.
- [35] E. Gartner and H. Hirao, “A review of alternative approaches to the reduction of CO<sub>2</sub> emissions associated with the manufacture of the binder phase in concrete,” *Cem Concr Res*, vol. 78, pp. 126–142, Dec. 2015, doi: 10.1016/J.CEMCONRES.2015.04.012.
- [36] A. Wesselsky and O. M. Jensen, “Synthesis of pure Portland cement phases,” *Cem Concr Res*, vol. 39, no. 11, pp. 973–980, Nov. 2009, doi: 10.1016/J.CEMCONRES.2009.07.013.
- [37] S. Telschow, “Clinker Burning Kinetics and Mechanism,” Technical University of Denmark, Kgs. Lyngby, 2012. Accessed: Feb. 25, 2021. [Online]. Available: <https://orbit.dtu.dk/en/publications/clinker-burning-kinetics-and-mechanism>
- [38] Á. G. de la Torre, R. N. de Vera, A. J. M. Cuberos, and M. A. G. Aranda, “Crystal structure of low magnesium-content alite: Application to Rietveld quantitative phase analysis,” *Cem Concr Res*, vol. 38, no. 11, pp. 1261–1269, Nov. 2008, doi: 10.1016/J.CEMCONRES.2008.06.005.
- [39] E. G. Shame and F. P. Glasser, “Stable Ca<sub>3</sub>SiO<sub>5</sub> solid solutions containing fluorine and aluminium made between 1050 and 1250 C,” *British ceramic Transactions and Journal*, vol. 86, no. 1, pp. 13–17, 1987.
- [40] T. T. Tran, D. Herfort, H. J. Jakobsen, and J. Skibsted, “Site preferences of fluoride guest ions in the calcium silicate phases of portland cement from <sup>29</sup>Si{<sup>19</sup>F} CP-REDOR NMR spectroscopy,” *J Am Chem Soc*, vol. 131, no. 40, pp. 14170–14171, Oct. 2009, doi: 10.1021/ja905223d.
- [41] R. Pérez-Bravo *et al.*, “Alite sulfoaluminate clinker: Rietveld mineralogical and SEM-EDX analysis,” <http://dx.doi.org/10.1680/adcr.12.00044>, vol. 26, no. 1, pp. 10–20, May 2015, doi: 10.1680/ADCR.12.00044.



- [42] D. Herfort, G. K. Moir, V. Johansen, F. Sorrentino, and H. B. Arceo, "The chemistry of Portland cement clinker," *Advances in Cement Research*, vol. 22, no. 4, pp. 187–194, Oct. 2010, doi: 10.1680/adcr.2010.22.4.187.
- [43] X. Liu and Y. Li, "Effect of MgO on the composition and properties of alite-sulphoaluminate cement," *Cem Concr Res*, vol. 35, no. 9, pp. 1685–1687, Sep. 2005, doi: 10.1016/J.CEMCONRES.2004.08.008.
- [44] I. Pajares, Á. G. de la Torre, S. Martínez-Ramírez, F. Puertas, M.-T. Blanco-Varela, and M. A. G. Aranda, "Quantitative analysis of mineralized white Portland clinkers: The structure of Fluorellestadite," *Powder Diffr*, vol. 17, no. 4, pp. 281–286, Dec. 2002, doi: 10.1154/1.1505045.
- [45] A. Seki, Y. Aso, M. Okubo, F. Sudo, and K. Ishizaka, "Development of Dusting Prevention Stabilizer for Stainless Steel Slag," no. 15, 1986.
- [46] I. M. Pritts and K. E. Daugherty, "The effect of stabilizing agents on the hydration rate of  $\beta$ -C<sub>2</sub>S," *Cem Concr Res*, vol. 6, no. 6, pp. 783–795, Nov. 1976, doi: 10.1016/0008-8846(76)90008-9.
- [47] B. Ziemer, B. Altrichter, and V. Jesenak, "Effect of SO<sub>3</sub> on formation and hydraulic reactivity of belite," *Cem Concr Res*, vol. 14, no. 5, pp. 686–692, Sep. 1984, doi: 10.1016/0008-8846(84)90032-2.
- [48] I. M. Pritts and K. E. Daugherty, "The effect of stabilizing agents on the hydration rate of  $\beta$ -C<sub>2</sub>S," *Cem Concr Res*, vol. 6, no. 6, pp. 783–795, Nov. 1976, doi: 10.1016/0008-8846(76)90008-9.
- [49] P. Fierens and J. Tirlocq, "Nature and concentration effect of stabilizing elements of beta-dicalcium silicate on its hydration rate," *Cem Concr Res*, vol. 13, no. 2, pp. 267–276, Mar. 1983, doi: 10.1016/0008-8846(83)90110-2.
- [50] S. Saidani, A. Smith, Y. el Hafiane, and L. ben Tahar, "Role of dopants (B, P and S) on the stabilization of  $\beta$ -Ca<sub>2</sub>SiO<sub>4</sub>," *J Eur Ceram Soc*, vol. 41, no. 1, pp. 880–891, Jan. 2021, doi: 10.1016/j.jeurceramsoc.2020.07.037.
- [51] C. K. Park, "Phase Transformation and Hydration of Dicalcium Silicate Containing Stabilizers," *Journal of the Ceramic Society of Japan*, vol. 109, no. 1269, pp. 380–385, May 2001, doi: 10.2109/JCERSJ.109.1269\_380.
- [52] A. J. M. Cuberos *et al.*, "Active iron-rich belite sulfoaluminate cements: Clinkering and hydration," *Environ Sci Technol*, vol. 44, no. 17, pp. 6855–6862, Sep. 2010, doi: 10.1021/ES101785N/SUPPL\_FILE/ES101785N\_SI\_001.PDF.
- [53] H. quan Zhao, Y. hong Qi, Y. lin Shi, X. zhao Na, and H. lin Feng, "Mechanism and Prevention of Disintegration of AOD Stainless Steel Slag,"

- Journal of Iron and Steel Research, International*, vol. 20, no. 4, pp. 26–30, Apr. 2013, doi: 10.1016/S1006-706X(13)60078-3.
- [54] D. Durinck *et al.*, “Borate Distribution in Stabilized Stainless-Steel Slag,” *Journal of the American Ceramic Society*, vol. 91, no. 2, pp. 548–554, Feb. 2008, doi: 10.1111/J.1551-2916.2007.02147.X.
- [55] G. S. , & G. E. M. Li, “High-belite sulfoaluminate clinker: fabrication process and binder preparation,” 2006
- [56] A. Cuesta, Á. G. de La Torre, E. R. Losilla, I. Santacruz, and M. A. G. Aranda, “Pseudocubic crystal structure and phase transition in doped ye’elimite,” *Cryst Growth Des*, vol. 14, no. 10, pp. 5158–5163, Oct. 2014, doi: 10.1021/CG501290Q/SUPPL\_FILE/CG501290Q\_SI\_002.CIF.
- [57] F. Bullerjahn, T. Scholten, K. L. Scrivener, M. ben Haha, and A. Wolter, “Formation, composition and stability of ye’elimite and iron-bearing solid solutions,” *Cem Concr Res*, vol. 131, p. 106009, May 2020, doi: 10.1016/j.cemconres.2020.106009.
- [58] A. Cuesta *et al.*, “Structure, atomistic simulations, and phase transition of stoichiometric yeelimite,” *Chemistry of Materials*, vol. 25, no. 9, pp. 1680–1687, May 2013, doi: 10.1021/cm400129z.
- [59] D. Kurokawa, S. Takeda, M. Colas, T. Asaka, P. Thomas, and K. Fukuda, “Phase transformation of Ca<sub>4</sub>[Al<sub>6</sub>O<sub>12</sub>]SO<sub>4</sub> and its disordered crystal structure at 1073 K,” *J Solid State Chem*, vol. 215, pp. 265–270, Jul. 2014, doi: 10.1016/J.JSSC.2014.03.040.
- [60] C. S. Hurlbut and C. Klein, *Manual of mineralogy (after James D. Dana)*. Wiley, 1977. Accessed: Feb. 25, 2021. [Online]. Available: <https://agris.fao.org/agris-search/search.do?recordID=US201300554480>
- [61] T. Hanein, A. Elhoweris, I. Galan, F. P. Glasser, and M. N. C. Bannerman, “Thermodynamic data of ye’elemite (C<sub>4</sub>A<sub>3</sub> $\bar{S}$ ) for cement clinker equilibrium calculations.” Aug. 26, 2015. Accessed: Mar. 31, 2021. [Online]. Available: <https://abdn.pure.elsevier.com/en/publications/thermodynamic-data-of-yeelemite-c4a3s-for-cement-clinker-equilibr>
- [62] K. Zhang, P. Shen, L. Yang, M. Rao, S. Nie, and F. Wang, “Development of high-ferrite cement: Toward green cement production,” *J Clean Prod*, vol. 327, p. 129487, Dec. 2021, doi: 10.1016/J.JCLEPRO.2021.129487.
- [63] T. CHABAYASHI, H. NAGATA, A. NAKAMURA, and H. KATO, “REDUCTION OF BURNING TEMPERATURE OF CEMENT CLINKER BY ADJUSTING OF MINERAL COMPOSITION,” *Cement*

- Science and Concrete Technology*, vol. 66, no. 1, pp. 217–222, 2012, doi: 10.14250/CEMENT.66.217.
- [64] Y. Elakneswaran *et al.*, “Characteristics of ferrite-rich portland cement: Comparison with ordinary portland cement,” *Front Mater*, vol. 6, Apr. 2019, doi: 10.3389/FMATS.2019.00097.
- [65] R. H. Bogue, “Calculation of the Compounds in Portland Cement,” *Industrial and Engineering Chemistry - Analytical Edition*, vol. 1, no. 4, pp. 192–197, Oct. 1929, doi: 10.1021/AC50068A006.
- [66] G. J. Redhammer, G. Tippelt, G. Roth, and G. Amthauer, “Structural variations in the brownmillerite series  $\text{Ca}_2(\text{Fe}_{2-x}\text{Al}_x)\text{O}_5$ : Single-crystal X-ray diffraction at 25 °C and high-temperature X-ray powder diffraction ( $25\text{ °C} \leq T \leq 1000\text{ °C}$ ),” *American Mineralogist*, vol. 89, no. 2–3, pp. 405–420, Feb. 2004, doi: 10.2138/am-2004-2-322.
- [67] M. B. Marinho and F. P. Glasser, “Polymorphism and phase changes in the ferrite phase of cements induced by titanium substitution,” *Cem Concr Res*, vol. 14, no. 3, pp. 360–368, May 1984, doi: 10.1016/0008-8846(84)90054-1.
- [68] L. Žibret, K. Šter, M. Borštnar, M. Lončnar, and S. Dolenc, “The Incorporation of Steel Slag into Belite-Sulfoaluminate Cement Clinkers,” *Applied Sciences*, vol. 11, no. 4, p. 1840, Feb. 2021, doi: 10.3390/app11041840.
- [69] M. Ichikawa, S. Ikeda, and Y. Komukai, “Effect of cooling rate and  $\text{Na}_2\text{O}$  content on the character of the interstitial materials in portland cement clinker,” *Cem Concr Res*, vol. 24, no. 6, pp. 1092–1096, Jan. 1994, doi: 10.1016/0008-8846(94)90033-7.
- [70] J. Neubauer, R. Sieber, H. J. Kuzel, and M. Ecker, “Investigations on introducing Si and Mg into Brownmillerite—A Rietveld refinement,” *Cem Concr Res*, vol. 26, no. 1, pp. 77–82, Jan. 1996, doi: 10.1016/0008-8846(95)00178-6.
- [71] M. Murat and F. Sorrentino, “Effect of large additions of Cd, Pb, Cr, Zn, to cement raw meal on the composition and the properties of the clinker and the cement,” *Cem Concr Res*, vol. 26, no. 3, pp. 377–385, Mar. 1996, doi: 10.1016/S0008-8846(96)85025-3.
- [72] C. Hall and K. L. Scrivener, “Oilwell Cement Clinkers: X-ray Microanalysis and Phase Composition,” *Advanced Cement Based Materials*, vol. 7, no. 1, pp. 28–38, Jan. 1998, doi: 10.1016/S1065-7355(97)00035-7.

- [73] S. Stöber, G. Redhammer, S. Schorr, O. Prokhnenko, and H. Pöllmann, "Structure refinements of members in the brownmillerite solid solution series  $\text{Ca}_2\text{Al}_x(\text{Fe}_{0.5}\text{Mn}_{0.5})_{2-x}\text{O}_5+\delta$  with  $1/2 \leq x \leq 4/3$ ," *J Solid State Chem*, vol. 197, pp. 420–428, Jan. 2013, doi: 10.1016/J.JSSC.2012.08.032.
- [74] X. Yao, S. Yang, H. Dong, S. Wu, X. Liang, and W. Wang, "Effect of CaO content in raw material on the mineral composition of ferric-rich sulfoaluminate clinker," *Constr Build Mater*, vol. 263, p. 120431, Dec. 2020, doi: 10.1016/j.conbuildmat.2020.120431.
- [75] Q. Song *et al.*, "The occurrence of MgO and its influence on properties of clinker and cement: A review," *Constr Build Mater*, vol. 293, p. 123494, Jul. 2021, doi: 10.1016/J.CONBUILDMAT.2021.123494.
- [76] S. Chatterji, "Mechanism of expansion of concrete due to the presence of dead-burnt CaO and MgO," *Cem Concr Res*, vol. 25, no. 1, pp. 51–56, Jan. 1995, doi: 10.1016/0008-8846(94)00111-B.
- [77] H. Kabir, R. D. Hooton, and N. J. Popoff, "Evaluation of cement soundness using the ASTM C151 autoclave expansion test," *Cem Concr Res*, vol. 136, p. 106159, Oct. 2020, doi: 10.1016/j.cemconres.2020.106159.
- [78] D. Środek, M. Dulski, and I. Galuskina, "Raman imaging as a new approach to identification of the mayenite group minerals," *Sci Rep*, vol. 8, no. 1, p. 13593, Dec. 2018, doi: 10.1038/s41598-018-31809-4.
- [79] E. v. Galuskin, F. Gfeller, I. O. Galuskina, T. Armbruster, R. Bailau, and V. v. Sharygin, "Mayenite supergroup, part I: Recommended nomenclature," *European Journal of Mineralogy*, vol. 27, no. 1, pp. 99–111, Feb. 2015, doi: 10.1127/ejm/2015/0027-2418.
- [80] G. K. Moir, "Improvements in the early strength properties of Portland cement," in *Trans. R. Soc. Lond. A*, Royal Soc, Sep. 1983, pp. 127–138. doi: 10.1098/rsta.1983.0072.
- [81] K. Gijbels *et al.*, "Feasibility of incorporating phosphogypsum in ettringite-based binder from ladle slag," *J Clean Prod*, vol. 237, p. 117793, Nov. 2019, doi: 10.1016/j.jclepro.2019.117793.
- [82] H. Nguyen *et al.*, "Byproduct-based ettringite binder – A synergy between ladle slag and gypsum," *Constr Build Mater*, vol. 197, pp. 143–151, Feb. 2019, doi: 10.1016/j.conbuildmat.2018.11.165.
- [83] H. Nguyen *et al.*, "Ettringite-based binder from ladle slag and gypsum – The effect of citric acid on fresh and hardened state properties," *Cem Concr Res*, vol. 123, p. 105800, Sep. 2019, doi: 10.1016/j.cemconres.2019.105800.

- [84] F. Bullerjahn, M. Zajac, M. ben Haha, and K. L. Scrivener, "Factors influencing the hydration kinetics of ye'elimite; effect of mayenite," *Cem Concr Res*, vol. 116, pp. 113–119, Feb. 2019, doi: 10.1016/J.CEMCONRES.2018.10.026.
- [85] S. Giminez-Molina, M. T. Blanco, J. Marr, and F. P. Glasser, "Phase relations in the system  $\text{Ca}_2\text{SiO}_4\text{-CaO-CaSO}_4\text{-CaF}_2$  relevant to cement clinkering," *Advances in Cement Research*, vol. 4, no. 14, pp. 81–86, Apr. 1992, doi: 10.1680/adcr.1992.4.14.81.
- [86] M. T. Blanco-Varela, A. Palomo, F. Puertas, and T. Vázquez, "Influence of the joint incorporation of  $\text{CaF}_2$  and  $\text{CaSO}_4$  in the clinkerization process. Obtainment of new cements," *Materiales de Construcción*, vol. 45, no. 239, pp. 21–39, Sep. 1995, doi: 10.3989/mc.1995.v45.i239.551.
- [87] S. Giménez-Molina and M. T. Blanco-Varela, "Solid state phases relationship in the  $\text{CaOSiO}_2\text{Al}_2\text{O}_3\text{CaF}_2\text{CaSO}_4$  system," *Cem Concr Res*, vol. 25, no. 4, pp. 870–882, May 1995, doi: 10.1016/0008-8846(95)00078-Q.
- [88] I. Galan, T. Hanein, A. Elhoweris, M. N. Bannerman, and F. P. Glasser, "Phase compatibility in the system  $\text{CaO-SiO}_2\text{-Al}_2\text{O}_3\text{-SO}_3\text{-Fe}_2\text{O}_3$  and the effect of partial pressure on the phase stability," *Ind Eng Chem Res*, vol. 56, no. 9, pp. 2341–2349, Feb. 2017, doi: 10.1021/acs.iecr.6b03470.
- [89] I. Galan, A. Elhoweris, T. Hanein, M. N. Bannerman, and F. P. Glasser, "Advances in clinkering technology of calcium sulfoaluminate cement," *Advances in Cement Research*, vol. 29, no. 10, pp. 405–417, Nov. 2017, doi: 10.1680/jadcr.17.00028.
- [90] Y. el Khessaimi, Y. el Hafiane, A. Smith, R. Trauchessec, C. Diliberto, and A. Lecomte, "Solid-state synthesis of pure ye'elimite," *J Eur Ceram Soc*, vol. 38, no. 9, pp. 3401–3411, Aug. 2018, doi: 10.1016/j.jeurceramsoc.2018.03.018.
- [91] T. Hanein *et al.*, "Production of belite calcium sulfoaluminate cement using sulfur as a fuel and as a source of clinker sulfur trioxide: Pilot kiln trial," *Advances in Cement Research*, vol. 28, no. 10, pp. 643–653, Nov. 2016, doi: 10.1680/JADCR.16.00018.
- [92] Á. G. de La Torre, A. J. M. Cuberos, G. Álvarez-Pinazo, A. Cuesta, and M. A. G. Aranda, "In situ powder diffraction study of belite sulfoaluminate clinkering," *urn:issn:0909-0495*, vol. 18, no. 3, pp. 506–514, Mar. 2011, doi: 10.1107/S0909049511005796.

- [93] N. Chitvoranund, F. Winnefeld, C. W. Hargis, S. Sinthupinyo, and B. Lothenbach, "Synthesis and hydration of alite-calcium sulfoaluminate cement," *Advances in Cement Research*, vol. 29, no. 3, pp. 101–111, Mar. 2017, doi: 10.1680/jadcr.16.00071.
- [94] J. D. Zea-Garcia, A. G. de la Torre, M. A. G. Aranda, and I. Santacruz, "Processing and characterisation of standard and doped alite-belite-ye'elimité ecocement pastes and mortars," *Cem Concr Res*, vol. 127, p. 105911, Jan. 2020, doi: 10.1016/j.cemconres.2019.105911.
- [95] F. Winnefeld, L. H. J. Martin, C. J. Müller, and B. Lothenbach, "Using gypsum to control hydration kinetics of CSA cements," *Constr Build Mater*, vol. 155, pp. 154–163, Nov. 2017, doi: 10.1016/J.CONBUILDMAT.2017.07.217.
- [96] E. S. Newman and L. S. Wells, "HEATS OF HYDRATION AND TRANSITION OF CALCIUM SULFATE," vol. 20, 1938.
- [97] J. Bensted and S. Prakash, "Investigation of the Calcium Sulphate-Water System by Infrared Spectroscopy," *Nature 1968 219:5149*, vol. 219, no. 5149, pp. 60–61, 1968, doi: 10.1038/219060a0.
- [98] F. Winnefeld and B. Lothenbach, "Hydration of calcium sulfoaluminate cements — Experimental findings and thermodynamic modelling," *Cem Concr Res*, vol. 40, no. 8, pp. 1239–1247, Aug. 2010, doi: 10.1016/J.CEMCONRES.2009.08.014.
- [99] D. Ariño Montoya, N. Pistofidis, G. Giannakopoulos, R. I. Iacobescu, M. S. Katsiotis, and Y. Pontikes, "Revisiting the iron-rich 'ordinary Portland cement' towards valorisation of wastes: study of Fe-to-Al ratio on the clinker production and the hydration reaction," *Materials and Structures 2021 54:1*, vol. 54, no. 1, pp. 1–20, Jan. 2021, doi: 10.1617/S11527-020-01601-W.
- [100] N. Noguchi, K. Siventhirarajah, T. Chabayashi, H. Kato, T. Nawa, and Y. Elakneswaran, "Hydration of ferrite-rich Portland cement: Evaluation of Fe-hydrates and Fe uptake in calcium-silicate-hydrates," *Constr Build Mater*, vol. 288, p. 123142, Jun. 2021, doi: 10.1016/J.CONBUILDMAT.2021.123142.
- [101] A. Cuesta *et al.*, "Multiscale understanding of tricalcium silicate hydration reactions," *Scientific Reports 2018 8:1*, vol. 8, no. 1, pp. 1–11, Jun. 2018, doi: 10.1038/s41598-018-26943-y.
- [102] G. Adegoloye, A. L. Beaucour, S. Ortola, and A. Noumowé, "Concretes made of EAF slag and AOD slag aggregates from stainless steel process:

- Mechanical properties and durability,” *Constr Build Mater*, vol. 76, pp. 313–321, Feb. 2015, doi: 10.1016/J.CONBUILDMAT.2014.12.007.
- [103] R. M. Santos and T. van Gerven, “Process intensification routes for mineral carbonation\*,” *Greenhouse Gases: Science and Technology*, vol. 1, no. 4, pp. 287–293, Dec. 2011, doi: 10.1002/GHG.36.
- [104] H. Shen, E. Forssberg, and U. Nordström, “Physicochemical and mineralogical properties of stainless steel slags oriented to metal recovery,” *Resour Conserv Recycl*, vol. 40, no. 3, pp. 245–271, Feb. 2004, doi: 10.1016/S0921-3449(03)00072-7.
- [105] H. ming Wang, L. li Yang, G. rong Li, X. Zhu, H. Zhu, and Y. tao Zhao, “Effects of B<sub>2</sub>O<sub>3</sub> and CaF<sub>2</sub> on Melting Temperatures of CaO-SiO<sub>2</sub>-Fe<sub>2</sub>O<sub>3</sub> System Fluxes,” *Journal of Iron and Steel Research, International*, vol. 20, no. 6, pp. 21–24, Jun. 2013, doi: 10.1016/S1006-706X(13)60106-5.
- [106] J. J. Beaumont *et al.*, “Cancer mortality in a Chinese population exposed to hexavalent chromium in drinking water,” *Epidemiology*, vol. 19, no. 1, pp. 12–23, Jan. 2008, doi: 10.1097/EDE.0B013E31815CEA4C.
- [107] E. D. Adesanya, “A Cementitious binder from high-alumina slag generated in the steelmaking process,” doctoral thesis, University Of Oulu, Oulu, 2019.
- [108] S. Creedy, A. Glinin, R. Matuszewicz, S. Hughes, and M. A. Reuter, “Outotec® Ausmelt Technology for Treating Zinc Residues,” in *WORLD OF METALLURGY, ERZMETALL*, GDMB Informationsgesellschaft mbH, 2013, pp. 230–235. Accessed: Feb. 25, 2021. [Online]. Available: <https://research.aalto.fi/en/publications/outotec-ausmelt-technology-for-treating-zinc-residues>
- [109] M. Rämä, S. Nurmi, A. Jokilaakso, L. Klemettinen, P. Taskinen, and J. Salminen, “Thermal Processing of Jarosite Leach Residue for a Safe Disposable Slag and Valuable Metals Recovery,” *Metals (Basel)*, vol. 8, no. 10, p. 744, Sep. 2018, doi: 10.3390/met8100744.
- [110] A. Adediran, J. Yliniemi, and M. Illikainen, “Mineralogy and glass content of Fe-rich fayalite slag size fractions and their effect on alkali activation and leaching of heavy metals,” *International Journal of Ceramic Engineering & Science*, vol. 3, no. 6, pp. 287–300, Nov. 2021, doi: 10.1002/CES2.10107.
- [111] A. E. M. Warner, C. M. Díaz, A. D. Dalvi, P. J. Mackey, A. v. Tarasov, and R. T. Jones, “JOM world nonferrous smelter survey Part IV: Nickel:

- Sulfide,” *undefined*, vol. 59, no. 4, pp. 58–72, Apr. 2007, doi: 10.1007/S11837-007-0056-X.
- [112] A. M. Rashad, “Phosphogypsum as a construction material,” *Journal of Cleaner Production*, vol. 166. Elsevier Ltd, pp. 732–743, Nov. 10, 2017. doi: 10.1016/j.jclepro.2017.08.049.
- [113] I. Netinger Grubeša, I. Barišić, A. Fucic, and S. S. Bansode, “Applications of steel slag in civil engineering: Worldwide research,” *Characteristics and Uses of Steel Slag in Building Construction*, pp. 67–82, Jan. 2016, doi: 10.1016/B978-0-08-100368-8.00005-1.
- [114] Z. Fan and S. J. Friedmann, “Low-carbon production of iron and steel: Technology options, economic assessment, and policy,” *Joule*, vol. 5, no. 4, pp. 829–862, Apr. 2021, doi: 10.1016/J.JOULE.2021.02.018.
- [115] G. Belz, J. Beretka, M. Marroccoli, L. Santoro, N. Sherman, and G. L. Valenti, “Use of Fly Ash, Blast Furnace Slag, and Chemical Gypsum for the Synthesis of Calcium Sulfoaluminate-Based Cements,” *Special Publication*, vol. 153, pp. 513–530, Jun. 1995, doi: 10.14359/1086.
- [116] P. Arjunan, M. R. Silsbee, and D. M. Roy, “Sulfoaluminate-belite cement from low-calcium fly ash and sulfur-rich and other industrial by-products,” *Cem Concr Res*, vol. 29, no. 8, pp. 1305–1311, Aug. 1999, doi: 10.1016/S0008-8846(99)00072-1.
- [117] I. A. Chen and M. C. G. Juenger, “Incorporation of coal combustion residuals into calcium sulfoaluminate-belite cement clinkers,” *Cem Concr Compos*, vol. 34, no. 8, pp. 893–902, Sep. 2012, doi: 10.1016/J.CEMCONCOMP.2012.04.006.
- [118] T. Hertel, A. van den Bulck, S. Onisei, P. P. Sivakumar, and Y. Pontikes, “Boosting the use of bauxite residue (red mud) in cement - Production of an Fe-rich calciumsulfoaluminate-ferrite clinker and characterisation of the hydration,” *Cem Concr Res*, vol. 145, p. 106463, Jul. 2021, doi: 10.1016/J.CEMCONRES.2021.106463.
- [119] M. A. Khairul, J. Zanganeh, and B. Moghtaderi, “The composition, recycling and utilisation of Bayer red mud,” *Resour Conserv Recycl*, vol. 141, pp. 483–498, Feb. 2019, doi: 10.1016/J.RESCONREC.2018.11.006.
- [120] M. Katsioti, P. E. Tsakiridis, S. Agatzini-Leonardou, and P. Oustadakis, “Examination of the jarosite–alunite precipitate addition in the raw meal for the production of Portland and sulfoaluminate-based cement clinkers,” *Int J Miner Process*, vol. 76, no. 4, pp. 217–224, Aug. 2005, doi: 10.1016/J.MINPRO.2005.01.007.



- [121] D. Adolfsson, N. Menad, E. Viggh, and B. Björkman, “Steelmaking slags as raw material for sulfoaluminate belite cement,” <http://dx.doi.org/10.1680/adcr.2007.19.4.147>, vol. 19, no. 4, pp. 147–156, May 2015, doi: 10.1680/ADCR.2007.19.4.147.
- [122] V. Isteri *et al.*, “Alternative raw materials for the production of calcium sulfoaluminate cement: ladle slag and phosphogypsum,” in *Proceedings of the 1st International Conference on Innovation in Low-Carbon Cement & Concrete Technology*, 2019.
- [123] L. Žibret, K. Šter, M. Borštnar, M. Lončnar, and S. Dolenc, “The Incorporation of Steel Slag into Belite-Sulfoaluminate Cement Clinkers,” *Applied Sciences* 2021, Vol. 11, Page 1840, vol. 11, no. 4, p. 1840, Feb. 2021, doi: 10.3390/APP11041840.
- [124] M. Mahoutian and Y. Shao, “Low temperature synthesis of cement from ladle slag and fly ash,” <http://dx.doi.org/10.1080/21650373.2015.1047913>, vol. 5, no. 4, pp. 247–258, Jul. 2015, doi: 10.1080/21650373.2015.1047913.
- [125] R. I. Iacobescu, G. N. Angelopoulos, P. T. Jones, B. Blanpain, and Y. Pontikes, “Ladle metallurgy stainless steel slag as a raw material in Ordinary Portland Cement production: a possibility for industrial symbiosis,” *J Clean Prod*, vol. 112, pp. 872–881, Jan. 2016, doi: 10.1016/J.JCLEPRO.2015.06.006.
- [126] A. di Maria, M. Salman, M. Dubois, and K. van Acker, “Life cycle assessment to evaluate the environmental performance of new construction material from stainless steel slag,” *The International Journal of Life Cycle Assessment* 2018 23:11, vol. 23, no. 11, pp. 2091–2109, Feb. 2018, doi: 10.1007/S11367-018-1440-1.
- [127] Z. Huaiwei and H. Xin, “An overview for the utilization of wastes from stainless steel industries,” *Resour Conserv Recycl*, vol. 55, no. 8, pp. 745–754, Jun. 2011, doi: 10.1016/J.RESCONREC.2011.03.005.
- [128] M. Salman *et al.*, “Alkali Activation of AOD Stainless Steel Slag Under Steam Curing Conditions,” *Journal of the American Ceramic Society*, vol. 98, no. 10, pp. 3062–3074, Oct. 2015, doi: 10.1111/JACE.13776.
- [129] M. Salman *et al.*, “Effect of accelerated carbonation on AOD stainless steel slag for its valorisation as a CO<sub>2</sub>-sequestering construction material,” *Chemical Engineering Journal*, vol. 246, pp. 39–52, Jun. 2014, doi: 10.1016/J.CEJ.2014.02.051.
- [130] H. Nguyen, V. Carvelli, E. Adesanya, P. Kinnunen, and M. Illikainen, “High performance cementitious composite from alkali-activated ladle slag

- reinforced with polypropylene fibers,” *Cem Concr Compos*, vol. 90, pp. 150–160, Jul. 2018, doi: 10.1016/j.cemconcomp.2018.03.024.
- [131] T. A. Branca and V. Colla, “Possible Uses of Steelmaking Slag in Agriculture: An Overview,” *Material Recycling - Trends and Perspectives*, Mar. 2012, doi: 10.5772/31804.
- [132] J. M. Manso, M. Losañez, J. A. Polanco, and J. J. Gonzalez, “Ladle Furnace Slag in Construction,” *Journal of Materials in Civil Engineering*, vol. 17, no. 5, pp. 513–518, Oct. 2005, doi: 10.1061/(ASCE)0899-1561(2005)17:5(513).
- [133] E. K. Anastasiou, I. Papayianni, and M. Papachristoforou, “Behavior of self compacting concrete containing ladle furnace slag and steel fiber reinforcement,” *Mater Des*, vol. 59, pp. 454–460, Jul. 2014, doi: 10.1016/J.MATDES.2014.03.030.
- [134] M. Skaf, V. Ortega-López, J. A. Fuente-Alonso, A. Santamaría, and J. M. Manso, “Ladle furnace slag in asphalt mixes,” *Constr Build Mater*, vol. 122, pp. 488–495, Sep. 2016, doi: 10.1016/J.CONBUILDMAT.2016.06.085.
- [135] V. Hallet, N. de Belie, and Y. Pontikes, “The impact of slag fineness on the reactivity of blended cements with high-volume non-ferrous metallurgy slag,” *Constr Build Mater*, vol. 257, p. 119400, Oct. 2020, doi: 10.1016/J.CONBUILDMAT.2020.119400.
- [136] M. A. Rahman, P. K. Sarker, F. U. A. Shaikh, and A. K. Saha, “Soundness and compressive strength of Portland cement blended with ground granulated ferronickel slag,” *Constr Build Mater*, vol. 140, pp. 194–202, Jun. 2017, doi: 10.1016/J.CONBUILDMAT.2017.02.023.
- [137] K. Komnitsas, L. Yurramendi, G. Bartzas, V. Karmali, and E. Petrakis, “Factors affecting co-valorization of fayalitic and ferronickel slags for the production of alkali activated materials,” *Science of The Total Environment*, vol. 721, p. 137753, Jun. 2020, doi: 10.1016/J.SCITOTENV.2020.137753.
- [138] A. Adediran, J. Yliniemi, and M. Illikainen, “Development of Sustainable Alkali-Activated Mortars Using Fe-Rich Fayalitic Slag as the Sole Solid Precursor,” *Front Built Environ*, vol. 7, p. 39, Mar. 2021, doi: 10.3389/FBUIL.2021.653466/BIBTEX.
- [139] I. Maragkos, I. P. Giannopoulou, and D. Panias, “Synthesis of ferronickel slag-based geopolymers,” *Miner Eng*, vol. 22, no. 2, pp. 196–203, Jan. 2009, doi: 10.1016/J.MINENG.2008.07.003.
- [140] A. Adediran, J. Yliniemi, V. Carvelli, E. Adesanya, and M. Illikainen, “Durability of alkali-activated Fe-rich fayalite slag-based mortars subjected

- to different environmental conditions,” *Cem Concr Res*, vol. 162, p. 106984, Dec. 2022, doi: 10.1016/J.CEMCONRES.2022.106984.
- [141] S. C. B. Myneni, S. J. Traina, T. J. Logan, and G. A. Waychunas, “Oxyanion behavior in alkaline environments: Sorption and desorption of arsenate in ettringite,” *Environ Sci Technol*, vol. 31, no. 6, pp. 1761–1768, Jun. 1997, doi: 10.1021/ES9607594/SUPPL\_FILE/ES1761.PDF.
- [142] S. Peysson, J. Péra, and M. Chabannet, “Immobilization of heavy metals by calcium sulfoaluminate cement,” *Cem Concr Res*, vol. 35, no. 12, pp. 2261–2270, Dec. 2005, doi: 10.1016/J.CEMCONRES.2005.03.015.
- [143] P. Kumarathanan, G. J. McCarthy, D. J. Hassett, and D. F. Pflughoeft-Hassett, “Oxyanion Substituted Ettringites: Synthesis and Characterization; and their Potential Role In Immobilization of As, B, Cr, Se and V,” *MRS Online Proceedings Library (OPL)*, vol. 178, 1989, doi: 10.1557/PROC-178-83.
- [144] K. Piekkari, V. Isteri, K. Ohenoja, and M. Illikainen, “Effect of Gypsum Content on CSAB Cement-Based Immobilization of Se and SO<sub>4</sub> from Industrial Filter Sludge and Sodium–Selenium Salts,” *J Hazard Toxic Radioact Waste*, vol. 25, no. 3, p. 04021018, Jul. 2021, doi: 10.1061/(ASCE)HZ.2153-5515.0000623.
- [145] K. Piekkari, K. Ohenoja, V. Isteri, P. Tanskanen, and M. Illikainen, “Immobilization of heavy metals, selenate, and sulfate from a hazardous industrial side stream by using calcium sulfoaluminate-belite cement,” *J Clean Prod*, vol. 258, p. 120560, Jun. 2020, doi: 10.1016/j.jclepro.2020.120560.
- [146] L. Qin, X. Gao, and A. Zhang, “Potential application of Portland cement–calcium sulfoaluminate cement blends to avoid early age frost damage,” *Constr Build Mater*, vol. 190, pp. 363–372, Nov. 2018, doi: 10.1016/J.CONBUILDMAT.2018.09.136.
- [147] SFS (Finnish Standards Association), “SFS-EN 196-1:2016:en: Methods of testing cement. Part 1: Determination of strength,” 2016.
- [148] ISO 13320:2009, “Particle size analysis — Laser diffraction methods,” 2009. <https://www.iso.org/standard/44929.html> (accessed Feb. 25, 2021).
- [149] W. G. Mumme, R. J. Hill, G. Bushnell-Wye, and E. R. Segnit, “Rietveld crystal structure refinements, crystal chemistry and calculated powder diffraction data for the polymorphs of dicalcium silicate and related phases.” 1995.

- [150] W. Mumme, L. M. D. Cranswick, and B. Chakoumakos, “Rietveld crystal structure refinements from high temperature neutron powder diffraction data for the polymorphs of dicalcium silicate,” *Neues Jahrbuch für Mineralogie, Abhandlungen*, vol. 170, no. 2, pp. 171–188, 1996.
- [151] H. Morikawa, I. Minato, T. Tomita, and S. Iwai, “Anhydrite: a refinement,” *Acta Crystallogr B*, vol. 31, no. 8, pp. 2164–2165, Aug. 1975, doi: 10.1107/s0567740875007145.
- [152] L. Palacios, A. Cabeza, S. Bruque, S. García-Granda, and M. A. G. Aranda, “Structure and electrons in mayenite electrides,” *Inorg Chem*, vol. 47, no. 7, pp. 2661–2667, Apr. 2008, doi: 10.1021/ic7021193.
- [153] S. Sasaki, Y. Takeuchi, and K. Fujino, “X-Ray Determination of Electron-Density Distributions in Oxides, MgO, MnO, CoO, and NiO, and Atomic Scattering Factors of their Constituent Atoms,” *Proceedings of the Japan Academy, Series B*, vol. 55, no. 2, pp. 43–48, 1979, doi: 10.2183/PJAB.55.43.
- [154] P. Norby, “Synchrotron Powder Diffraction using Imaging Plates: Crystal Structure Determination and Rietveld Refinement,” *J Appl Crystallogr*, vol. 30, no. 1, pp. 21–30, Feb. 1997, doi: 10.1107/S0021889896009995.
- [155] E. Bykova *et al.*, “Structural complexity of simple Fe<sub>2</sub>O<sub>3</sub> at high pressures and temperatures,” *Nature Communications 2016 7:1*, vol. 7, no. 1, pp. 1–6, Feb. 2016, doi: 10.1038/ncomms10661.
- [156] A. Cuesta, E. R. Losilla, M. A. G. Aranda, J. Sanz, and Á. G. de La Torre, “Reactive belite stabilization mechanisms by boron-bearing dopants,” *Cem Concr Res*, vol. 42, no. 4, pp. 598–606, Apr. 2012, doi: 10.1016/j.cemconres.2012.01.006.
- [157] M. Y. Benarchid, A. Diouri, A. Boukhari, J. Aride, J. Rogez, and R. Castanet, “Elaboration and thermal study of iron-phosphorus-substituted dicalcium silicate phase,” *Cem Concr Res*, vol. 34, no. 10, pp. 1873–1879, Oct. 2004, doi: 10.1016/j.cemconres.2004.01.030.
- [158] I. Jelenić, A. Bezjak, and M. Bujan, “Hydration of B<sub>2</sub>O<sub>3</sub>-stabilized  $\alpha'$ - and  $\beta$ -modifications of dicalcium silicate,” *Cem Concr Res*, vol. 8, no. 2, pp. 173–180, Mar. 1978, doi: 10.1016/0008-8846(78)90006-6.
- [159] H. F. W. Taylor, *Cement chemistry*, 2nd ed. London: Thomas Telford Publishing, 1997. doi: 10.1680/cc.25929.
- [160] G. Álvarez-Pinazo *et al.*, “Rietveld quantitative phase analysis of Yeelimite-containing cements,” *Cem Concr Res*, vol. 42, no. 7, pp. 960–971, Jul. 2012, doi: 10.1016/j.cemconres.2012.03.018.

- [161] Y. Shen, J. Qian, J. Chai, and Y. Fan, "Calcium sulphoaluminate cements made with phosphogypsum: Production issues and material properties," *Cem Concr Compos*, vol. 48, no. 48, pp. 67–74, Apr. 2014, doi: 10.1016/j.cemconcomp.2014.01.009.
- [162] F. Puertas, M. T. B. Varela, and S. G. Molina, "Kinetics of the thermal decomposition of  $C_4A_3\bar{S}$  in air," *Cem Concr Res*, vol. 25, no. 3, pp. 572–580, Apr. 1995, doi: 10.1016/0008-8846(95)00046-F.
- [163] W. G. Mumme, R. J. Hill, G. Bushnell-Wye, and E. R. Segnit, "Rietveld crystal structure refinements, crystal chemistry and calculated powder diffraction data for the polymorphs of dicalcium silicate and related phases," *Neues Jahrbuch fuer Mineralogie - Abhandlungen*, vol. 169, no. 1, pp. 35–68, 1995.
- [164] M. Merlini, M. Gemmi, G. Cruciani, and G. Artioli, "High-temperature behaviour of melilite: In situ X-ray diffraction study of gehlenite-kermanite-Na melilite solid solution," *Phys Chem Miner*, vol. 35, no. 3, pp. 147–155, Apr. 2008, doi: 10.1007/s00269-007-0206-2.
- [165] V. G. Tsirelson, A. S. Avilov, Y. A. Abramov, E. L. Belokoneva, R. Kitaneh, and D. Feil, "X-ray and Electron Diffraction Study of  $MgO$ ," *Acta Crystallogr B*, vol. 54, no. 1, pp. 8–17, Feb. 1998, doi: 10.1107/S0108768197008963.
- [166] V. v. Sharygin *et al.*, "Shulamitite  $Ca_3TiFe_3+AlO_8$  - a new perovskite-related mineral from Hatrurim Basin, Israel," *European Journal of Mineralogy*, vol. 25, no. 1, pp. 97–111, Feb. 2013, doi: 10.1127/0935-1221/2013/0025-2259.
- [167] Y. Takéuchi and F. Nishi, "Crystal-chemical characterization of the  $3CaO \cdot Al_2O_3 - Na_2O$  solid-solution series," *Z Kristallogr Cryst Mater*, vol. 152, no. 1–4, pp. 259–308, Nov. 1980, doi: 10.1524/ZKRI.1980.152.14.259.
- [168] J. A. McGinnety and IUCr, "Redetermination of the structures of potassium sulphate and potassium chromate: the effect of electrostatic crystal forces upon observed bond lengths," *urn:issn:0567-7408*, vol. 28, no. 9, pp. 2845–2852, Sep. 1972, doi: 10.1107/S0567740872007022.
- [169] D. M. Töbrens, N. Stüßer, K. Knorr, H. M. Mayer, and G. Lampert, "E9: The New High-Resolution Neutron Powder Diffractometer at the Berlin Neutron Scattering Center," *Materials Science Forum*, vol. 378–381, no. I, pp. 288–293, 2001, doi: 10.4028/WWW.SCIENTIFIC.NET/MSF.378-381.288.

- [170] H. F. Kay, P. C. Bailey, and IUCr, "Structure and properties of  $\text{CaTiO}_3$ ," *urn:issn:0365-110X*, vol. 10, no. 3, pp. 219–226, Mar. 1957, doi: 10.1107/S0365110X57000675.
- [171] B. A. Wechsler and C. T. Prewitt, "Crystal structure of ilmenite ( $\text{FeTiO}_3$ ) at high temperature and at high pressure," *American Mineralogist*, vol. 69, no. 1–2, pp. 176–185, 1984.
- [172] P. B. Moore and T. Araki, "Atomic arrangement of merwinite,  $\text{Ca}_3\text{Mg}[\text{SiO}_4]_2$ , an unusual dense-packed structure of geophysical interest," *American Mineralogist: Journal of Earth and Planetary Materials*, vol. 57, no. 9–10, pp. 1355–1374, 1972.
- [173] J. Neubauer, R. Sieber, H. J. Kuzel, and M. Ecker, "Investigations on introducing Si and Mg into Brownmillerite - A Rietveld refinement," *Cem Concr Res*, vol. 26, no. 1, pp. 77–82, Jan. 1996, doi: 10.1016/0008-8846(95)00178-6.
- [174] V. v. Sharygin, E. v. Sokol, and Y. Vapnik, "Minerals of the pseudobinary perovskite-brownmillerite series from combustion metamorphic larnite rocks of the Hatrurim Formation (Israel)," *Russian Geology and Geophysics*, vol. 49, no. 10, pp. 709–726, Oct. 2008, doi: 10.1016/j.rgg.2008.03.001.
- [175] T. Hanein, F. P. Glasser, and M. N. Bannerman, "Thermodynamic data for cement clinkering," *Cem Concr Res*, vol. 132, p. 106043, Jun. 2020, doi: 10.1016/j.cemconres.2020.106043.
- [176] W. G. Mumme, "Crystal structure of tricalcium silicate from a Portland cement clinker and its application to quantitative XRD analysis," *Neues Jahrbuch Für Mineralogie-Monatshefte*, vol. 1995, no. 4, pp. 146–160, 1995.
- [177] D. Redaoui, F. Sahnoune, M. Heraiz, and A. Raghdhi, "Mechanism and kinetic parameters of the thermal decomposition of gibbsite  $\text{Al}(\text{OH})_3$  by thermogravimetric analysis," *Acta Phys Pol A*, vol. 131, no. 3, pp. 562–565, Mar. 2017, doi: 10.12693/APHYSPOLA.131.562.
- [178] L. Trusilewicz, F. Fernández-Martínez, V. Rahhal, and R. Talero, "TEM and SAED Characterization of Metakaolin. Pozzolanic Activity," *Journal of the American Ceramic Society*, vol. 95, no. 9, pp. 2989–2996, Sep. 2012, doi: 10.1111/J.1551-2916.2012.05325.X.
- [179] D. N. Batchelder and R. O. Simmons, "Lattice Constants and Thermal Expansivities of Silicon and of Calcium Fluoride between 6° and 322°K," *J Chem Phys*, vol. 41, no. 8, p. 2324, Jul. 2004, doi: 10.1063/1.1726266.

- [180] P. D. Brotherton, J. M. Epstein, M. W. Pryce, and A. H. White, "Crystal structure of 'calcium sulphosilicate',  $\text{Ca}_5(\text{SiO}_4)_2\text{SO}_4$ ," *Aust J Chem*, vol. 27, no. 3, pp. 657–660, 1974, doi: 10.1071/CH9740657.
- [181] M. Z. Stout and P. Bayliss, "Crystal structure of two ferrian ulvospinel from British Columbia," *The Canadian Mineralogist*, vol. 18, no. 3, pp. 339–341, 1980.
- [182] J. Asha Goclawska, "The Mineral Industry of Finland in 2017-2018".





# Appendices

## Appendix 1.

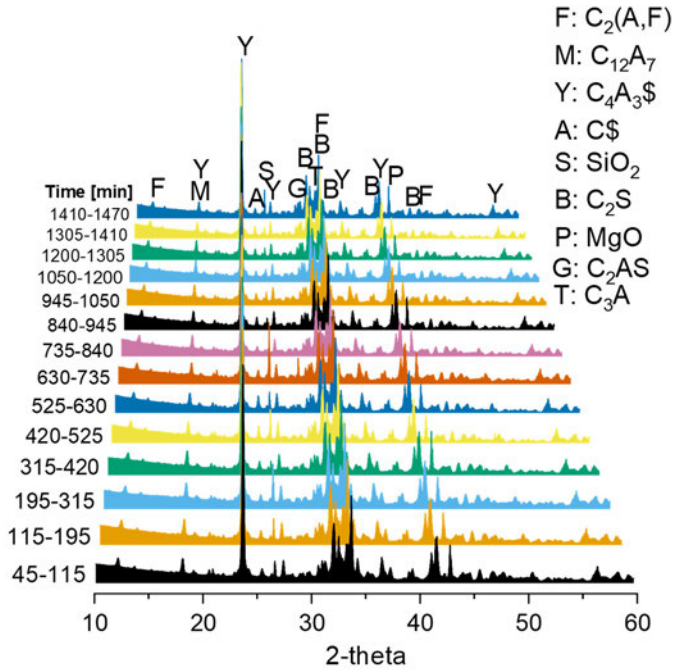
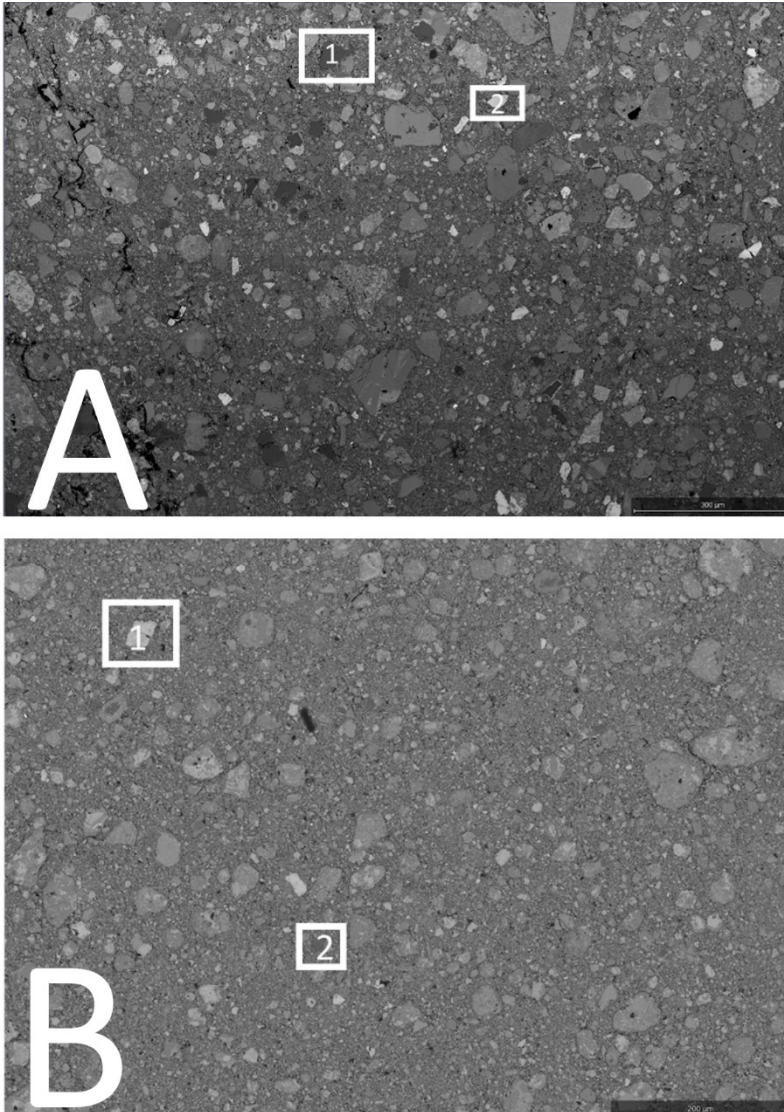


Fig. A1. XRD analyses of clinkers at increasing burning times. F: ferrite  $C_2(A,F)$ , M: mayenite  $C_{12}A_7$ , Y: ye'elimite  $C_4A_3\$$ , A: anhydrite  $C\$$ , S: quartz  $SiO_2$ , B: belite  $C_2S$ , P: periclase  $MgO$ , G: gehlenite, and T: tricalcium aluminate (under CC BY 4.0 license from Paper III © 2022 Authors).

Appendix 2.



**Fig. A2.** Large area BSE images of A) pilot clinker: 1-Mg-rich silicate, 2-FeO; B) reference clinker prepared from ground granules. Mg-rich silicate (1) and FeO (2) indicate that residual raw material is present to a larger extent in the pilot clinker (adapted under CC BY 4.0 license from Paper III © 2022 Authors).

Appendix 3.

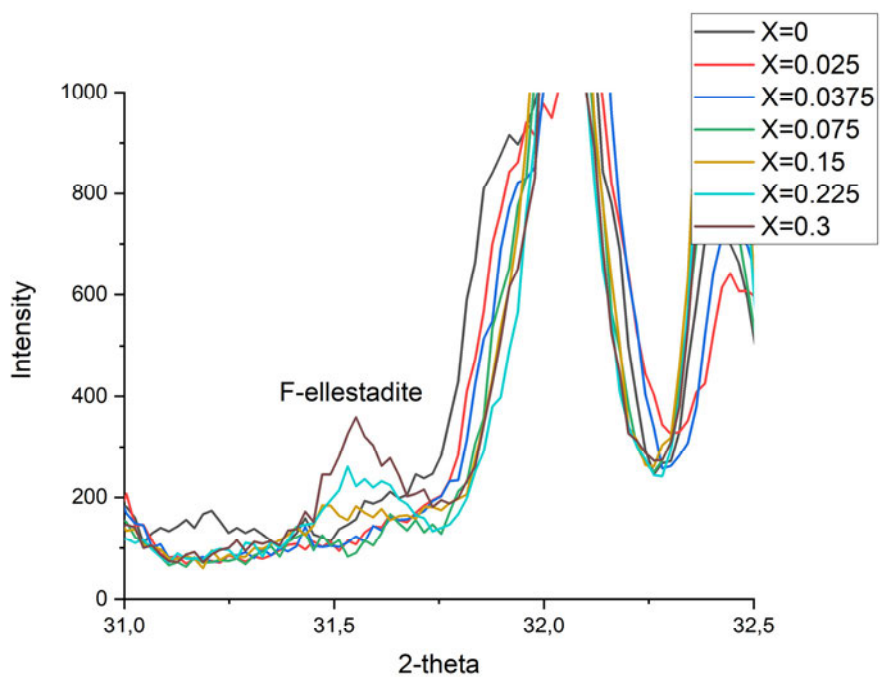
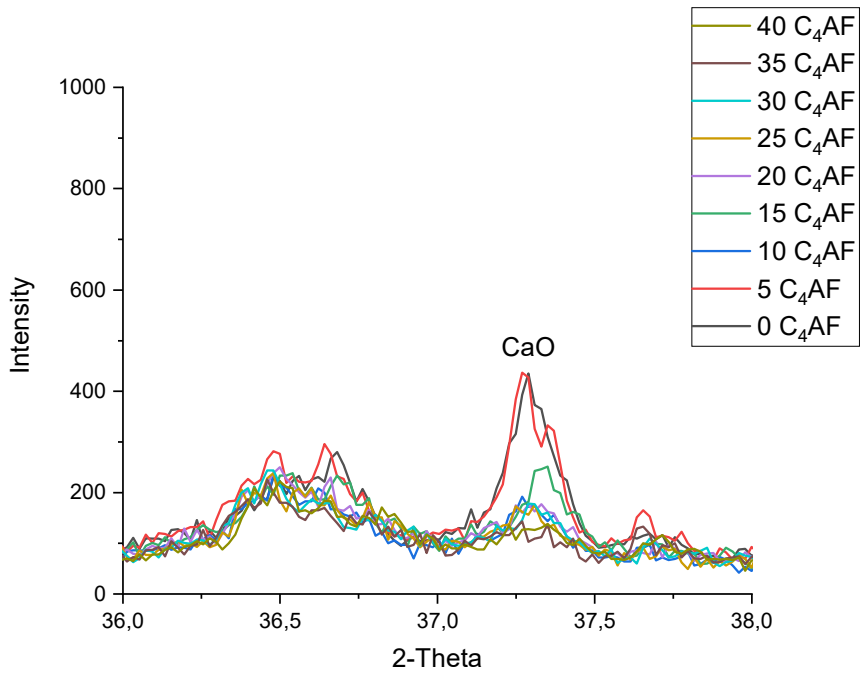
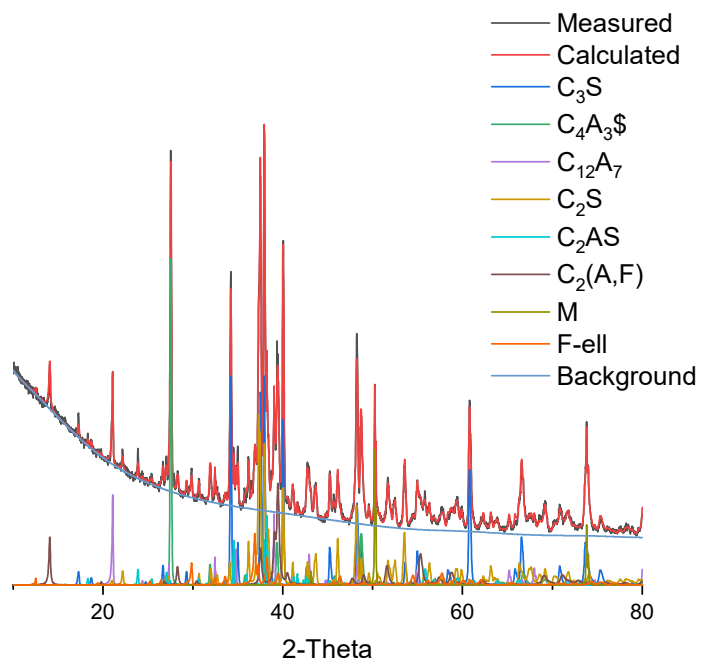


Fig. A3. Series 1 of Paper II, XRD pattern with peaks of fluorellestadite (adapted under CC BY 4.0 license from Paper II © 2021 Authors).



**Fig. A4. Series 3 of Paper II, XRD pattern with peaks of free lime (adapted under CC BY 4.0 license from Paper II © 2021 Authors).**

Appendix 4.



**Fig. A5. XRD of PRE AOD 20 clinker with phase identification and intensities calculated with the Rietveld method (Paper IV). The black line represents the measured diffractogram; the red line refers to the calculated intensities. Alite = C<sub>3</sub>S, belite = C<sub>2</sub>S, ye'elimite = C<sub>4</sub>A<sub>3</sub>\$, ferrite = C<sub>2</sub>(A,F), mayenite = C<sub>12</sub>A<sub>7</sub>, periclase = M, gehlenite = C<sub>2</sub>AS, and Fell = fluorellestadite.**

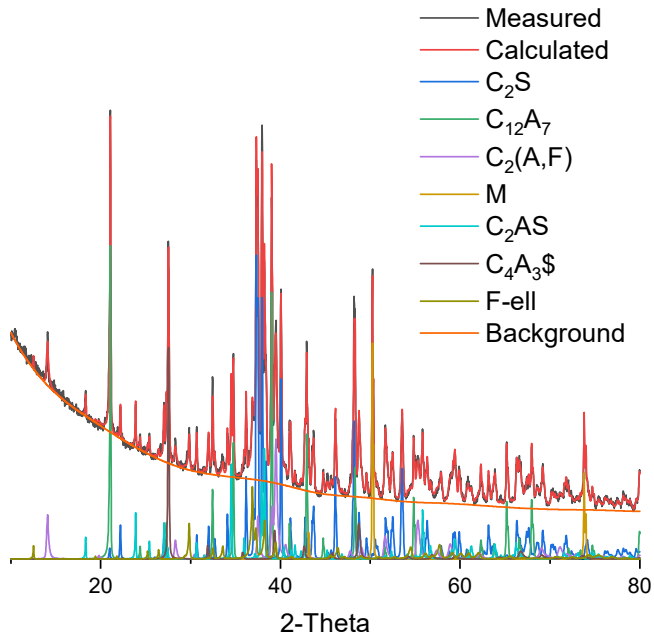


**Fig. A6.** XRD of After Lab clinker prepared from AOD slag used for pilot (Paper IV). Phase identification and intensities calculated with the Rietveld method. The black line represents the measured diffractogram; the red line refers to the calculated intensities. Belite =  $C_2S$ , ye'elinite =  $C_4A_3\$$ , ferrite =  $C_2(A,F)$ , mayenite =  $C_{12}A_7$ , periclase = M, gehlenite =  $C_2AS$ , and fell = fluorellestadite.

Appendix 5.

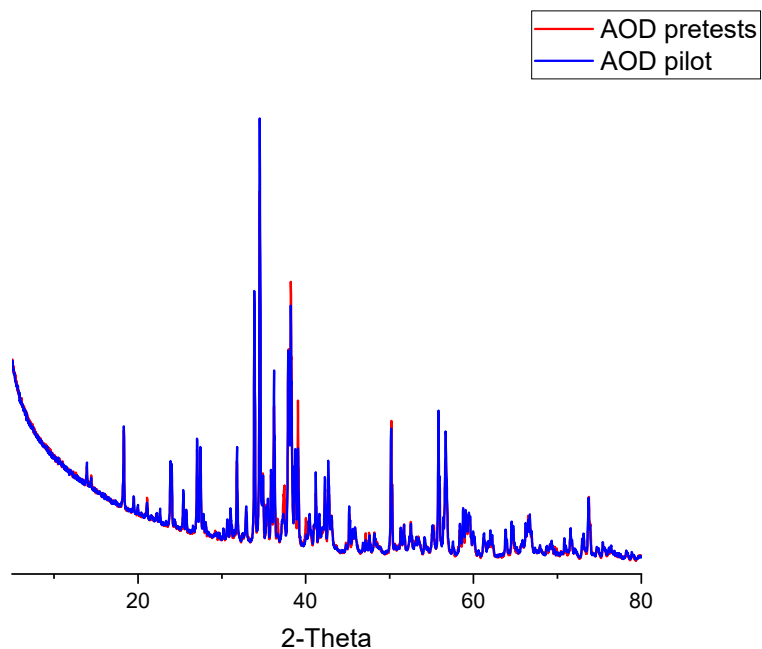


**Fig. A7. XRD patterns of AOD slags used for pre-tests and pilot (Paper IV)**

**Table A1. Average chemical compositions of the phases of pilot AOD slag (Paper IV).**

at.%	O	F	Mg	Al	Si	S	Ca	Ti	Cr	Mn	Fe
Cuspidine	49.57	13.17	0.14	0.25	12.04		24.68	0.14			
Belite	57.15		0.18	0.06	14.22	0.02	28.37				
Merwinite	57.05		7.01	0.11	14.01		21.7		0.05	0.07	
Bredigite	57.09		3.05	0.11	14.12		25.64				
Periclase	50.04	0.09	49.31	0.1	0.12		0.34				
Mayenite	53.89	4.04	0.13	21.54	0.81	0.06	19.25			0.04	0.23
Al-belite	57.29		0.17	0.63	13.02	0.48	27.91	0.13	0.05		0.29
CaF <sub>2</sub>	23.4	53.28			0.09		23.23				

Appendix 6.

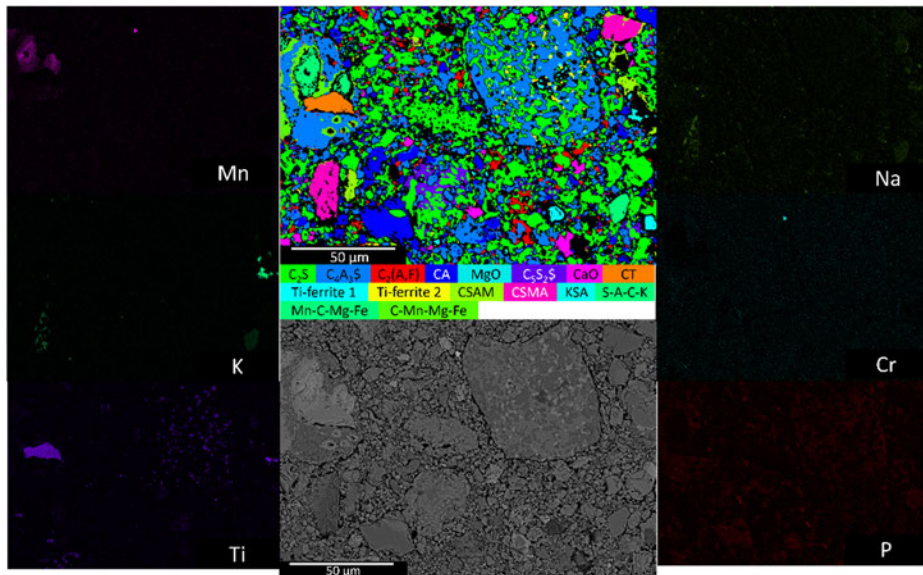


**Fig. A8.** Results of the EDX mapping analysis at an acceleration voltage of 7 kV (Paper IV): Elemental distribution maps were used to segment phase maps (PM) of each phase. The minor elements/impurities are from industrial byproducts.

**Table A2.** Phase composition of PILOT B LAB clinker (at.%) determined by EDX analysis (Paper IV). The sum was normalized to 100%.

Phase	O	F	Na	Mg	Al	Si	S	K	Ca	Ti	Cr	Mn	Fe	Zn
S-Al-belite	58.1		0.1	0.2	0.7	12.8	0.3		27.4	0.1			0.3	
C\$A	58.9		0.1	0.3	20.0	0.8	3.6		15.6	0.1	0.1		0.7	
MgO	50.3			48.1	0.3	0.2	0.1		0.6			0.1	0.2	
CA	55.1	2.8	0.1	0.3	20.2	0.7	0.6	0.1	18.8	0.1			1.4	
Mg-Si ferrite	57.9		0.1	1.5	9.1	1.5	0.5	0.1	20.5	1.1	0.1	0.8	6.9	
\$-C <sub>2</sub> S	57.6	2.0	0.1	0.2	0.9	10.4	2.4	0.1	25.7	0.1	0.1		0.2	
belite	33.7		0.1	0.2	0.8	17.9	0.4	0.1	46.7	0.2				
ternesite	57.8	4.5	0.1	0.1	1.4	6.8	5.6	0.1	22.9	0.2	0.2		0.3	
belite-2	57.4		0.1	0.3	5.9	8.6	1.1	0.1	24.4	0.3	0.1	0.1	1.6	
CAF	59.1			1.0	6.8	0.8	0.1		20.7	0.7		0.6	10.2	
CA-2	55.7			0.2	19.8	0.5	0.2		22.2				1.3	0.2
CF	57.1	0.6	0.3	1.1	6.9	2.6	2.4	0.4	22.1	0.9	0.1	0.6	4.9	
CAF	56.1			0.7	4.8	2.7	0.2	0.1	22.3	1.1	0.1	0.5	11.3	0.2
CaF <sub>2</sub>	16.0	57.6			2.6	1.0			22.8					



## Appendix 7.

### Hydration and workability of CSAB(F) (Paper III)

Fig. A8 shows the heat flow of calorimetric studies conducted using an 8-channel TAM Air (TA instruments) isothermal calorimeter at 20 °C for 24 hours. The dry formulation for calorimetry mixtures contained 0, 5, 10, 15, and 20 wt.% gypsum and anhydrite and 100, 95, 90, 85, 80 wt.% pilot clinker. The water to solid ratio for the calorimetry samples was 0.5. The dry materials were first mixed, and then water was added, and the mix was stirred using a spatula for one minute. 3–6 g of each sample were poured into 20 ml glass ampoules and placed in calorimeter slots. A 40 min baseline was run for each analysis before the recording started. The weight of the samples was used to normalize the recorded data.

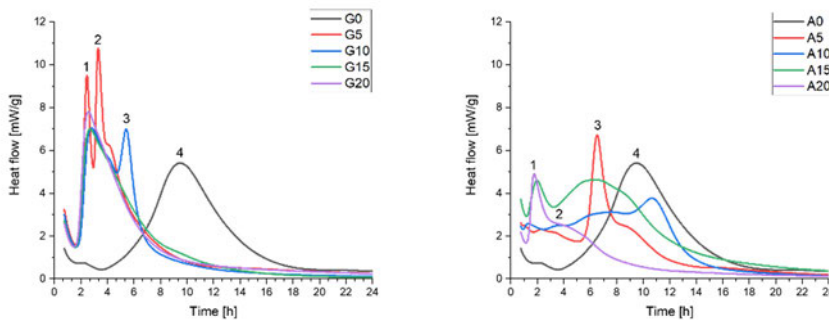


**Fig. A8.** Rate of heat evolution from isothermal calorimetry results of pilot clinker with 0, 5, 10, 15, and 20 wt.% gypsum and anhydrite replacement. The recording started after a 40-minute baseline run and was collected for 24 hours at 20 °C at a w/c ratio of 0.5.

Fig. A8 shows that the hydration speed with anhydrite was slower and distributed for a longer period. The hydrations of ye’elinite with gypsum/anhydrite to ettringite can be expressed with the equation  $(C_4A_3S + 2C_2S + 32H + 2AH_3) \rightarrow C_3A \cdot 3C_2S \cdot 32H + 2AH_3$ . According to the equation, to complete the precipitation of ettringite, the replacement of pilot clinker (title study) with gypsum and anhydrite was calculated to be 18.8 wt.% and 15.5 wt.% respectively. 15 wt.% anhydrite was selected for XRD and compressive strength studies according to the assumption that it would lead to most ettringite formation and had the longest hydration period, which was assumed to lead to the best workability.

To confirm the hydration products of A15, hydrated paste samples were prepared to determine the hydration products of pilot clinker with curing times of

1, 7, and 28 days. Three samples were prepared by replacing 15 wt.% of cement clinker with anhydrite with a water/binder ratio of 0.5. The effect of citric acid on hydration was studied by preparing three samples for each curing time by dissolving 0.5 vol.% citric acid in DI water. Pastes were cured in a humidity chamber with 98% air humidity at 22 °C. After curing, the hydrated pastes were crushed (>4 mm) and submerged in isopropanol for 48 h to stop the hydration. After removal from the isopropanol bath, the samples were dried in a 40 °C furnace and ground with an agate mortar. The amorphous content and corrected content of crystalline phases of hydrated samples were determined with an internal standard method, in which amorphous content is determined by replacing material with a known weight fraction of a crystalline internal standard material. In this case, the sample was replaced with 10 wt.% of TiO<sub>2</sub> (Alfa Aesar, titanium (IV) oxide, rutile, 99.9%, metals basis). The XRD analysis was conducted using the same parameters as for laboratory clinkers, and the crystalline phases were identified using PDXL 2 software. The phase composition of 1-, 3-, 7-, and 28-day cured cement pastes is shown in Table A3. The XRD data show that the main hydration product is Aft, ettringite. The formation of ettringite is already complete after one day of hydration, but the amount of amorphous content evolves as the hydration continues. The hydration of belite is negligible because of impurities, and the ferrite remained mostly unreacted.

**Table A3. The phase composition of 1-, 3-, 7-, and 28-day cured cement pastes. The amorphous content is determined using an internal standard method. Anhydrite 15 wt.% + 0.5 vol.% citric acid.**

XRD phases	Start	1d	3d	7d	28d
AFt	0	36	36	39	42
C <sub>2</sub> S	16	13	12	11	12
C <sub>4</sub> A <sub>3</sub> \$	22	2	1	1	1
C <sub>4</sub> AF	10	10	8	7	8
MgO	3	3	3	3	3
SiO <sub>2</sub>	1	1	0	1	0
C\$	11	4	1	0	0
C <sub>12</sub> A <sub>7</sub>	2	0	0	0	0
C <sub>2</sub> AS	2	0	0	0	0
ACn	0	32	39	38	33
Water	33				
Total	100	100	100	100	100
Unreacted cement phases		33	25	23	23.2
Crystalline reaction products		36	36	39	42
Amorphous/unidentified content		32	39	38	33

Setting time for CSAB(F) with 15 wt.% anhydrite and 20 wt.% gypsum additions with a citric acid content of 0–0.5 vol.% water – DI water solutions were measured using a VICAT testing machine. The results are presented in Table A4. It was seen that citric acid addition postponed the initial and final setting time effectively. Most of the benefits from the retarder could already be achieved with a 0.2 vol.% citric acid – water solution.

**Table A4. Setting times of pilot CSA with anhydrite/gypsum addition with different citric acid additions.**

Sample	Initial setting time	Final setting time
	[min]	[min]
CSA + anhyd (15%) + 0.1% CA	79	121-126
	74	114
CSA + anhyd (15%) + 0.2% CA	118	163
	99	194
CSA + anhyd (15%) + 0.3% CA	103	158
	102	152
CSA + anhyd (15%) + 0.4% CA	104	185
	87	187
CSA + anhyd (15%) + 0.5%-CA	95	190
	78	175
CSA + anhyd (15%)	34	84
	45	70
CSA + gypsum (20%) + 0.1% CA	67	87
	98	123
CSA + Gypsum (20%) + 0.2% CA	88	118
	108	143
CSA + gypsum (20%) + 0.1% CA	67	87
	98	123
CSA + Gypsum (20%) + 0.2% CA	88	118
	108	143
CSA + Gypsum (20%) + 0.3% CA	108	148
	128	193
CSA + Gypsum (20%) + 0.4% CA	120	158
	128	248
CSA + Gypsum (20%) + 0.5% CA	75	180
	109	193
CSA + Gypsum (20%)	58	83
	63	88

Appendix 8.

**Table A5. Target phase composition, target oxides, and raw mixes of clinkers of pretesting to determine sufficient AOD slag content needed for mineralization of alite.**

Phase	C <sub>3</sub> S	C <sub>2</sub> S	C <sub>4</sub> A <sub>3</sub> S	C <sub>4</sub> AF	CS (anhydrite)	C
Wt. %	40	25	20	15	0	0
Target oxide composition and required fluorine content						
Oxide	Al <sub>2</sub> O <sub>3</sub>	CaO	F	Fe <sub>2</sub> O <sub>3</sub>	SiO <sub>2</sub>	SO <sub>3</sub>
Wt. %	13.2	60	0.5	4.9	19.2	2.6
PRE AOD 17.5						
Raw material	AOD slag	CaO	Pgypum	Fayalite slag	Ladle slag	SiO <sub>2</sub>
Wt. %	17.5	31	4.8	7.8	39.0	7.8
PRE AOD 22.5						
Raw material	AOD slag	CaO	Pgypum	Fayalite slag	Ladle slag	SiO <sub>2</sub>
Wt. %	22.5	28.3	4.4	7.5	39.6	6.6

**Table A6. QXRD pretesting to determine sufficient AOD slag content needed for mineralization of alite. Diffractograms are presented in Figures A5 and A6.**

Clinker	17.5 AOD	22.5 AOD
C <sub>4</sub> A <sub>3</sub> S	5.74	3.68
C <sub>3</sub> S	19.49	20.79
C <sub>2</sub> S	40	38.2
C <sub>2</sub> (A,F)	17.19	17.61
γ-C <sub>2</sub> S	2.81	0
C <sub>12</sub> A <sub>7</sub>	9.8	11.98
M	4.16	5.13
C\$	0.75	0
C	0.11	0
R <sub>wp</sub> [%]	6.1	5.7



## Original publications

This thesis is based on the following publications, which are referred to throughout the text by their Roman numerals:

- I Isteri, V., Ohenoja, K., Hanein, T., Kinoshita, H., Tanskanen, P., Illikainen, M., Fabritius, T. (2020). Production and properties of ferrite-rich CSAB cement from metallurgical industry residues, *Science of The Total Environment*, 712, 136208. <https://doi.org/10.1016/j.scitotenv.2019.136208>.
- II Isteri, V., Ohenoja, K., Hanein, T., Kinoshita, H., Tanskanen, P., Illikainen, M., Fabritius, T. (2021). The Effect of Fluoride and Iron Content on the Clinkering of Alite-Ye'elimite-Ferrite (AYF) Cement Systems, *Frontiers in Built Environment*, 7, 89. <https://doi.org/10.3389/fbuil.2021.698830>.
- III Isteri, V., Ohenoja, K., Hanein, T., Kinoshita, H., Kletti, H., Rößler, C., Tanskanen, P., Illikainen, M., Fabritius, T. (2022). Ferritic calcium sulfoaluminate belite cement from metallurgical industry residues and phosphogypsum: Clinker production, scale-up, and microstructural characterization. *Cement and Concrete Research*, 154, 106715. <https://doi.org/10.1016/j.cemconres.2022.106715>.
- IV Isteri, V., Ohenoja, K., Hanein, T., Kinoshita, H., Kletti, H., Rößler, C., Tanskanen, P., Illikainen, M., Fabritius, T. (manuscript). The effect of slag variability and the fate of minor elements in the attempted manufacture of AYF (alite-ye'elimite-ferrite) cement clinker at both laboratory and pilot scale.

Reprinted under CC BY 4.0 license<sup>1</sup> (Papers I–III © 2020, 2021, 2022 Authors).

The original publications are not included in the electronic version of the dissertation.

---

<sup>1</sup> <https://creativecommons.org/licenses/by/4.0/>





864. Tervo, Henri (2023) Non-metallic inclusions in steels and their effect on the toughness and ductility : ultra-high-strength steels and high strength offshore steels
865. Siponkoski, Tuomo (2022) Advanced piezoelectric composites : development and properties
866. Shi, Henglin (2023) Learning-based human action and affective gesture analysis
867. Pálvölgyi, Petra (2023) Synthesis of porous dielectric materials for future wireless high frequency applications
868. Kovacevic, Ivana (2023) Advanced network slicing and computational offloading for latency limited communications
869. Ikkala, Lauri (2023) Airborne remote sensing as a tool for monitoring topographical and hydrological changes on northern degraded and restored peatlands
870. Virpiranta, Hanna (2023) Development of biological treatment for sulfate- and metals-containing cold mining-impacted waters
871. Alzaza, Ahmad (2023) Cementitious binders for construction in northern cold regions
872. Kantanen, Pekka (2023) The role of finely divided retained austenite on the mechanical properties of QP and ART processed novel 0.3C ultrahigh strength steels
873. Markkula, Juho (2023) Communicating smart grid demand response and control data through LTE network related solutions
874. Laukkanen, Johanna (2023) Alkali-activation of industrial aluminosilicate sidestreams : application for mine water treatment and sediment remediation
875. Ismail, Mostafa (2023) Advanced imaging of lignocellulosic and cellulose materials
876. Abdelrahim, Ahmed (2023) Towards lower CO<sub>2</sub> emissions in iron and steelmaking : hydrogen-assisted reduction and cement-free briquettes
877. Zhou, Jin (2023) Conductive composites of engineered nanomaterials with excellent gas sensing properties
878. Ali, Farooq (2023) A framework for analyzing, developing, and managing stakeholder network relationships in collaborative hospital construction projects
879. Rönkkö, Pasi (2023) Circular economy as an enabler of improved resilience and material availability in supply chains

Book orders:

Virtual book store

<https://verkkokauppa.omapumu.com/fi/>

S E R I E S E D I T O R S

**A**  
**SCIENTIAE RERUM NATURALIUM**

*University Lecturer Mahmoud Filali*

**B**  
**HUMANIORA**

*University Lecturer Santeri Palviainen*

**C**  
**TECHNICA**

*Senior Research Fellow Antti Kajjalainen*

**D**  
**MEDICA**

*University Lecturer Pirjo Kaakinen*

**E**  
**SCIENTIAE RERUM SOCIALIUM**

*University Lecturer Henri Pettersson*

**E**  
**SCRIPTA ACADEMICA**

*Strategy Officer Mari Katvala*

**G**  
**OECONOMICA**

*University Researcher Marko Korhonen*

**H**  
**ARCHITECTONICA**

*Associate Professor Anu Soikkeli*

**EDITOR IN CHIEF**

*University Lecturer Santeri Palviainen*

**PUBLICATIONS EDITOR**

*Publications Editor Kirsti Nurkkala*

ISBN 978-952-62-3663-6 (Paperback)

ISBN 978-952-62-3664-3 (PDF)

ISSN 0355-3213 (Print)

ISSN 1796-2226 (Online)